Parity Nonconservation in Neutron Radiative Capture Reactions(Dissertation_全文)

AUTHOR(S):

Shimizu, Hirohiko

Parity Nonconservation in Neutron Radiative Capture Reactions

Submitted to the Faculty of Science
of
Kyoto University
in Partial Fulfillment of the Requirements
for the Degree of Doctor of Science
by

Hirohiko M. Shimizu

1991

Abstract

Parity nonconserving effect in neutron induced nuclear reactions has been investigated in low energy (n,γ) reactions for several p-wave compound resonances. Large asymmetries with respect to the incident neutron helicity ($A_{L,\gamma}$) have been observed in p-wave resonance cross sections for several target nuclei. Obtained results are $A_{L,\gamma} = (9.8 \pm 0.3)\%$, $(2.1 \pm 0.1)\%$ and $-(1.3^{+0.7}_{-0.4})\%$ for the targets of $^{139}La(E_n = 0.734eV)$, $^{81}Br(E_n = 0.88eV)$ and $^{111}Cd(E_n = 4.53eV)$, respectively. The phenomena are explained as very large enhancement of interference terms between s- and p-wave amplitudes due to the statistical nature of compound states and the difference of centrifugal potential barriers between the two amplitudes. Dependences of resonance cross sections and their asymmetries with respect to the incident neutron helicity on the angle of emitted γ-rays have been measured, and found to be very small. The dependence of $A_{L,\gamma}$ on γ-ray energy has been measured for ^{139}La, and has been found to be independent of γ-ray energy within experimental errors. The results show that the large values of $A_{L,\gamma}$ are due to parity mixing in the entrance channel.

The $\sigma_n \cdot \hat{k}_\gamma$ correlation term for ^{139}La has been also measured to study parity mixing effects in exit channels.

Table of Contents

§1 Introduction

The parity (P) is a discrete symmetry of a physical system under a space reflection. The parity violation has been established to be a nature of the weak interaction since it was introduced by Lee and Yang [1] in 1956, and it was observed experimentally by Wu et al.[2] in 1957. In nucleon-nucleon (N-N) interactions where the strong interaction is dominant, the parity-nonconserving (PNC) effect is very small. A possibility to observe a PNC effect in N-N interactions was first discussed by Wilkinson[3] †. The total amplitude (f) consists of parity-conserving (PC) part (f_{PC}) and PNC part (f_{PNC}),

$$f = f_{PC} + f_{PNC}. \tag{1-1}$$

The size of f_{PNC} relative to that of f_{PC} is crudely given by the ratio of PC and PNC light-meson-exchange potentials (V_{PC} and V_{PNC}) :

$$\begin{aligned} \alpha_{NN} \equiv \frac{V_{PNC}}{V_{PC}} &\sim G_F m_\pi^2 \sim 2 \times 10^{-7} \\ &\sim \frac{|f_{PNC}|}{|f_{PC}|}, \end{aligned} \tag{1-2}$$

where G_F and m_π are the Fermi coupling constant and the pion mass, respectively. The absolute square of f is to be observed in experiments.

$$\begin{aligned} |f|^2 &= |f_{PC}|^2 + 2Re f_{PC} f_{PNC}^* + |f_{PNC}|^2 \\ &\sim |f_{PC}|^2 (1 + 2\alpha_{NN} + \alpha_{NN}^2) \end{aligned} \tag{1-3}$$

Two types of experiments were suggested. The first one is the measurement of $|f_{PNC}|^2$ which is pure PNC part. For example, search for violation of "absolute" selection rules which are imposed by parity-conservation belongs to this type. The second one is the measurement of $Re f_{PC} f_{PNC}^*$ which is an interference term. The measurement of P-odd correlation terms belongs to this type. Larger PNC effect is expected in the second-type experiment since the PNC effect in the second-type experiment is the order of $\alpha_{NN} \sim 10^{-7}$ while that in the first-type is the order of $\alpha_{NN}^2 \sim 10^{-14}$.

The longitudinal asymmetry in proton-proton scattering which is given as

$$A_L(pp) = \frac{\sigma^+(pp) - \sigma^-(pp)}{\sigma^+(pp) + \sigma^-(pp)}, \tag{1-4}$$

where $\sigma^+(pp)$ ($\sigma^-(pp)$) is the scattering cross section with incident positive- (negative -) helicity protons. It has been measured at several incident proton energies. The

† He discussed in the context of parity violation in the strong interaction.

incident energy [MeV]	$A_L(pp)$	
15	$-(1.7 \pm 0.8) \times 10^{-7}$	Los Alamos [4]
45	$-(2.3 \pm 0.8) \times 10^{-7}$	SIN [5]
45	$-(1.3 \pm 0.8) \times 10^{-7}$	Berkeley [6]
800	$(2.4 \pm 1.1 \pm 0.1) \times 10^{-7}$	Los Alamos [7]

Table 1-1. Longitudinal asymmetry in p-p scattering.

experimental results are listed in Table 1-1. These results are consistent with theoretical estimations.

The first successful observation of large PNC effect in nuclear process was the measurement of left-right asymmetry of capture γ-rays from unpolarized ^{113}Cd target induced by transversely polarized incident thermal neutrons from a reactor in 1964 [8]. They measured a parity violating term A_γ in angular distribution of the capture γ-ray intensity given as

$$W(\theta_{\gamma\sigma_n}) \propto (1 + p_n A_\gamma \cos\theta_{\gamma\sigma_n}), \qquad (1-5)$$

where p_n and $\theta_{\gamma\sigma_n}$ are the incident neutron polarization and the angle between the direction of the incident neutron spin and the emitted γ-ray momentum. The obtained value is $A_\gamma = -(4.1 \pm 0.8) \times 10^{-4}$. The large PNC effect arises from interference between parity-favored transition (M1) and parity-unfavored transition (E1) in $^{114}Cd(1^+ \rightarrow 0^+)$. Another large PNC effect was found in the measurement of circular polarization of γ-ray (P_γ) from unpolarized ^{114}Cd nuclei[9]. The obtained value is $P_\gamma = -(6.0 \pm 1.5) \times 10^{-4}$. These types of PNC effect have been studied for a number of nuclei as listed in Table 1-2. The existence of the large interference term implies that the initial (compound) state or the final state of the γ-ray transition is a parity mixed state. It is natural to assume that the parity is mixed in the intial state, since the level density is much higher in the initial state than in the final state. Therefore, a large PNC effect is expected also in the entrance channel of the compound state. The A_γ and P_γ are related to parity mixing in exit channel.

In 1980, very large PNC effect caused by an interference between two opposite-parity amplitudes in the entrance channel was observed in spin rotation angle of transversely polarized thermal neutrons with respect to the beam axis on propagation through ^{117}Sn [21]. The obtained value is $d\phi/dz = (3.7 \pm 0.3) \times 10^{-5} rad/cm$. The spin rotation angle corresponds to the real part of the interference term between PC and PNC part of the amplitude.

transition	value	reference
$n + p \rightarrow D(1^+) + \gamma$	$A_\gamma = (0.6 \pm 2.1) \times 10^{-7}$	10
	$P_\gamma = -(1.30 \pm 0.45) \times 10^{-6}$	11
$^{18}F(0^- \rightarrow 1^+)$	$P_\gamma = -(0.5 \pm 20) \times 10^{-3}$	12
$^{19}F(\frac{1}{2}^- \rightarrow \frac{1}{2}^+)$	$A_\gamma = -(18 \pm 9) \times 10^{-5}$	13
$^{41}K(\frac{7}{2}^- \rightarrow \frac{3}{2}^+)$	$P_\gamma = (2.0 \pm 0.4) \times 10^{-5}$	14
$^{114}Cd(1^+ \rightarrow 0^+)$	$A_\gamma = -(4.0 \pm 0.8) \times 10^{-4}$	8
	$P_\gamma = -(6 \pm 1.5) \times 10^{-4}$	9
$^{118}Sn(1^+ \rightarrow 0^+)$	$A_\gamma = (4.4 \pm 0.6) \times 10^{-4}$	15
	$P_\gamma = (8.5 \pm 1.5) \times 10^{-4}$	16
$^{175}Lu(\frac{9}{2}^- \rightarrow \frac{7}{2}^-)$	$P_\gamma = (5.5 \pm 20) \times 10^{-5}$	17
$^{180}Hf(8 \rightarrow 6)$	$P_\gamma = -(2.4 \pm 0.3) \times 10^{-3}$	18
	$A_\gamma = -(1.7 \pm 0.2) \times 10^{-3}$	19
$^{181}Ta(\frac{5}{2}^+ \rightarrow \frac{3}{2}^+)$	$P_\gamma = -(5.2 \pm 0.5) \times 10^{-6}$	20

Table. 1-2. PNC effects in nuclear γ-ray transitions.

Another important observable which arises from the imaginary part of the interference term is the longitudinal asymmetry (A_L) of a compound resonance cross section. The A_L is given as

$$A_L = \frac{\sigma^+_{res} - \sigma^-_{res}}{\sigma^+_{res} + \sigma^-_{res}}, \qquad (1-6)$$

where σ^+_{res} (σ^-_{res}) is the resonance cross section for a radiative capture reaction with incident positive- (negative-) helicity neutrons. We discuss the case of radiative capture reactions induced by epithermal neutrons. The total cross section σ_{tot} consists of potential scattering cross section (σ_{sc}) and the radiative capture cross section (σ_{cap}). The value of σ_{sc} is almost constant against E_n, while that of σ_{cap} varies with E_n. The σ_{cap} consists of a number of compound resonances well separated from each other. Most of them are s-wave resonances, and small p-wave resonances are also observed. When we look at vicinity of a resonance, we can observe a component which changes slowly with E_n in addition to the component of the resonance. The slowly varying component is the sum of the contributions of tails of other resonances. The cross section for the narrow compound resonance is referred to as resonance cross section (σ_{res}), and that of the slowly changing component as continuum cross section (σ_{con}). Very large A_L's have been observed only in p-wave resonances. The phenomena can be explained by an interference between amplitudes of the p-wave resonance and the tail of a neighboring s-wave resonance (s-p mixing) [22]. The interference term between two opposite-parity amplitudes has a possibility of large contribution in low energy neutron capture reaction cross section, since nucleons in the compound nucleus have much longer time to

interact with each other than in the case of direct processes. The small PNC effect of N-N interaction may be accumulated or cancelled during the long life time of the compound state. In this case, it tends to be accumulated as discussed in §6. Another theoretical approach based on an S-matrix formalism is proposed in which the large PNC effect arises from an interference between amplitudes of p- and d-wave resonances (p-d mixing) [23,24].

The large PNC effect in neutron-nucleus (n-A) interaction introduces a new possibility for testing the time-reversal-invariance (TRI) [23–29].

The CP violation was observed in the decay of neutral K mesons by Christenson et al.[30] in 1964, but the origin of CP violation still remains unknown. If the CPT theorem[31] is true, it implies that TRI is broken. Direct measurement of T-violating effect is very important to study the origin of CP-violation, since the theoretical prediction of T-violating effect in an observable is model dependent because of lack of the knowledge about the origin of CP-violation [32]. No finite T-violating effect has been observed so far in spite of a number of intensive efforts. The experimental upper limits for T-odd amplitudes relative to T-even amplitudes are $\sim 10^{-3}$ for strong, electromagnetic and weak interactions. The difficulty of the experiments on the TRI test is due to the anti-unitarity of T-operator [33]. Even if the interaction is TRI, T-odd correlation term may exist because of the effect of final state interaction (FSI). We must evaluate the FSI effect and subtract it from the observed T-odd correlation term. The measurement of T-odd correlation term in nuclear β-decay is a good example to see the problem of FSI effects. The T-odd correlation term $D\hat{\mathbf{J}}\cdot\vec{\mathbf{p}}_e\times\vec{\mathbf{p}}_\nu/(\mathbf{E}_e\cdot\mathbf{E}_\nu)$ in $^{19}Ne \rightarrow ^{19}F + e^+ + \nu$ was measured [34] where $\hat{\mathbf{J}}$, $\vec{p}_e$, $\vec{p}_\nu$, E_e and E_ν are unit vectors parallel to the nuclear spin of ^{19}Ne, momenta of the emitted positron and the neutrino, kinetic energies of the positron and the neutrino, respectively. The obtained result is $D = (4 \pm 8) \times 10^{-4}$, while the contribution of FSI (D_{FSI}) is $\sim 2.6 \times 10^{-4} p_e/(p_e)_{max}$, where $(p_e)_{max}$ is the maximum value of p_e [35]. The experimental sensitivity to T-violation is limited to a few times 10^{-4} by the value of the contribution of the FSI effect. The FSI effect appears in all decay or reaction processes. But it does not exist when the system is static, or the process is elastic scattering where momenta of incoming and outgoing particles are the same. In such cases, there is no contribution of FSI effect to a T-odd correlation term, and a non-zero value of T-odd correlation is equivalent to the existence of T-violation. This feature is suitable for the measurement of small T-violation effects.

A non-zero value of an electric-dipole-moment (EDM) of a fermion violates TRI and it is an observable in a static system. The measurement of the EDM of neutron

(d_n) has provided the most reliable upper limit for TRI. Recent improvement of techniques to storage ultra-cold-neutrons in a bottle has greatly reduced the systematic error due to the Larmor precession about an effective magnetic field induced by Lorentz transformation from the electric field which is applied to detect the EDM. The upper limits $d_n = (0.6 \pm 0.6) \times 10^{-25}\mathrm{e}\cdot cm$ and $d_n = -(1.4 \pm 0.6) \times 10^{-25}\mathrm{e}\cdot cm$ have been obtained at ILL[36] and Leningrad[37], respectively †. These results give upper limit of the order of 10^{-3} [32] for the strength of T-odd interaction relative to that of T-even interaction (g_T).

All the TRI tests give upper limit for g_T as the order of 10^{-3} in the strong, weak, and electromagnetic interactions [38].

In neutron transmission experiments through matter, kinds and momenta of incoming and outgoing particles are the same, and no FSI effect is contained in T-odd correlation terms. In most of these cases, we can test TRI only in the strong interaction since the strong interaction is dominant in n-A interaction. But a sizable contribution of the weak interaction is contained in the vicinity of p-wave resonances where large PNC effects are observed. Therefore, if we observe T-odd correlation terms in the vicinity of such p-wave resonances, we can study T-violating effect in the weak interaction free from FSI.

It is very important to study the reaction mechanism of p-wave resonances which show large PNC effects, in order to find the most suitable nucleus and the most efficient method for TRI experiment.

There have been two types of experiments for the measurement of A_L. One of them is the measurement of helicity dependence of neutron beam attenuation in which the number of neutron is counted on the beam line behind the target. This method is referred to as neutron transmission method hereafter. The total cross section (σ_{tot}) is measured in the neutron transmission method. The other one is the measurement of helicity dependence of the cross section of neutron radiative capture reaction. Capture γ-rays are measured in this method which is referred to as γ-ray detection method hereafter. The γ-ray detection method is more efficient than the neutron transmission method for the measurement of A_L, since the γ-ray detection method is insensitive to very large potential scattering cross section which shows no large PNC effect.

† The latter one is interpreted as an upper limit of $|d_n| < 2.6 \times 10^{-25}\mathrm{e}\cdot cm$ at a 95% confidence level.

The γ-ray detection method has further merit. In the neutron-transmission method, the capture cross section consists of only two terms, that is, a spin independent term and a helicity dependent term $(\sigma_{\mathbf{n}} \cdot \hat{\mathbf{k}}_{\mathbf{n}})$ where $\sigma_{\mathbf{n}}$ and $\hat{\mathbf{k}}_{\mathbf{n}}$ are unit vectors parallel to neutron spin and neutron momentum, respectively. In the γ-ray detection method, the differential capture cross section $(\sigma_{cap}(\theta_\gamma))$ has more correlation terms [39] which depend on the neutron spin, the polar angle of the γ-ray momentum with respect to the beam axis (θ_γ) and the helicity of the γ-ray. Each correlation term is an interference term between two amplitudes. A different amplitude arises from a different reaction mechanism. Therefore, the measurement of such terms enables us to understand the reaction mechanism which is responsible for the large PNC effect.

The A_L for the p-wave resonance of ^{139}La target at $E_n = 0.734eV$ had been measured by Dubna[40,41] and Kyoto-KEK[42] groups. The Dubna group obtained $A_L = (7.3 \pm 0.5)\%$ using neutron-transmission method, while Kyoto-KEK group obtained $A_L = (9.5 \pm 0.3)\%$ using γ-ray detection method †. In general, the A_L in γ-ray detection method $(A_{L,\gamma})$ is not equivalent to the A_L in neutron-transmission method $(A_{L,n})$ because of the correlation terms which depend on θ_γ. The $A_{L,\gamma}$ is equivalent to $A_{L,n}$ only when the γ-rays are detected in whole solid angle. Vanhoy et al.[44] suggested a possibility that the contribution of polarization and angular correlation terms, especially 2nd order Legendre term $(\cos^2\theta_\gamma - 1/3)$, explains the inconsistency between those two values, since the $A_{L,\gamma}$ had been measured for incomplete solid angle around $\theta_\gamma = 90°$. The determination of such correlation terms is very important to solve this discrepancy.

In this work, we have carried out a precise measurement of polarization and angular correlations in $(\vec{n}, \gamma)$ reactions with improved equipment to investigate the PNC effect in n-A interactions. The $A_{L,\gamma}$'s have been measured in p-wave resonances for the targets of $^{81}Br(E_n = 0.88eV)$, $^{93}Nb(E_n = 35.9eV,\ \ E_n = 42.3eV)$, $^{108}Pd(E_n = 2.96eV)$, $^{111}Cd(E_n = 4.53eV)$, $^{124}Sn(E_n = 62.0eV)$ and $^{139}La(E_n = 0.734eV)$. The experiment has been carried out using a longitudinally polarized epithermal neutron beam from the spallation neutron source at KEK. All the correlation coefficients have been determined for ^{139}La and ^{81}Br targets by measuring the angular distribution of the resonance cross section for unpolarized incident neutrons $(\sigma_{res}^{Unpol}(\theta_\gamma))$ and the θ_γ dependence of the

† Recently, Los Alamos group obtained the value of the A_L which confirmed Kyoto-KEK group's result[43].

longitudinal asymmetry $(a_{L,\gamma}(\theta_\gamma))$.

The $A_{L,\gamma}$ for the target of ^{139}La has been measured as a function of γ-ray energy. If the $A_{L,\gamma}$ is independent of γ-ray energy, only the parity mixing in the entrance channel is responsible for the large value of $A_{L,\gamma}$.

The parity-violating angular distribution of γ-rays with respect to the spin direction of incident neutrons which corresponds to the $\sigma_{\mathbf{n}} \cdot \hat{\mathbf{k}}_\gamma$ correlation term has been measured where $\hat{\mathbf{k}}_\gamma$ is the unit vector parallel to γ-ray momentum. The compound state is longitudinally polarized due to helicity dependence of the capture cross section. We write the angular distribution of γ-rays as

$$W(\theta_\gamma) \propto (1 + p_n A_L)(1 + p_n a_\gamma \cos\theta_\gamma), \qquad (1-7)$$

where the a_γ is the asymmetry of γ-ray intensity with respect to the polarization of the compound state (forward-backward asymmetry). The a_γ contains information of parity mixing in the exit channel.

Dependence of $A_{L,\gamma}$ on E_n has also been studied by using cold targets in order to reduce a Doppler broadening which smears out the structure of $A_{L,\gamma}$.

The formalism of correlation terms in $(\vec{n}, \gamma)$ reaction is given in §2. The experimental arrangement and characteristics of the counters are described in §3 and §4. The method of data analysis and experimental results are discussed in §5. Theoretical interpretation based on s-p mixing in first order perturbation is discussed in §6 and §7. In §8, we will give an overview of further study of PNC effects. We also point out a feasibility of TRI experiment to measure the P-odd T-odd triple vector correlation term $(\sigma_{\mathbf{n}} \cdot (\hat{\mathbf{I}} \times \hat{\mathbf{k}}_{\mathbf{n}}))$ in total scattering amplitude by using neutron transmission method, where $\hat{\mathbf{I}}$ is the unit vector parallel to target nuclear spin [45].

§2 Polarization and Angular Correlations in $(\vec{n},\gamma)$ Reaction

In this section, the polarization and angular correlations in $(\vec{n},\gamma)$ reaction cross section are discussed based on s-p mixing [39] (Appendix A).

The differential cross section of radiative capture reaction induced by polarized neutrons ($\sigma_{cap}(\sigma_n,\hat{k}_n,\sigma_\gamma,\hat{k}_\gamma)$) is given as

$$\begin{aligned}\sigma_{cap}(\sigma_n,\hat{k}_n,\sigma_\gamma,\hat{k}_\gamma) = \frac{1}{2}\Big(& a_0 + a_1\hat{k}_n\cdot\hat{k}_\gamma + a_2\sigma_n\cdot(\hat{k}_n\times\hat{k}_\gamma) + a_3((\hat{k}_n\cdot\hat{k}_\gamma)^2-\frac{1}{3})\\ &+a_4(\hat{k}_n\cdot\hat{k}_\gamma)(\sigma_n\cdot(\hat{k}_n\times\hat{k}_\gamma)) + a_5(\sigma_\gamma\cdot\hat{k}_\gamma)(\sigma_n\cdot\hat{k}_\gamma)\\ &+a_6(\sigma_\gamma\cdot\hat{k}_\gamma)(\sigma_n\cdot\hat{k}_n)\\ &+a_7(\sigma_\gamma\cdot\hat{k}_\gamma)((\sigma_n\cdot\hat{k}_\gamma)(\hat{k}_\gamma\cdot\hat{k}_n)-\frac{1}{3}\sigma_n\cdot\hat{k}_n)\\ &+a_8(\sigma_\gamma\cdot\hat{k}_\gamma)((\sigma_n\cdot\hat{k}_n)(\hat{k}_n\cdot\hat{k}_\gamma)-\frac{1}{3}\sigma_n\cdot\hat{k}_\gamma)\\ &+a_9\sigma_n\cdot\hat{k}_\gamma + a_{10}\sigma_n\cdot\hat{k}_n\\ &+a_{11}((\sigma_n\cdot\hat{k}_\gamma)(\hat{k}_\gamma\cdot\hat{k}_n)-\frac{1}{3}\sigma_n\cdot\hat{k}_n)\\ &+a_{12}((\sigma_n\cdot\hat{k}_n)(\hat{k}_n\cdot\hat{k}_\gamma)-\frac{1}{3}\sigma_n\cdot\hat{k}_\gamma)\\ &+a_{13}\sigma_\gamma\cdot\hat{k}_\gamma + a_{14}(\sigma_\gamma\cdot\hat{k}_\gamma)(\hat{k}_n\cdot\hat{k}_\gamma) + a_{15}(\sigma_\gamma\cdot\hat{k}_\gamma)\sigma_n\cdot(\hat{k}_n\times\hat{k}_\gamma)\\ &+a_{16}(\sigma_\gamma\cdot\hat{k}_\gamma)((\hat{k}_n\cdot\hat{k}_\gamma)^2-\frac{1}{3})\\ &+a_{17}(\sigma_\gamma\cdot\hat{k}_\gamma)(\hat{k}_n\cdot\hat{k}_\gamma)(\sigma_n\cdot(\hat{k}_n\times\hat{k}_\gamma))\Big),\end{aligned} \tag{2-1}$$

where σ_n, $\hat{k}_n$, σ_γ and $\hat{k}_\gamma$ are unit vectors parallel to neutron spin, neutron momentum, γ-ray spin and γ-ray momentum, respectively. When the circular polarization of γ-ray $(\sigma_\gamma\cdot\hat{k}_\gamma)$ is not observed and the incident neutrons are longitudinally polarized, we write

$$\sigma_n\cdot\hat{k}_n = p_n, \qquad \hat{k}_n\cdot\hat{k}_\gamma = \cos\theta_\gamma, \tag{2-2}$$

where p_n is the polarization of incident neutrons and θ_γ is the polar angle of the emitted γ-ray momentum with respect to the beam axis. Then we obtain

$$\begin{aligned}\sigma_{cap}(\theta_\gamma) = \frac{1}{2}\Big(& a_0 + a_1\cos\theta_\gamma + a_3(\cos^2\theta_\gamma-\frac{1}{3})\\ &+ p_n\left(a_{10} + (a_9+\frac{2}{3}a_{12})\cos\theta_\gamma + a_{11}(\cos^2\theta_\gamma-\frac{1}{3})\right)\Big).\end{aligned} \tag{2-3}$$

The a_0 consists of s- and p-wave cross sections ($a_0 = a_{0s} + a_{0p}$). The differential cross section of a p-wave resonance ($\sigma_{res}(\theta_\gamma)$) in the vicinity of the p-wave resonance is

$$\begin{aligned}\sigma_{res}(\theta_\gamma) \propto & 1 + A_1\cos\theta_\gamma + A_3(\cos^2\theta_\gamma-\frac{1}{3})\\ &+ p_n\left(A_{10} + (A_9+\frac{2}{3}A_{12})\cos\theta_\gamma + A_{11}(\cos^2\theta_\gamma-\frac{1}{3})\right),\end{aligned} \tag{2-4}$$

where $A_i = a_i/a_{0p}$ †. If the γ-rays are detected for the whole solid angle, the resonance cross section (σ_{res}) is given as

$$\sigma_{res} = \int d\Omega_\gamma\sigma_{res}(\theta_\gamma) \propto 1 + A_{10}p_n. \tag{2-5}$$

In this case, only A_{10} term remains, which is equivalent to the longitudinal asymmetry measured in neutron-transmission method ($A_{L,n}$). But if γ-rays are detected only for some angle, the σ_{res} depends on other correlation terms. The longitudinal asymmetry in the γ-ray detection method at the angle of θ_γ is given as

$$\begin{aligned}a_{L,\gamma}(\theta_\gamma) &= \frac{(\sigma_{res}(\theta_\gamma))^{p_n=+1} - (\sigma_{res}(\theta_\gamma))^{p_n=-1}}{(\sigma_{res}(\theta_\gamma))^{p_n=+1} + (\sigma_{res}(\theta_\gamma))^{p_n=-1}}\\ &= \frac{A_{10} + (A_9+\frac{2}{3}A_{12})\cos\theta_\gamma + A_{11}(\cos^2\theta_\gamma-\frac{1}{3})}{1 + A_1\cos\theta_\gamma + A_3(\cos^2\theta_\gamma-\frac{1}{3})}.\end{aligned} \tag{2-6}$$

This quantity depends on θ_γ and is not equivalent to the $A_{L,n}$ which is given as

$$A_{L,n} = \frac{(\sigma_{res})^{p_n=+1} - (\sigma_{res})^{p_n=-1}}{(\sigma_{res})^{p_n=+1} + (\sigma_{res})^{p_n=-1}} = A_{10}. \tag{2-7}$$

There are two ways to determine the A_{10} term in $(\vec{n},\gamma)$ reactions. One is to measure $a_{L,\gamma}(\theta_\gamma)$ in the whole solid angle. The other is to measure $a_{L,\gamma}(\theta_\gamma)$ at two θ_γ's which satisfy $\cos^2\theta_\gamma - 1/3 = 0$. From Eq. (2-3), the resonance cross sections are given as

$$\begin{cases}\sigma_{res}(\theta_{\gamma 0}) \propto 1 + A_1\cos\theta_{\gamma 0} + p_n\left(A_{10} + (A_9+\frac{2}{3}A_{12})\cos\theta_{\gamma 0}\right)\\ \sigma_{res}(\pi-\theta_{\gamma 0}) \propto 1 - A_1\cos\theta_{\gamma 0} + p_n\left(A_{10} - (A_9+\frac{2}{3}A_{12})\cos\theta_{\gamma 0}\right)\end{cases}, \tag{2-8}$$

† The A_i's are defined as $A_i = a_i/a_0$ in *Ref.*39.

for $\theta_{\gamma 0} = 54.7°$, that is, $\cos^2\theta_{\gamma 0} - 1/3 = 0$. The A_{10} term is obtained as

$$A_{10} = \frac{\langle\sigma_{res}\rangle^{p_n=+1} - \langle\sigma_{res}\rangle^{p_n=-1}}{\langle\sigma_{res}\rangle^{p_n=+1} + \langle\sigma_{res}\rangle^{p_n=-1}}, \qquad (2-9)$$

where $\langle\sigma_{res}\rangle$ is

$$\langle\sigma_{res}\rangle = \sigma_{res}(\theta_{\gamma 0}) + \sigma_{res}(\pi - \theta_{\gamma 0}) = 1 + A_{10}p_n. \qquad (2-10)$$

The symbol $A_{L,\gamma}$ is used to represent a longitudinal asymmetry measured under those conditions hereafter.

For determination of A_i's, we must measure not only the $a_{L,\gamma}(\theta_\gamma)$ at various θ_γ's but also the θ_γ dependence of the denominator of Eq. (2-6). The differential cross section of a resonance for unpolarized incident neutrons ($\sigma_{res}^{Unpol}(\theta_\gamma)$) is obtained substituting $p_n = 0$ in Eq. (2-4) as

$$\sigma_{res}^{Unpol}(\theta_\gamma) \propto 1 + A_1\cos\theta_\gamma + A_3(\cos^2\theta_\gamma - \frac{1}{3}). \qquad (2-11)$$

Values of A_i's can be determined combining the experimental results of $a_{L,\gamma}(\theta_\gamma)$ and $\sigma_{res}^{Unpol}(\theta_\gamma)$.

The forward-backward asymmetry (a_γ) defined in Eq.(1-7) is discussed below. If we define the a_{FB} as

$$a_{FB} = \frac{\sigma_{res}^F - \sigma_{res}^B}{\sigma_{res}^F + \sigma_{res}^B} = p_n\cos\theta_\gamma \cdot \frac{A_9 + A_{12}\frac{2}{3}}{1 + A_3(\cos^2\theta_\gamma - \frac{1}{3})}, \qquad (2-12)$$

where

$$\begin{cases} \sigma_{res}^F = (\sigma_{res}(\theta_\gamma))^{p_n=+1} + (\sigma_{res}(\pi-\theta_\gamma))^{p_n=-1} \\ \quad \propto 1 + A_3(\cos^2\theta_\gamma - \frac{1}{3}) + (A_9 + \frac{2}{3}A_{12})p_n\cos\theta_\gamma, \\ \sigma_{res}^B = (\sigma_{res}(\pi-\theta_\gamma))^{p_n=+1} + (\sigma_{res}(\theta_\gamma))^{p_n=-1} \\ \quad \propto 1 + A_3(\cos^2\theta_\gamma - \frac{1}{3}) - (A_9 + \frac{2}{3}A_{12})p_n\cos\theta_\gamma, \end{cases} \qquad (2-13)$$

it is approximately equivalent to a_γ if $A_{L,\gamma}a_\gamma \ll 1$. If the detection system is insensitive to A_3 term or the A_3 term is negligible, the a_{FB} is almost equivalent to A_9. Therefore, the a_γ is almost equivalent to A_9, since the A_{12} is negligibly small compared with A_9 (see Appendix A).

The a_9 has a dispersive E_n dependence (see §7), and so does the $\epsilon_\gamma^{tot} = a_\gamma \cdot (\sigma_{res}/\sigma_{cap})$ as shown in Fig. 2-1. Therefore, a_γ must be calculated in left- or right-half side of the resonance. We use $a_{\gamma,<}$ and $a_{\gamma,>}$ to represent the a_γ calculated in left- and right-hand side of the resonance, respectively. The $a_{\gamma,<}$, $a_{\gamma,>}$ and

$a_{\gamma,<>}$ are calculated in the regions of $E_0 - \Gamma \le E_n \le E_0$, $E_0 \le E_n \le E_0 + \Gamma$ and $E_0 - \Gamma \le E_n \le E_0 + \Gamma$, respectively, where the E_0 is the resonance energy and the Γ is the resonance width. We define the difference of $a_{\gamma,<}$ and $a_{\gamma,>}$ as

$$\langle a_\gamma\rangle = \frac{a_{\gamma,<} - a_{\gamma,>}}{2}. \qquad (2-14)$$

§3 Neutron Beam

In this section, we describe the method to obtain a longitudinally polarized epithermal neutron beam.

§3-1 Spallation Neutron Source

The experiment has been carried out at the Polarized-Epithermal-Neutron (PEN) beam line of KEK-Neutron-Source (KENS). A pulsed $500MeV$ proton beam from the booster synchrotron at KEK was used to bombard a uranium target block for producing neutrons by spallation reactions [46]. The repetition rate of the primary proton beam is $20Hz$. The intensity of the proton beam is $(5 \sim 15) \times 10^{11}$ per bunch. Neutrons are moderated in a polyethylene block which is placed next to the uranium target (see Fig. 3-1-1). The uranium target and the moderator are shielded by a $4m$ thick biological shield made of iron and concrete. The size of the neutron beam was defined by a collimator embedded in the shield.

The neutron energy was determined by the time-of-flight (TOF) method using a multi-channel-scaler (MCS: CANBERRA-7880 and an equivalent CAMAC module). A sweep of the MCS was started by a pulse of the primary proton beam, and γ-ray pulses and neutron pulses were histogramed against the time difference from the starting of the sweep. Accuracy of neutron energy determination is limited by the length of primary proton beam bunch and the size of the moderator.

Fig. 3-1-2 shows a typical time structure of the induced current in a current transformer installed in the beam duct which transports the primary proton beam. The beam size is $40nsec$ in FWHM which corresponds to $0.00017eV$ for $1eV$ neutrons when the flight pass length is $6.6m$.

The dimension of the moderator is $10.0cm^W \times 10.0cm^H \times 5.0cm^T$. The moderator's thickness of the beam line PEN is about $5.2cm$ which causes an energy spread of $0.009eV$ in standard deviation for $1eV$ neutrons.

The neutron intensity was measured using a ^{10}B loaded liquid scintillator (NE311A) placed at $9.4m$ from the neutron source. A typical intensity versus neutron energy is

shown in Fig. 3-1-3. The number of incident neutrons was monitored by counting capture γ-rays from an annular indium foil placed at $4.5m$ from the neutron source on the beam axis [47].

§3-2 Neutron Polarizer

Incident neutrons were transversely polarized upon transmission through a dynamically polarized proton filter which was installed at $5.2m$ from the neutron source. A typical neutron polarization was approximately 70% for $E_n \sim 1eV$. The neutron spin was rotated from transverse to longitudinal direction gradually following an adiabatic passage. The magnetic field was designed to rotate the neutron spin parallel and antiparallel to the beam axis (positive- and negative-helicity). The helicity of neutron was reversed every 2.5 or 4 *sec*.

A dynamically polarized proton filter [48–53] was used to obtain the neutron polarization (Appendix B). The neutron polarization was obtained from the spin dependence of $p-n$ cross section [50–52]. The numbers of spin-up and spin-down neutrons after transmission are given as

$$\begin{cases} N_n^{\uparrow} = \dfrac{N_n^{in}}{2}\exp\left(-\dfrac{n_p}{2}((1+p_p)\sigma_{pn}^{\uparrow\uparrow}+(1-p_p)\sigma_{pn}^{\uparrow\downarrow})t\right), \\ N_n^{\downarrow} = \dfrac{N_n^{in}}{2}\exp\left(-\dfrac{n_p}{2}((1-p_p)\sigma_{pn}^{\uparrow\uparrow}+(1+p_p)\sigma_{pn}^{\uparrow\downarrow})t\right), \end{cases} \qquad (3-2-1)$$

respectively, where n_p is the number density of protons, t is the thickness of the filter, p_p is the proton polarization, $\sigma_{pn}^{\uparrow\uparrow}$ ($\sigma_{pn}^{\uparrow\downarrow}$) is the total cross section for parallel (anti-parallel) spin, and N_n^{in} is the number of incident neutrons. The neutron polarization p_n is given as

$$p_n = \frac{N_n^{\uparrow}-N_n^{\downarrow}}{N_n^{\uparrow}+N_n^{\downarrow}} = \tanh\left(\frac{n_p}{2}p_p\Delta\sigma_{pn}t\right), \qquad (3-2-2)$$

where

$$\Delta\sigma_{pn} = \sigma_{pn}^{\uparrow\uparrow}-\sigma_{pn}^{\uparrow\downarrow}. \qquad (3-2-3)$$

The number of neutrons transmitted through polarized filter (N_n^{Pol}) is

$$\begin{aligned} N_n^{Pol} &= N_n^{\uparrow}+N_n^{\downarrow} \\ &= N_n^{in}\exp\left(-n_p\sigma_{pn}^{0}t\right)\cosh\left(\frac{n_p}{2}p_p\Delta\sigma_{pn}t\right), \end{aligned} \qquad (3-2-4)$$

where

$$\sigma_{pn}^{0} = \frac{\sigma_{pn}^{\uparrow\uparrow}+\sigma_{pn}^{\uparrow\downarrow}}{2}. \qquad (3-2-5)$$

The number of neutrons transmitted through unpolarized filter (N_n^{Unpol}) is

$$N_n^{Unpol} = N_n^{in}\exp\left(-n_p\sigma_{pn}^{0}t\right). \qquad (3-2-6)$$

The neutron transmittance of polarized filter (T_n^{Pol}) relative to that of unpolarized filter (T_n^{Unpol}) is

$$\frac{T_n^{Pol}}{T_n^{Unpol}} = \frac{N_n^{Pol}}{N_n^{Unpol}} = \cosh\left(\frac{n_p}{2}p_p\Delta\sigma_{pn}t\right). \qquad (3-2-7)$$

Combining Eq. (3-2-2) and (3-2-7), the neutron polarization p_n is given as

$$p_n = \sqrt{1-\left(\frac{T_n^{Unpol}}{T_n^{Pol}}\right)^2}. \qquad (3-2-8)$$

This formula is based on the incoherence of scattering. It is not valid for very slow neutrons since their wave length is longer than the distance between nuclei in the filter. The validity of this formula was confirmed within the accuracy of 3% relative to the neutron polarization for $E_n > 200meV$ [53,48] which covers the region of our interest.

The layout of the polarized proton filter is shown in Fig. 3-2-1. Superconducting coils and a ^3He cryostat were installed in the same liquid-helium container. The magnetic flux density at the center of the filter was $2.5T$ with homogeneity of 0.5×10^{-4} in a volume of $3cm$ diameter and $4cm$ height. The coils were designed to be asymmetric with respect to the medium plane so that no zero crossing point of magnetic field exists along the neutron-beam path. Therefore, the neutron spin is held in the same direction with respect to the field direction during passage. The ^3He cryostat was a continuous-flow type and was installed at the center of the liquid helium container. The ^3He gas was pumped out by a Roots pump system (Alcatel RSV2000 + RSV350 + 2060H). The temperature of liquid ^3He was less than $0.5K$. The polarized proton filter was placed in a copper box as shown in Fig. 3-2-2. The filter consisted of 5 layers of plates ($3.3\times2.4\times0.2cm^3$) with spacing of $0.2cm$. This box was cooled by liquid ^3He from outside through heat exchanging copper fins which were attached from inside and outside of the box. The box was filled with ^4He superfluid liquid which worked as a heat exchanger between the box and the filter layers. The neutron beam passed through these plates in their normal direction. Neutron absorption by the ^3He gas in the neutron flight path was negligible since the ^3He gas pressure was less than $0.16Torr$ and the length of the flight path was $4cm$.

Microwave of $70GHz$ was supplied to the filter through the wave guide. The microwave was obtained by using a klystron (OKI-KA701A). The microwave power was estimated to be about $35mW$ at the filter.

The filter material was cooked in chemical reaction. The $50cm^3$ ethylene-glycol was kept at the temperature of $70°C$. Powder of potassium dichromate ($K_2Cr_2O_7$) of $22g$ was added to it, and the mixture was stirred for $12min$ at $70°C$. Complexes of Cr^V were produced in the reaction. The Cr^V was used as free radicals for the dynamic polarization. The optimum density of Cr^V was approximately one per 200 hydrogens. The proton polarization of about 90% was obtained at $0.5K$. The neutron transmittance of the polarizer was measured by the liquid scintillator. A typical neutron polarization is shown in Fig. 3-2-3.

An NMR-coil was embedded in the filter material. The proton polarization in the filter was measured by the NMR system every minute. The fluctuation of the polarization was within a few percent for a few weeks.

The transversely polarized neutrons pass through an inhomogeneous magnetic field which is superposition of fringing field of superconducting coils and longitudinal field of the $150G$ solenoid placed downstream the polarizer. The depolarization due to the inhomogeneous magnetic field is discussed below.

We write the polar angle of magnetic field $\vec{H}$ with respect to the beam axis as θ_H. The θ_H is given as

$$\tan\theta_H = \frac{H_\perp}{H_{//}}, \qquad (3-2-9)$$

where $H_\perp$ ($H_{//}$) is perpendicular (parallel) component of ($\vec{H}$) with respect to the beam axis. If neutrons do not move in the magnetic field, their spins precess about the direction of $\vec{H}$ with a Larmor frequency

$$\omega_n = \gamma_n\sqrt{H_{//}^2 + H_\perp^2}, \qquad (3-2-10)$$

where γ_n is the gyromagnetic ratio of neutron. In this experiment, neutrons move along the beam axis. We denote the direction of neutron propagation as z-axis. On the rest frame of neutrons whose velocity is v_n, the magnetic field rotates with the angular velocity $\dot{\theta}_H$ which is given as

$$\begin{aligned}\dot{\theta}_H &= \frac{d\theta_H}{dt} \\ &= \frac{\frac{\partial H_\perp}{\partial z}H_{//} - \frac{\partial H_{//}}{\partial z}H_\perp}{H_\perp^2 + H_{//}^2}v_n. \end{aligned} \qquad (3-2-11)$$

In this case, neutron spins precess about the magnetic field $\vec{H}'$ given as

$$\vec{H}' = \vec{H} + \vec{H}_{rot}, \qquad (3-2-12)$$

where $\vec{H}_{rot}$ is a field perpendicular to $\vec{H}$. The absolute value of $\vec{H}_{rot}$ is given as

$$H_{rot} = \frac{\dot{\theta}_H}{\gamma_n}. \qquad (3-2-13)$$

Here we define η as

$$\tan\eta = \frac{H_{rot}}{H} = \frac{\dot{\theta}_H}{\omega_n}. \qquad (3-2-14)$$

The neutron polarization becomes $p_n\cos\eta$. The $\cos\eta$ is calculated from the actual field as shown in Fig. 3-2-4.

The adiabatic condition is

$$|\tan\eta| = \left|\frac{\dot{\theta}_H}{\omega_n}\right| \ll 1. \qquad (3-2-15)$$

The neutron polarization at the target point was calculated by a numerical simulation based on the Larmor precession of the classical magnetic moment. As a result, the depolarization due to the rotation of the magnetic field is calculated to be less than 1% for $E_n \leq 10eV$. (see Table 3-2-1)

$E_n[eV]$	positive helicity	negative helicity
1	0.998	0.996
10	0.990	0.991
100	0.995	0.989

Table 3-2-1. The results of numerical simulation of neutron polarization at the target divided by the original polarization (p_n). Small depolarizations are due to the rotation of the magnetic field direction.

§4 Experimental Procedure

In this section, the experimental procedures are described.

nucleus	material	thickness [cm]	areal density $[\times 10^{22} nuclei/cm^2]$	target temperature
^{81}Br	CBr_4	3.0	2.9	room temp.
	CBr_4	5.0	5.2	room temp.
^{93}Nb	metal	2.5	13.9	room temp.
^{108}Pd	metal	0.7	1.8	room temp.
^{111}Cd	metal	1.15	0.68	room temp.
^{124}Sn	metal	3.0	0.17	room temp.
^{139}La	metal	1.0	2.7	$35K$
	metal	0.3	0.8	$9K$

Table 4-1-1. List of target materials. The areal densities of relevant isotopes are shown.

§4-1 Measurement of Longitudinal Asymmetry

In this section, we describe the experimental procedure of the measurement of the longitudinal asymmetry ($A_{L,\gamma}$) with low γ-ray energy threshold in p-wave resonances for the targets of ^{81}Br, ^{93}Nb, ^{108}Pd, ^{111}Cd, ^{124}Sn and ^{139}La. Experimental arrangement and γ-ray counters are shown in Fig. 4-1-1 and Fig. 4-1-2 [47], respectively. Target disks of $2.5cm$ in diameter were placed at $6.6m$ from the neutron source in a $50G$ solenoid which holds the neutron spin direction, and were bombarded by longitudinally polarized neutrons. The targets with natural abundance were used. Experimental conditions are listed in Table 4-1-1.

The lanthanum targets were cooled down to $35K$ using a helium refrigerator, and to $9K$ using a liquid helium cryostat, to reduce the Doppler broadening of the resonances to $0.008eV$ and $0.004eV$, respectively. The energy spread due to Doppler broadening in room temperature is $0.023eV$ which is wider than the half width of the p-wave resonance of ^{139}La target at $E_n = 0.734eV$. Other targets were used in room temperature since the Doppler-broadenings are small enough compared with resonance widths.

The BaF_2 crystal was used as a γ-ray detector[54]. The BaF_2 crystal has various attractive properties. Its radiation length is short ($X_0 = 2.1cm$) and its density is high ($\rho = 4.88g/cm^3$). The light output of the crystal amounts to $\sim 1/5$ of that obtained with $NaI(Tl)$. The BaF_2 crystal has two light emission peaks at 220 and $310nm$ in wave length. The decay constants for the two components are 0.6 and $620ns$, respectively. Hamamatsu R329QTE photomultiplier with $CsTe$ photocathode was used to detect only the fast component of the scintillation light with good timing characteristics. A quartz-glass plate was used as a window for R329QTE so as to transmit the fast component

of the light which is in the ultra violet region. The energy threshold was set at about $1MeV$. The energy resolution was about 20% at $E_\gamma \sim 1MeV$.

Three γ-ray counters were arranged to detect γ-rays at $\bar{\theta}_\gamma = 55.5°$, 90° and 124.5°, where $\bar{\theta}_\gamma$ is the averaged value of θ_γ weighted by the absorption probability of γ-rays in BaF_2 crystals. In total, solid angle of $\theta_\gamma = 30° \sim 150°$ and $\phi_\gamma = 0° \sim 360°$ which is 85% of whole solid angle was covered. The thickness of the crystal in γ-ray emission direction was more than $6cm$.

A cylinder made of sintered B_4C was inserted inside the solenoid to absorb scattered neutrons from the target so that the scattered neutron does not produce capture γ-rays outside the target. The beam was collimated to a circle of $1.8cm$ in diameter. The scintillator and PMT sets were magnetically shielded. They were covered with lead and boric acid resin of $5cm$ thick to reduce room background γ-rays and neutrons, respectively. The B_4C filled the space between the counter box and the lead. The counter box was made of iron to shield the PMT's from external magnetic fields. A $2cm$ thick B_4C covered the surface of the counter box to absorb neutrons coming from the neutron source and other beam lines.

§4-2 Measurement of the Angular Distribution

The experimental procedure of the measurement of angular distribution of γ-rays from resonance for unpolarized incident neutrons ($\sigma_{res}^{Unpol}(\theta_\gamma)$) is discussed in this section.

The experimental arrangement is shown in Fig. 4-2-1. Unpolarized neutrons were obtained by removing the neutron polarizer from the beam line. The beam size was $1.8cm$ in diameter.

The $\sigma_{res}^{Unpol}(\theta_\gamma)$ was measured for p-wave resonances for the targets of ^{139}La and ^{81}Br and for an s-wave resonance of the target of ^{107}Ag. All the elements in the targets had natural abundance. The lanthanum target was a metal column of $2.5cm$ in diameter and $3.0cm$ in height. Carbon tetrabromide of the same size was used as the bromine target. The silver target was a thin self-supported foil of $50\mu m$ thick. The silver target was used to check the detection system since the s-wave resonance of the target of ^{107}Ag at $E_n = 16.30eV$ has a zero total angular momentum and must have a uniform angular distribution.

A bismuth germanate ($Bi_4Ge_3O_{12}$:BGO) crystal of $5cm\phi \times 5cm$ was used to detect γ-rays from the target with high detection efficiency. Its radiation length is very short ($X_0 = 1.1cm$) and its density is very high ($\rho = 7.1g/cm^3$). The detection efficiency

is more important than the timing characteristics since the solid angle covered by the crystal is small and the γ-ray counting rate is low. The BGO crystal has a light emission peak at $480nm$ in wave length and its decay constant is $300ns$. The scintillation light was detected by Hamamatsu H1161 photomultipliers. The detector set was magnetically shielded by iron. The $5cm$ thick lead shield was used to reduce the γ-ray background. The thickness of B_4C for neutron shield was more than $2cm$. The energy threshold was set to $1MeV$. The γ-ray intensity was measured at $\theta_\gamma = 35°$, $50°$, $70°$, $90°$, $110°$, $130°$ and $145°$. The angular acceptance was $\pm 4°$ in standard deviation.

§4-3 Measurement of E_γ Dependence of Longitudinal Asymmetry

The longitudinal asymmetry for the target of ^{139}La was measured as a function of $E_{\gamma,thres}$, where $E_{\gamma,thres}$ is the threshold of γ-ray energy †. The schematic view of the BGO counter is shown in Fig. 4-3-1. The target disk of $2.3cm$ in diameter and $3.0cm$ in thickness was placed at $6.75m$ from the neutron source in a $50G$ solenoid which holds the neutron spin to longitudinal direction. The target was put in room temperature. The beam was collimated to a circle of $2.0cm$ in diameter.

The γ-ray counter was designed for observation of the p-wave resonance of the target of ^{139}La with a better absorption efficiency and a better energy resolution than the BaF_2 counter described in §4-1. Bismuth germanate (BGO) crystal was used in this measurement to provide better absorption efficiency for γ-rays compared with BaF_2 crystals of the same dimension. The dimension of the whole counter is important to obtain better γ-ray counting efficiency for true signal than that for room background, since the counting rate for room background is proportional to the dimension of the counter. The thickness of BGO crystal in the γ-ray emission direction was more than $6cm$.

A typical pulse height spectrum for γ-rays from $^{12}C^*(4.43MeV)$ of Am/Be radioactive source obtained using this counter is shown in Fig. 4-3-2. The energy resolution for 4.43-MeV γ-rays was 13%. The pulse height spectrum for γ-rays from $La(n,\gamma)$ ($E_n = 0.46 \sim 1.4eV$) obtained using the same counter is shown in Fig. 4-3-3. Bumps are observed around 4.3 and $5MeV$. The arrows in the figure indicate the energies where single γ-ray transitions are expected. The expected single γ-ray transitions are listed in Table 4-3-1[55,56]. The $E_{\gamma,thres}$'s were set to 1.1 ± 0.1, 3.2 ± 0.2, 4.2 ± 0.2 and 4.8 ± 0.3 [MeV] †.

† The $E_{\gamma,thres}$ is defined as the output pulse height of PMT which is not equivalent to γ-ray energy (E_γ) because of the contribution of compton scattering, single escape and double escape peaks.

E_γ [MeV]	spin/parity of final state
5.101 ± 0.005	4^-
4.845 ± 0.005	5^-
4.416 ± 0.005	$4, 5^-$
4.390 ± 0.005	$4, 5^-$

Table 4-3-1 The list of spin/parity of final state of relatively intense γ-ray transitions of $^{139}La(n,\gamma)^{140}La$ reported in $Ref.55,56$. The spin/parity of the ground state of ^{140}La is $J^\pi = 3^-$.

Two γ-ray counters were arranged to detect the γ-rays for $\theta_\gamma = 20° \sim 70°, \phi_\gamma = 0° \sim 360°$ and $110° \sim 160°, \phi_\gamma = 0° \sim 360°$. In total, about 60% of whole solid angle is covered. A cylinder of 0.8cm thick made of sintered B_4C was inserted inside the solenoid to absorb scattered neutrons from the target. The PMT's were magnetically shielded by iron boxes. Lead walls of $5cm$ thick covered the iron boxes to reduce background γ-rays coming from outside. B_4C walls of $2cm$ thick covered the lead walls to absorb background neutrons coming from outside.

The sensitivity of the counter for the term of $\cos^2\theta_\gamma - 1/3$ is important for the determination of the value of $A_{L,\gamma}$ using Eq. (2-9). It was calculated as

$$\frac{\int_{\Omega_{det}} e^{-\ell(\Omega)/\lambda_{BGO}}(\cos^2\theta - \frac{1}{3})d\Omega}{\int_{\Omega_{det}} e^{-\ell(\Omega)/\lambda_{BGO}}d\Omega}. \qquad (4-3-1)$$

The Ω_{det} is the solid angle covered by scintillators. The $\ell(\Omega)$ is the length of BGO crystal for the direction of Ω. The λ_{BGO} is the mean free path of γ-rays in BGO crystal. The sensitivity depends on γ-ray energy since the λ_{BGO} depends on γ-ray energy. The value of (4-3-1) was calculated by averaging in the region of γ-ray energy of ~ 1 to $\sim 5MeV$. Finally, the value of (4-3-1) is calculated to be 0.04.

§5 Data Analysis and Results

In this section, the method of data analysis and the experimental results are described.

† The Q-value of $^{139}La + n \rightarrow ^{140}La$ is $5.2MeV$.

§5-1 Longitudinal Asymmetry

The longitudinal asymmetries ($A_{L,\gamma}$) and their θ_γ dependences ($a_{L,\gamma}(\theta_\gamma)$, Eq. (2-6)) have been measured with low γ-ray energy thresholds using the γ-ray counter described in §4-1. The γ-rays consisted of three components which have different origins. One of them was the γ-ray coming from the resonance cross section (σ_{res}). The second one was the γ-ray coming from the continuum cross section (σ_{con}). There were also γ-rays which did not come from the target. The component of γ-rays coming from the σ_{res} was obtained after subtracting the contribution of σ_{con} and that of room background γ-rays. The contribution of σ_{con} has been evaluated by least χ^2 fitting with a linear function of $1/v_n$ † where v_n is the velocity of incident neutron. The γ-ray counting rates are plotted in Fig. 5-1-1 for the targets of lanthanum, carbon tetrabromide, cadmium, tin, niobium and palladium. In the case of cadmium target, the σ_{con} has a nonlinear $1/v_n$ dependence because a large s-wave resonance of the target of ^{113}Cd exists close to the plotted region (at $E_n = 0.178eV$). A 3rd order polynomial of $1/v_n$ has been used for the evaluation of σ_{con}, since it is the lowest order polynomial to reproduce the shape of σ_{con}.

We write the γ-ray counting rates of whole BaF_2 counters after subtracting the component of room background γ-rays for incident positive- (negative-) helicity neutrons as n_γ^+ (n_γ^-). The $n_\gamma^\pm$ consists of the contribution of σ_{res} and that of σ_{con}. The $\epsilon_{L,\gamma}^{tot}$ is plotted in Fig. 5-1-2 where

$$\epsilon_{L,\gamma}^{tot} = \frac{n_\gamma^+ - n_\gamma^-}{n_\gamma^+ + n_\gamma^-}. \qquad (5-1-1)$$

The $\epsilon_{L,\gamma}^{tot}$'s deviate from zero systematically at p-wave resonances of the targets of $^{139}La(E_n = 0.734eV)$, $^{81}Br(E_n = 0.88eV)$ and $^{111}Cd(E_n = 4.53eV)$ while no significant deviation has been found at p-wave resonances of the targets of $^{93}Nb(E_n = 35.9eV)$, $^{93}Nb(E_n = 42.3eV)$, $^{108}Pd(E_n = 2.96eV)$ and $^{124}Sn(E_n = 62.0eV)$.

We write the component of γ-ray counting rates of whole BaF_2 counters which come from σ_{res} for incident positive- (negative-) helicity neutrons as n_γ^{r+} (n_γ^{r-}). The $n_\gamma^{r\pm}$ can be written as

$$\begin{cases} n_\gamma^{r+} = C\Omega\eta^+(1 + p_n A_{L,\gamma}^{UC}), \\ n_\gamma^{r-} = C\Omega\eta^-(1 - p_n A_{L,\gamma}^{UC}). \end{cases} \qquad (5-1-2)$$

The C is a common constant to $n_\gamma^{r\pm}$. The Ω is the geometrical acceptance of the counter. The p_n is the incident neutron polarization. The $A_{L,\gamma}$ with superscript "UC" is different from the "true" $A_{L,\gamma}$ due to the multiple scattering effect discussed in the latter part of this section. The η^+ and η^- are the counter efficiencies. The superscripts $\pm$ represent the magnetic field direction of the solenoid. A small difference of photomultiplier gain ($< 10^{-3}$) was found for two magnetic field directions.

The small difference between η^+ and η^- was cancelled by the following procedure. The proton polarization can be reversed by changing the microwave frequency in the same magnetic field (Appendix B). We write the counting rate of γ-rays with the "reversed-polarizer" for incident positive- (negative-) helicity neutrons as $\bar{n}_\gamma^{r+}$ ($\bar{n}_\gamma^{r-}$). The relation between neutron helicity and magnetic field is reversed in the measurement with the "reversed-polarizer". The $\bar{n}_\gamma^{r\pm}$ are given as

$$\begin{cases} \bar{n}_\gamma^{r+} = C\Omega\eta^-(1 + \bar{p}_n A_{L,\gamma}^{UC}), \\ \bar{n}_\gamma^{r-} = C\Omega\eta^+(1 - \bar{p}_n A_{L,\gamma}^{UC}). \end{cases} \qquad (5-1-3)$$

The $\bar{p}_n$ is the incident neutron polarization with the "reversed-polarizer". Here we write n_1 and n_2 as

$$\begin{cases} n_1 = n_\gamma^{r+}\bar{n}_\gamma^{r+}, \\ n_2 = n_\gamma^{r-}\bar{n}_\gamma^{r-}. \end{cases} \qquad (5-1-4)$$

If we define $\epsilon_{L,\gamma}$ as,

$$\epsilon_{L,\gamma} = \frac{n_1 - n_2}{n_1 + n_2}, \qquad (5-1-5)$$

the $\eta^\pm$ are cancelled in the $\epsilon_{L,\gamma}$. The longitudinal asymmetry can be written using $\epsilon_{L,\gamma}$ as

$$A_{L,\gamma}^{UC} = \frac{\epsilon_{L,\gamma}}{\langle p_n \rangle} \frac{1}{1 + \sqrt{1 + \left(\frac{\epsilon_{L,\gamma}}{\langle p_n \rangle}\right)^2 p_n \bar{p}_n}}, \qquad (5-1-6)$$

where $\langle p_n \rangle = (p_n + \bar{p}_n)/2$.

The longitudinal asymmetry obtained by Eq. (5-1-6) contains a multiple scattering effect which comes from the finite thickness of the target. Some of incident neutrons change their helicity states by elastic scattering, since the neutron momentum is changed in elastic scattering but neutron spin direction is not changed †. The neutron helicity is lost almost completely on scattering since the angular distribution of elastic scattering is uniform for low energy incident neutrons. If the scattered neutron is captured by another nucleus, it decreases the helicity dependence of the γ-ray counting rate. We

† The capture cross section obeys the $1/v_n$ rule at zero-energy limit if no large resonance exists.

† The neutron spin is reversed by the incoherent scattering cross section. It becomes important in the measurement of forward-backward asymmetry (see §5-3).

write the number of captured neutrons due to the resonance cross section for incident positive- (negative-) helicity neutrons as N^+ (N^-). The N^+ (N^-) can be written as the sum of N_i^+ (N_i^-) which represents the number of neutrons which are captured due to the resonance cross section after being scattered elastically for i-times.

$$N^{\pm} = \sum_{i=0}^{\infty} N_i^{\pm} \qquad (5-1-7)$$

The $N_i^{\pm}$'s were calculated as functions of $A_{L,\gamma}$ by a numerical simulation (Appendix D). If we define the "calculated" asymmetry as

$$\epsilon_{L,\gamma}^{cal} = \frac{N^+ - N^-}{N^+ + N^-}, \qquad (5-1-8)$$

the "calculated" longitudinal asymmetry is given as

$$A_{L,\gamma}^{cal} = \frac{\epsilon_{L,\gamma}^{cal}}{p_n}. \qquad (5-1-9)$$

The $A_{L,\gamma}$ was determined so that $A_{L,\gamma}^{cal}$ reproduces $A_{L,\gamma}^{UC}$.

The E_n dependence of $\epsilon_{L,\gamma}$ for ^{139}La target is shown in Fig. 5-1-3 together with that of $\epsilon_{L,\gamma}^{cal}$. The target was a $1.0cm$-thick lanthanum metal disk of $2.5cm$ in diameter which was cooled down to $35K$. The E_n dependence of $\epsilon_{L,\gamma}$ is well reproduced by the numerical simulation described above, assuming that the $A_{L,\gamma}$ is independent of E_n. The E_n dependence of $\epsilon_{L,\gamma}$ for the lanthanum target which was cooled down to $9K$ is shown in Fig. 5-1-4. No significant E_n dependence of $A_{L,\gamma}$ has been observed in either case.

The obtained results of $A_{L,\gamma}$ are listed in Table 5-1-1. The error of neutron polarization (p_n) is mainly due to the uncertainty in determination of p_n using Eq. (3-2-8). The statistical error of p_n is negligible (less than 0.1%). The error of $A_{L,\gamma}^{UC}$ consists of statistical error and the error of p_n. Its main component is statistical error except for the case of ^{139}La. The error of $A_{L,\gamma}$ contains the uncertainty of correction of multiple scattering effect (Eq. (5-1-9)) which is smaller than the statistical error and the error of p_n. The asymmetries of continuum cross section with respect to the helicity of incident neutrons ($A_{L,\gamma}^{con}$) are also listed. In all cases, the $A_{L,\gamma}^{con}$'s are zero within experimental errors. The value of $A_{L,\gamma} = 0.0 \pm 0.1\%$ has been obtained for the s-wave resonance of the target of ^{138}La at $E_n = 2.99eV$.

We write the γ-ray counting rate for incident positive- (negative-) helicity neutrons measured at a specific polar angle θ_γ after subtracting the component of room background γ-rays as $n_\gamma^+(\theta_\gamma)$ ($n_\gamma^-(\theta_\gamma)$). Corresponding to Eq. (5-1-1), we write the $\epsilon_{L,\gamma}^{tot}(\theta_\gamma)$

target nucleus	E_n [eV]	p_n [%]	$A_{L,\gamma}^{UC}$ [%]	$A_{L,\gamma}$ [%]		$A_{L,\gamma}^{con}$ [%]
^{81}Br	0.88	69 ± 2	1.8 ± 0.2	2.1 ± 0.2	3cm thick	-0.05 ± 0.04
		69 ± 2	1.7 ± 0.1	2.1 ± 0.2	5cm thick	0.04 ± 0.03
				2.1 ± 0.1	average	0.02 ± 0.02
^{93}Nb	35.9	46 ± 1	0.2 ± 0.2	0.3 ± 0.5		-0.05 ± 0.05
	42.3	45 ± 1	-0.0 ± 0.3	-0.0 ± 0.6		-0.05 ± 0.05
^{108}Pd	2.96	61 ± 2	0.1 ± 0.1	0.2 ± 0.2		-0.08 ± 0.10
^{111}Cd	4.53	63 ± 2	$-(1.1^{+0.5}_{-0.3})$	$-(1.3^{+0.7}_{-0.4})$		-0.07 ± 0.05
^{124}Sn	62	47 ± 1	0.1 ± 0.2	0.2 ± 0.4		-0.13 ± 0.23
^{139}La	0.734	67 ± 2	8.1 ± 0.2	9.8 ± 0.3		0.02 ± 0.04

Table 5-1-1. The experimental values of $A_{L,\gamma}$ for the p-wave resonances of several target nuclei. The $A_{L,\gamma}^{UC}$ is uncorrected value of $A_{L,\gamma}$. The $A_{L,\gamma}^{con}$ is the asymmetry of continuum cross section with respect to the helicity of incident neutrons.

as

$$\epsilon_{L,\gamma}^{tot}(\theta_\gamma) = \frac{n_\gamma^+(\theta_\gamma) - n_\gamma^-(\theta_\gamma)}{n_\gamma^+(\theta_\gamma) + n_\gamma^-(\theta_\gamma)}. \qquad (5-1-10)$$

The $a_{L,\gamma}(\theta_\gamma)$ was determined in the same way as $A_{L,\gamma}$ by replacing γ-ray counting rates of whole BaF_2 counters which come from the σ_{res} ($n_\gamma^{r\pm}$ and $\bar{n}_\gamma^{r\pm}$) with those measured at a specific polar angle θ_γ ($n_\gamma^{r\pm}(\theta_\gamma)$ and $\bar{n}_\gamma^{r\pm}(\theta_\gamma)$). In Fig. 5-1-5, the $\epsilon_{L,\gamma}^{tot}(\theta_\gamma)$'s are plotted in the vicinity of the p-wave resonance of ^{139}La target at three θ_γ's. No significant difference has been found among them. The $a_{L,\gamma}(\theta_\gamma)$'s are plotted in Fig. 5-1-6 for the targets of ^{139}La, ^{81}Br and ^{111}Cd. In all cases, the $a_{L,\gamma}(\theta_\gamma)$ has been found to be independent of θ_γ within experimental errors.

§5-2 Angular Distribution

The angular distribution of γ-rays induced by unpolarized neutrons ($\sigma_{res}^{Unpol}(\theta_\gamma)$, Eq. (2-11)) has been measured using the γ-ray counter described in §4-2. The angular distribution of the γ-ray counting rate contains several effects due to the finite thickness of the target.

1) The attenuation of the γ-ray between the reaction point and the counter.
2) The inhomogeneous distribution of the reaction point due to the neutron attenuation in the target.
3) Capture of scattered neutrons by another nucleus.

These effects can be calculated from the geometry of the target and the mean free path of γ-rays in the target (λ_{tgt}). The analysis has been carried out with several values of λ_{tgt} to evaluate the effect of E_γ dependence of the λ_{tgt}. The uncertainty in determination of A_1 and A_3 due to the E_γ dependence of λ_{tgt} was added to experimental errors. Its size is comparable with the size of statistical error.

The results of the measurement of $\sigma_{res}^{Unpol}(\theta_\gamma)$ are plotted in Fig. 5-2-1. The solid lines in the figure are the best fit curves obtained with Eq. (2-11). The numerical data after corrections are listed in Table 5-2-1. The angular distribution of the s-wave resonance of the target of ^{107}Ag at $E_n = 16.30eV$ has been measured as a calibration since it must be uniform. The observed angular distributions are uniform for p-wave resonances of the targets of ^{139}La and ^{81}Br within experimental errors. All correlation coefficients have been obtained as listed in Table 5-2-2 for the targets of ^{139}La and ^{81}Br, from the results of $a_{L,\gamma}(\theta_\gamma)$ and $\sigma_{res}^{Unpol}(\theta_\gamma)$.

target nucleus	$E_n[eV]$	$A_1[\%]$	$A_3[\%]$
^{139}La	0.734	-1.3 ± 3.1	2.1 ± 2.3
^{81}Br	0.88	-1.7 ± 2.7	3.0 ± 4.1
^{107}Ag	16.30	-0.7 ± 2.0	-0.9 ± 2.0

Table 5-2-1 The experimental values of A_1 and A_3. The energy threshold for γ-ray energy was set to $\sim 1MeV$.

target nucleus	E_n [eV]	A_1 [%]	A_3 [%]	A_{10} [%]	$A_9 + \frac{2}{3}A_{12}$ [%]	A_{11} [%]
^{139}La	0.734	-1.3 ± 3.0	2.1 ± 2.4	10.1 ± 0.7	0.1 ± 1.2	2.9 ± 3.8
^{81}Br	0.88	-1.7 ± 3.0	2.8 ± 4.2	2.2 ± 0.7	-0.5 ± 1.2	0.1 ± 3.8

Table 5-2-2 The experimental values of A_i's. The energy threshold for γ-ray energy was set to $\sim 1MeV$.

§5-3 The E_γ Dependence of Longitudinal Asymmetry

The longitudinal asymmetry for the p-wave resonance of the target of ^{139}La at $E_n = 0.734eV$ has been measured with different γ-ray energy thresholds using the γ-ray counter described in §4-3.

The γ-ray counting rates versus incident neutron energy are plotted in Fig. 5-3-1 for the p-wave resonance of the target of ^{139}La with different γ-ray energy thresholds ($E_{\gamma,thres}$). The p-wave resonance has been clearly observed in each $E_{\gamma,thres}$. The $A_{L,\gamma}$ was evaluated following the Eq. (2-9). The $A_{L,\gamma}$'s for several γ-ray energy thresholds are listed in Table 5-3-1 and plotted in Fig. 5-3-2. The error of $E_{\gamma,thres}$ is the accuracy of threshold adjustment and gain adjustment of photomultiplier and amplifier for all BGO counters. The error of neutron polarization (p_n) is mainly due to the uncertainty in determination of p_n using Eq. (3-2-8). Statistical error of p_n is negligible. The error of $A_{L,\gamma}^{UC}$ consists of statistical error and the error of p_n. Its main component is the error of p_n for the cases of $E_{\gamma,thres} = 1.1$ and $3.2MeV$, and is statistical error for the cases of $E_{\gamma,thres} = 4.2$ and $4.8MeV$. The asymmetries of the continuum cross section with respect to the helicity of incident neutrons ($A_{L,\gamma}^{con}$) are also listed in Table 5-3-1 and found to be zero within experimental errors. The $A_{L,\gamma}$ is independent of $E_{\gamma,thres}$ within experimental errors. The longitudinal asymmetry for the s-wave resonance of the target of ^{138}La at $E_n = 2.99eV$ have been found to be less than 0.3%.

The forward-backward asymmetry (a_γ) given by Eq. (1-7) has been measured. The γ-rays were detected at two angles (θ_γ and $\pi - \theta_\gamma$). Following notations in §5-1, the γ-ray counting rates are given as

$$\begin{cases} n_\gamma^{r+}(\theta_\gamma) = C\Omega_F\eta^+(1 + p_n A_{L,\gamma}^{UC})(1 + p_n a_\gamma^{UC}\cos\theta_\gamma), \\ n_\gamma^{r+}(\pi - \theta_\gamma) = C\Omega_B\eta^+(1 + p_n A_{L,\gamma}^{UC})(1 - p_n a_\gamma^{UC}\cos\theta_\gamma), \\ n_\gamma^{r-}(\theta_\gamma) = C\Omega_F\eta^-(1 - p_n A_{L,\gamma}^{UC})(1 + p_n a_\gamma^{UC}\cos\theta_\gamma), \\ n_\gamma^{r-}(\pi - \theta_\gamma) = C\Omega_B\eta^-(1 - p_n A_{L,\gamma}^{UC})(1 - p_n a_\gamma^{UC}\cos\theta_\gamma), \end{cases} \quad (5-3-1)$$

$E_{\gamma,thres}$ $[MeV]$	p_n [%]	$A^{UC}_{L,\gamma}$ [%]	$A_{L,\gamma}$ [%]	$A^{con}_{L,\gamma}$ [%]
1.1 ± 0.1	63 ± 2	7.2 ± 0.2	9.4 ± 0.3	-0.02 ± 0.03
3.2 ± 0.2	65 ± 2	7.1 ± 0.2	9.3 ± 0.2	0.04 ± 0.04
4.2 ± 0.2	65 ± 2	7.7 ± 0.5	9.9 ± 0.7	-0.04 ± 0.07
4.8 ± 0.3	67 ± 2	7.3 ± 1.4	9.5 ± 1.9	0.22 ± 0.18

Table 5-3-1. The experimental values of $A_{L,\gamma}$ for the p-wave resonance of the target of ^{139}La at $E_n = 0.734eV$ obtained with several γ-ray threshold energies ($E_{\gamma,thres}$). The $A^{UC}_{L,\gamma}$ is uncorrected value of $A_{L,\gamma}$. The $A^{con}_{L,\gamma}$ is the asymmetry of continuum cross section with respect to the helicity of incident neutrons.

where Ω_F and Ω_B are the geometrical acceptances of the counters at θ_γ and $\pi - \theta_\gamma$, respectively. The a_γ with superscript "UC" is different from the "true" a_γ due to multiple scattering effect discussed in the latter part of this section. If we define n_F and n_B as

$$\begin{cases} n_F = n^{r+}_\gamma(\theta_\gamma) n^{r-}_\gamma(\pi - \theta_\gamma), \\ n_B = n^{r+}_\gamma(\pi - \theta_\gamma) n^{r-}_\gamma(\theta_\gamma), \end{cases} \qquad (5-3-2)$$

the $\Omega_{F(B)}$ and $\eta^\pm$ † are cancelled in the quantity ϵ_γ given as

$$\epsilon_\gamma = \frac{n_F - n_B}{n_F + n_B}. \qquad (5-3-3)$$

The a^{UC}_γ is obtained from ϵ_γ as

$$a^{UC}_\gamma = \frac{\epsilon_\gamma}{p_n \cos\theta_\gamma} \frac{1}{1 + \sqrt{1 - \epsilon^2_\gamma}}. \qquad (5-3-4)$$

The neutron polarization becomes $(1 - 4R_{incoh}/3)$ times of original polarization due to the incoherent scattering cross section on every elastic scattering[57], where $R_{incoh} = \sigma_{incoh}/(\sigma_{incoh} + \sigma_{coh})$. The σ_{coh} and σ_{incoh} are coherent- and incoherent-scattering cross sections, respectively. Therefore, the polarization of incident neutrons becomes p'_n effectively where p'_n is given as

$$p'_n = p_n \frac{\sum_i N_i (1 - \frac{3}{4} R_{inc})^i}{\sum_i N_i}, \qquad (5-3-5)$$

† We assumed $\eta^\pm_F = \eta^\pm_B$ for simplicity. The behaviors of $\eta^\pm_F$ and $\eta^\pm_B$ were confirmed to be same within experimental errors where $\eta^\pm_{F(B)}$ represent the $\eta^\pm$ of the two counters. In actual case, we cancelled the $\eta^\pm_F$ and $\eta^\pm_B$ using the results of the "reversed-polarizer" measurement (see §5-1).

where $N_i = (N^+_i + N^-_i)/2$. The $N^\pm_i$ is given in Eq. (5-1-7). The a_γ is evaluated from the following relation.

$$p_n a^{UC}_\gamma = p'_n a_\gamma \qquad (5-3-6)$$

The obtained results of $a_{\gamma,<}$, $a_{\gamma,>}$, $a_{\gamma,<>}$ and $\langle a_\gamma \rangle$ (see §2) are listed in Table 5-3-2 for the cases of $E_{\gamma,thres} = 1.1 \pm 0.1MeV$ and $4.8 \pm 0.3MeV$. The main component of the error is statistical error. In all cases, the forward-backward asymmetry of continuum cross section has been found to be less than 0.3%. The $\langle a_\gamma \rangle$'s for the s-wave resonance of the target of ^{138}La at $E_n = 2.99eV$ have been observed to be less than 0.2%.

$E_{\gamma,thres}$ $[MeV]$	$a_{\gamma,<}$ [%]	$a_{\gamma,>}$ [%]	$a_{\gamma,<>}$ [%]	$\langle a_\gamma \rangle$ [%]
1.1 ± 0.1	-0.1 ± 0.4	-0.2 ± 0.3	-0.2 ± 0.2	0.1 ± 0.3
4.8 ± 0.3	3.3 ± 1.4	-6.1 ± 4.0	-1.8 ± 2.7	4.7 ± 2.1

Table 5-3-2. The experimental values of the forward-backward asymmetry for the p-wave resonance of the target of ^{139}La at $E_n = 0.734eV$ obtained with low and high γ-ray threshold energies.

§6 Theoretical Interpretation

In this section, the mechanism which is responsible for a large PNC effect in n-A interaction is discussed in the context of s-p mixing, since it is natural to assume that all processes in this energy region can be described by the contributions of s- and p-wave components of incident neutron †. It is assumed below that only an s-wave resonance and a p-wave resonance exist in the energy region of our interest.

Total Hamiltonian of a compound nucleus consists of PC part (H_{PC}) and PNC part (H_{PNC}). The s- and p-wave compound states represented by $|s\rangle$ and $|p\rangle$, respectively, are mixed up by a small non-orthogonal component H_{PNC}. The mixed states $|s'\rangle$ and $|p'\rangle$ are given by

$$\begin{cases} |s'\rangle = |s\rangle - \dfrac{\langle s|H_{PNC}|p\rangle}{E_p - E_s}|p\rangle, \\ |p'\rangle = |p\rangle + \dfrac{\langle s|H_{PNC}|p\rangle}{E_p - E_s}|s\rangle, \end{cases} \qquad (6-1)$$

in the first order perturbation, where E_s and E_p are incident neutron energies at s- and p-wave resonance centers, respectively.

† Another approach based on p-d mixing is also argued to explain the large PNC effects[23,24].

The value of $A_{10}(A_L)$ in the p-wave resonance is given as [22,39],

$$A_{10} \sim -\frac{2W}{E_p - E_s}\sqrt{\frac{\Gamma_s^n}{\Gamma_p^n}}\eta_{p\frac{1}{2}}\sqrt{\frac{\Gamma_{p\frac{1}{2}}^n}{\Gamma_p^n}}, \qquad (6-2)$$

where $W = i\langle s|H_{PNC}|p\rangle$, and Γ_s^n and Γ_p^n are neutron widths of s-wave and p-wave resonances, respectively. The $\Gamma_{p\frac{1}{2}}^n$ is the partial neutron width of p-wave resonance of $j = 1/2$, where j is the total angular momentum of incident neutron. The $\eta_{p\frac{1}{2}}$ is the sign factor of the reduced T-matrix element (see Eq. (A-5) in Appendix A). Two kinds of mechanisms are responsible for the large PNC effect. One is "dynamical enhancement" $(W/(E_p - E_s))$, and the other is "structural enhancement" $(\sqrt{\Gamma_s^n/\Gamma_p^n})$. The factor $\sqrt{\Gamma_{p\frac{1}{2}}^n/\Gamma_p^n}$ is not responsible for the large PNC effect.

The "dynamical enhancement" arises from a statistical nature of compound state. A typical time scale of a capture reaction through a compound state is $\hbar/\Gamma \sim 10^{-14}s$ for $\Gamma \sim 0.1eV$, while that of direct process is given by the time in which a neutron passes through a nucleus, that is, $2R/v_n \sim 10^{-18}s$ for $E_n \sim 1eV$, where $R \sim 10fm$ is a typical nuclear radius. The nucleons have much longer time to interact with each other in the compound state than in the direct process. Small PNC effects of N-N interaction are accumulated during the long life time as discussed below[22]. The s- and p-wave compound states ($|s\rangle$ and $|p\rangle$) can be expanded by a number of single particle-hole states in nuclear shell model as

$$|s\rangle = \sum_i^N a_i|\phi_i\rangle, \qquad |p\rangle = \sum_i^N b_i|\phi_i'\rangle. \qquad (6-3)$$

The magnitudes of the coefficients a_i and b_j are the order of $1/\sqrt{N}$ because of the normalization conditions of $|s\rangle$ and $|p\rangle$. If we write the scale of excitation energy of single particle-hole states and the average level spacing of compound states as ΔE and D, respectively, the number N is given as

$$N \sim \frac{\Delta E}{D}. \qquad (6-4)$$

If we use typical values of $\Delta E \sim 10^6 eV$ and $D \sim 10eV$, we obtain $N \sim 10^5$. The magnitude of PNC matrix element W in compound state is expressed as

$$|W| = |\langle s|H_{PNC}|p\rangle| = \left|\langle\sum_i a_i\phi_i|H_{PNC}|\sum_j b_j\phi_j'\rangle\right|$$
$$= \left|\sum_{i,j} a_i^* b_j\langle\phi_i|H_{PNC}|\phi_j'\rangle\right|. \qquad (6-5)$$

It is natural to assume the signs of a_i and b_j appear at random. Therefore, the $|W|$ is given as

$$|W| \sim \frac{|\langle H_{PNC}\rangle|}{N} \times \sqrt{N}, \qquad (6-6)$$

and it leads to

$$\left|\frac{W}{E_p - E_s}\right| \sim \frac{|W|}{D} \sim \frac{|\langle H_{PNC}\rangle|}{\sqrt{N}}\frac{1}{\frac{\Delta E}{N}} = \frac{|\langle H_{PNC}\rangle|}{\Delta E}\sqrt{N}, \qquad (6-7)$$

where the $\langle H_{PNC}\rangle$ is the average value of the $\langle\phi_i|H_{PNC}|\phi_i'\rangle$. The factor $|\langle H_{PNC}\rangle/\Delta E|$ is a typical size of parity mixing in single particle states which is the same order as that of N-N interaction (α_{NN}). The small PNC effect in N-N interaction is accumulated up to $\sqrt{N} = 10^2 \sim 10^3$ times.

The "structural enhancement" arises from the difference of the centrifugal potential barrier between s- and p-wave incident neutrons. The s- and p-wave neutron widths (Γ_s^n and Γ_p^n) are

$$\begin{cases} \Gamma_s^n \propto k_n R, \\ \Gamma_p^n \propto (k_n R)^3, \end{cases} \qquad (6-8)$$

and the structural enhancement factor is given as

$$\sqrt{\frac{\Gamma_s^n}{\Gamma_p^n}} \sim \frac{1}{k_n R}. \qquad (6-9)$$

In the energy region of $1eV$, the neutron momentum k_n is $\sim 2 \times 10^{-4} fm^{-1}$. If we use a typical value of $R \sim 10fm$, we obtain $\sqrt{\Gamma_s^n/\Gamma_p^n} \sim 10^3$.

From these two mechanisms, the PNC effect in s-p mixing becomes $10^5 \sim 10^6$ times larger than in N-N interaction.

Here we discuss the remained factor $\sqrt{\Gamma_{p\frac{1}{2}}^n/\Gamma_p^n}$. The total angular momentum of compound state $\vec{J}$ is the sum of the target nucleus spin $\vec{I}$, the neutron spin $\vec{s}$ $(s = \frac{1}{2})$ and the orbital angular momentum $\vec{l}$ $(l = 0$ or $1)$.

$$\vec{J} = \vec{I} + \vec{s} + \vec{l} \qquad (6-10)$$

We sum these three vectors in the following order.

$$\vec{J} = \vec{I} + \vec{j}, \qquad \vec{j} = \vec{s} + \vec{l} \qquad (6-11)$$

The vector $\vec{j}$ is the total angular momentum of the incident neutron. The absolute value of j is given as

$$j = \frac{1}{2} \qquad \text{for s-wave,}$$
$$j = \frac{1}{2} \text{ or } \frac{3}{2} \qquad \text{for p-wave.}$$

For simplicity, let us consider the case of $I = 0$. In this case, $\vec{J}$ is identical with $\vec{j}$, and J is given as

$$J = j = \frac{1}{2} \qquad \text{for s-wave,}$$
$$J = j = \frac{1}{2} \text{ or } \frac{3}{2} \qquad \text{for p-wave.}$$

The $j = 3/2$ component of p-wave does not interfere with s-wave component, since its total angular momentum is different from that of s-wave component. It can be generalized to the case of $I \neq 0$ and the factor $\sqrt{\Gamma^n_{p\frac{1}{2}}/\Gamma^n_p}$ gives the interfering part out of all p-wave contribution. We define x and y as

$$x = \eta_{p\frac{1}{2}}\sqrt{\frac{\Gamma^n_{p\frac{1}{2}}}{\Gamma^n_p}}, \quad y = \eta_{p\frac{3}{2}}\sqrt{\frac{\Gamma^n_{p\frac{3}{2}}}{\Gamma^n_p}}, \qquad (6-12)$$

where $\Gamma^n_p = \Gamma^n_{p\frac{1}{2}} + \Gamma^n_{p\frac{3}{2}}$. The η_{pj}'s are sign factors (see Eq. (A-5) in Appendix A). The absolute value of x cannot exceed unity because of the relation of $x^2 + y^2 = 1$. The x does not contribute to enlarge the PNC effect.

Explicit expressions of other correlation coefficients in the vicinity of the p-wave resonance for a single γ-ray transition are discussed below (see *Ref.*39 and Appendix A). Intrinsic parities of the compound state and the final state are assumed to be the same. The dominant parity-favored transition is M1 transition while the dominant parity unfavored one is E1. The A_i's defined in §2 are given as

$$A_1 \sim \eta_\gamma \frac{1}{(E_p - E_s)}\sqrt{\frac{\Gamma^n_s}{\Gamma^n_p}\frac{\Gamma_{M1}}{\Gamma_{E1}}}(E_n - E_p)\sum_j \xi_j P(J_s J_p \tfrac{1}{2} j 1 I F), \qquad (6-13a)$$

$$A_3 = 3\sqrt{10}\sum_{jj'} \xi_j \xi_{j'} P(J_p J_p j j' 2 I F) \begin{Bmatrix} 2 & 1 & 1 \\ 0 & \frac{1}{2} & \frac{1}{2} \\ 2 & j & j' \end{Bmatrix}, \qquad (6-13b)$$

$$A_9 \sim -2\eta_\gamma \frac{W}{(E_p - E_s)^2}\frac{\Gamma^n_s}{\Gamma^n_p}\sqrt{\frac{\Gamma_{M1}}{\Gamma_{E1}}}(E_n - E_p)P(J_s J_s \tfrac{1}{2}\tfrac{1}{2} 1 I F), \qquad (6-13c)$$

$$A_{11} \sim \sqrt{3} y \frac{W}{E_p - E_s}\sqrt{\frac{\Gamma^n_s}{\Gamma^n_p}} P(J_s J_p \tfrac{1}{2}\tfrac{3}{2} 2 I F), \qquad (6-13d)$$

$$A_{12} \sim -36\eta_\gamma \frac{W}{E_p - E_s}\sqrt{\frac{\Gamma_{M1}}{\Gamma_{E1}}}\sum_{jj'} \xi_j \xi_{j'} P(J_p J_p j j' 1 I F) \begin{Bmatrix} 2 & 1 & 1 \\ 1 & \frac{1}{2} & \frac{1}{2} \\ 1 & j & j' \end{Bmatrix}, \qquad (6-13e)$$

in the vicinity of the p-wave resonance, where J_s, J_p and F are spins of the s-wave resonance, p-wave resonance and final state, respectively. The Γ_{M1} and Γ_{E1} are widths of the M1 and E1 transitions, respectively. The $\eta_\gamma = \pm 1$[39] is a sign factor and we define the ξ_j and the function P as

$$\xi_j = \begin{cases} x & \text{for} \quad j = \frac{1}{2}, \\ y & \text{for} \quad j = \frac{3}{2}, \end{cases} \qquad (6-14)$$

$$P(JJ'jj'kIF) = (-1)^{J+J'+j'+I+F}\frac{3}{2}\sqrt{(2J+1)(2J'+1)}\begin{Bmatrix} k & j & j' \\ I & J' & J \end{Bmatrix} \times \begin{Bmatrix} k & 1 & 1 \\ F & J' & J \end{Bmatrix}. \qquad (6-15)$$

The A_i's are classified into two types of E_n dependence. The A_3, A_{10}, A_{11} and A_{12} are constant functions of E_n in the vicinity of the p-wave resonance while the A_1 and A_9 change their signs at $E_n = E_p$. The values of A_i's of the former type can be discussed at $E_n = E_p$ while those of the latter type must be discussed at $E_n = E_p \pm \Gamma_p/2$. The A_{10} contains no quantity which depends on the γ-ray transition. Therefore the A_{10} is predicted to be independent of the γ-ray transition. On the other hand, other A_i's contain the quantities which depend on γ-ray transitions, that is, the sign factor η_γ, the function P, the 9-j symbol and the factor $\sqrt{\Gamma_{M1}/\Gamma_{E1}}$. If a number of γ-ray transitions are detected without identification of individual γ-ray transition (which is referred to as "integrated γ-detection" below), the contributions of γ-ray transitions cancel each other since they have different signs and magnitudes, and the A_i's become very small (except for A_{10}).

In a measurement of single γ-ray transition, large values of A_i's which depend on γ-ray transitions can be observed if the size of the factor $\sqrt{\Gamma_{M1}/\Gamma_{E1}}$ ($= 10^{-2} \sim 10^2$) is not very small.

§7 Discussion

In this section, we discuss the properties of large PNC effect in $(\vec{n},\gamma)$ reaction for the p-wave resonance of the target of $^{139}La(E_n = 0.734eV)$ and the origin of large values of $A_{L,\gamma}$ for p-wave resonances of several nuclei. We mention a PNC effect in exit channel of the target of ^{139}La in the latter part of this section.

We have studied properties of $A_{L,\gamma}$ in the p-wave resonance for the target of $^{139}La(E_n = 0.734eV)$.

$< E_\gamma$ dependence of $A_{L,\gamma} >$ The longitudinal asymmetry has been measured with several γ-ray energy thresholds. It has been found that the value of $A_{L,\gamma}$ is independent of γ-ray energy within experimental errors. It implies that the large $A_{L,\gamma}$ has no immediate connection with the PNC effect of exit channels. It means that the large value of $A_{L,\gamma}$ is caused by entrance-channel parity-mixing between two opposite-parity amplitudes.

$< \theta_\gamma$ dependences $>$ All the values of correlation coefficients (A_i) which appear in radiative capture reactions induced by longitudinally polarized incident neutrons have been determined in "integrated γ-ray detection" by measuring the angular dependence of longitudinal asymmetry ($a_{L,\gamma}(\theta_\gamma)$, Eq. (2-6)) and angular distribution of γ-rays induced by unpolarized neutrons ($\sigma_{res}^{Unpol}(\theta_\gamma)$, Eq. (2-11)). The A_i's which contain the exit-channel parity-mixing are very small in "integrated γ-ray detection", since the contributions of many γ-ray transitions cancel each other. The A_i's expect for A_{10} have been found to be zero within experimental errors in "integrated γ-ray detection", while the A_{10} term has a large value. The discrepancy between the results of Kyoto-KEK group and Dubna group (see §1) cannot be explained by the contribution of exit-channel parity-mixing.

$< E_n$ dependence of $A_{L,\gamma} >$ It has been found that $A_{L,\gamma}$ is independent of E_n within the resonance width in the case of lanthanum target, which was cooled down to $35K$ and $9K$. At these temperatures, we can avoid the effect of Doppler broadening of the resonance. It is consistent with Eq. (6-2) which is based on s-p mixing scheme. The results are also consistent with the p-d mixing scheme.

The large PNC effects are consistent with the theory based on the parity mixing in entrance channel discussed in §6. It is important for the TRI experiment in neutron transmission method. If the large PNC effects are due to exit-channel parity mixing, we must observe the contributions of individual γ-ray transitions separately where large

FSI effects contribute.

The θ_γ dependences have been studied also for the p-wave resonance of the target of $^{81}Br(E_n = 0.88eV)$ by "integrated γ-ray detection" method. All the A_i's except for A_{10} have been found to be zero within experimental errors, and the A_{10} term has a large value. The θ_γ dependence of longitudinal asymmetry ($a_{L,\gamma}(\theta_\gamma)$) has been studied also for the p-wave resonance of the target of $^{111}Cd(E_n = 4.53eV)$ by "integrated γ-ray detection" method, and no sizable θ_γ dependence has been observed.

The $A_{L,\gamma}$ has been measured for p-wave resonances of the targets of ^{81}Br, ^{93}Nb, ^{108}Pd, ^{111}Cd, ^{124}Sn and ^{139}La, by "integrated γ-ray detection" method. We re-examine the results of $A_{L,\gamma}$ in the framework of the parity-mixing between an s- and a p-wave resonances. We do not discuss the cases of heavy nuclei here, since the level spacing is too small to assume that the parity-mixing is caused by two separate resonances. In order to discuss the origin of the large PNC effect, it is convenient to define α_{nA} as

$$\alpha_{nA} = \frac{2}{E_p - E_s}\sqrt{\frac{\Gamma_s^n}{\Gamma_p^n}}. \qquad (7-1)$$

Resonance parameters are listed in Table 7-1 with experimental values of the $A_{L,\gamma}$ and the calculated values of $|\alpha_{nA}|$. The magnitudes of xW are shown in the rightmost column. They are obtained by substituting our experimental results into the following relation.

$$|A_{L,\gamma}| = |xW||\alpha_{nA}| \qquad (7-2)$$

The values of $|W|$ for the targets of $^{139}La(E_n = 0.734eV)$, $^{81}Br(E_n = 0.88eV)$ and $^{111}Cd(E_n = 4.53eV)$ are in the same order of magnitude, if we assume $|x| = 1$. The $|A_{L,\gamma}|$ is roughly proportional to $|\alpha_{nA}|$. The large PNC effects are mainly caused by the large $|\alpha_{nA}|$. A pair of s- and p-wave resonances which are located closely does not always cause a large PNC effect. No large PNC effect has been observed for the targets of $^{124}Sn(E_n = 62.0eV)$, $^{93}Nb(E_n = 35.9eV)$ and $^{93}Nb(E_n = 42.3eV)$, since their $|\alpha_{nA}|$'s are very small compared with those of ^{139}La, ^{81}Br and ^{111}Cd.

Very large enhancement of PNC effect seems to occur only when Γ_p^n is very small. The fact that the large PNC effects are observed for only a few nuclei, can be explained by the fact that the cross sections of the p-wave resonances with very small Γ_p^n's are too small to be observed among a number of s-wave resonances whose cross sections are very large unless the p-wave resonances are well-separated from other s-wave resonances.

The nucleus which has a well-separated p-wave resonance is rarely to be found. As the average level spacings of the targets of ^{139}La and ^{81}Br are $D_0 = 208 \pm 10eV$ and $94 \pm 15eV$, respectively, a well-separated resonance is likely to be found [†].

No PNC effect has been found in the case of the p-wave resonance of the target of ^{108}Pd at $E_n = 2.96eV$, in spite of the fact that α_{nA} is large, that is, $7.8 \pm 0.3eV^{-1}$, if the resonance at $E_n = 33.10eV$ is taken as the neighboring s-wave resonance. The total angular momentum of the p-wave resonance is $3/2$, while that of the neighboring s-wave resonance is $1/2$. Two opposite-parity amplitudes cannot interfere if their total angular momenta are different.

Parity-mixing in exit channels is important when individual γ-ray transitions are observed separately. It is expected to be smeared in the "integrated γ-ray detection". The forward-backward asymmetry, which contains exit-channel parity-mixing, has been measured for the target of ^{139}La in the γ-ray energy region higher than $1.1 \pm 0.1MeV$ where many γ-ray transitions contribute. The obtained value is $\langle a_\gamma \rangle = 0.1 \pm 0.3\%$. On the other hand, the $\langle a_\gamma \rangle$ measured in the γ-ray energy region higher than $4.8 \pm 0.3MeV$, where only one or two γ-ray transitions are dominant, is $\langle a_\gamma \rangle = 4.7 \pm 2.1\%$. The result suggests the existence of exit-channel parity-mixing in a single γ-ray transition. If we assume that the $\langle a_\gamma \rangle$ is caused by a single γ-ray transition of $^{140}La(4^- \rightarrow 4^-)$, the value of $\sqrt{\Gamma_{M1}/\Gamma_{E1}}$ is obtained from the following relation between A_{10} and A_9 (see Eq. (6-2) and (6-13)). The $\sqrt{\Gamma_{M1}/\Gamma_{E1}}$ is referred to as the exit-channel structural enhancement factor.

$$\left| \frac{\langle a_\gamma \rangle}{A_{L,\gamma}} \right| \sim \frac{|A_9|_{E_n = E_p \pm \Gamma_p/2}}{|A_{10}|_{E_n = E_p}} \sim \frac{1}{|x|} \frac{\Gamma_p}{2\,|E_p - E_s|} \sqrt{\frac{\Gamma_s^n}{\Gamma_p^n}} \sqrt{\frac{\Gamma_{M1}}{\Gamma_{E1}}} \left| P(44\tfrac{1}{2}\tfrac{1}{2}1\tfrac{7}{2}4) \right| \qquad (7-3)$$

Substituting the experimental values, we obtain $\sqrt{\Gamma_{M1}/\Gamma_{E1}} \sim 5.6 \pm 2.5$ assuming $|x| = 1$. But if another γ-ray transition of $^{140}La(4^- \rightarrow 5^-)$ contributes to the $\langle a_\gamma \rangle$, exit-channel structural enhancement factor should be different. Further study is necessary to examine the parity-mixing in exit channels.

In summary, the properties of large PNC effects in n-A interactions have been studied in $(\vec{n}, \gamma)$ reactions for several nuclei. The phenomena can be explained by the

† $D_0 \leq 20eV$ for uranium and thorium.

target nucleus	E_p $[eV]$	$2g\Gamma_p^n$ $[meV]$	E_s $[eV]$	$2g\Gamma_s^{n0}$ $[meV]$	J_p	J_s	$A_{L,\gamma}$	$\lvert\alpha_{nA}\rvert$ $[eV^{-1}]$	$\lvert xW\rvert$ $[meV]$
^{81}Br	0.88 ± 0.01	0.000116 ± 0.000006	101.10 ± 0.14	20	unknown	unknown	0.021 ± 0.004	8.0 ± 0.2	2.6 ± 0.1
^{93}Nb	35.9 ± 0.1	0.112 ± 0.010	119.2 ± 0.2	0.37	5	5	0.003 ± 0.005	0.11 ± 0.01	
^{93}Nb	42.3 ± 0.1	0.0865 ± 0.0050	-105.39	33.24	4	4	-0.000 ± 0.006	0.68 ± 0.02	
^{108}Pd	2.96 ± 0.01	0.01008 ± 0.00010	33.10 ± 0.17	40.6 ± 2.8	$\frac{3}{2}$	$\frac{1}{2}$	0.002 ± 0.002	7.8 ± 0.3	
^{111}Cd	4.53 ± 0.03	0.00326 ± 0.00010	-4	1.9	unknown	0	$-(0.013^{+0.007}_{-0.004})$	8.3 ± 0.3	$1.6^{+0.9}_{-0.5}$
^{124}Sn	62.0 ± 0.1	14.4 ± 0.4	-20	0.30	$\frac{1}{2}$	$\frac{1}{2}$	0.002 ± 0.004	0.010 ± 0.003	
^{139}La	0.734 ± 0.005	0.000073 ± 0.000010	-48.63	168	unknown	4	0.098 ± 0.003	57 ± 4	1.7 ± 0.1

Table 7-1. Resonance parameters and spins of compound states are listed for p-wave resonances and their neighboring s-wave resonances. The nearest s-wave resonances from p-wave resonances are taken as neighboring s-wave resonances. The g is the statistical weight factor given as $g = \frac{2J+1}{2(2I+1)}$. The $\Gamma_s^{n0} = \Gamma_s^n \sqrt{1eV/E_s}$ is the reduced neutron width at $1eV$ for s-wave neutrons [59,40]. The values of $|\alpha_{nA}|$ calculated by substituting the resonance parameters into Eq. (7-1) are shown. The values of $A_{L,\gamma}$ are the experimental results obtained in this work. The values of $|xW|$ are shown in the rightmost column.

interference between two opposite parity amplitudes of compound resonances in the entrance channel.

They are very important candidates for the TRI test experiment which are free from FSI effect.

§8 Future Prospects

In this section, we point out several possibilities of further study of PNC effects. Feasibility of the TRI experiment by the measurement of triple vector correlation term in neutron transmission is pointed out in the latter part of this section.

If the magnitude of nuclear weak matrix element $|W|$ is almost in the same order for all nuclei, we can predict the value of PNC effect. For example, the $A_{L,\gamma}$ for the target of $^{93}Nb(E_n = 42.3eV)$ must be around a few times 10^{-3}. It is very important to study the magnitude of the nuclear weak matrix element for a number of p-wave resonances in various nuclei and to confirm the assumption that the magnitude of nuclear weak matrix element is almost in the same order for all nuclei †. Very precise data of neutron cross sections are necessary to predict the possibility of large PNC effect especially for small p-wave resonances, since large PNC effects have been found only in p-wave resonances which are well-separated from other resonances and have small neutron widths. The assignment of the total angular momentum and the orbital angular momentum of incident neutrons are also necessary.

For further understanding of the reaction mechanism which is responsible for large PNC effects, we can study exit-channel parity-mixing by measuring the correlation coefficients given in §2 for individual γ-ray transitions. The precise measurement of them enables us to predict the values of PNC effects based on s-p mixing scheme, and to check the consistency of the predicted values. Here we discuss the case of the p-wave resonance of ^{139}La at $E_n = 0.734eV$. The $A_{13}\sigma_\gamma \cdot \hat{\mathbf{k}}_\gamma$ term corresponds to the circular polarization of the emitted γ-rays induced by unpolarized incident neutrons (P_γ) through the relation $P_\gamma = A_{13}\sigma_{res}/\sigma_{cap}$. The A_{13} is related to A_9 as

$$\frac{A_9}{A_{13}} = -P(J_s J_s \frac{1}{2}\frac{1}{2} 1 I F), \qquad (8-1)$$

† In heavy nuclei, many p-wave resonances exist in slow-neutron capture reaction. In this case, we cannot apply the two level approximation since the resonances are located too close to each other. We can extract the nuclear matrix element applying a statistical procedure even in such cases[61,62].

for single γ-ray transitions (Appendix A). If we substitute $J_s = 4$, $I = 7/2$, $F = 4$, and $\langle a_\gamma \rangle = 4.7 \pm 2.1\%$, we obtain $|A_{13}|_{E_n = E_p \pm \Gamma_p/2} = 38 \pm 17\%$. Another interesting observable is the $A_2\sigma_n \cdot (\hat{\mathbf{k}}_n \times \hat{\mathbf{k}}_\gamma)$ term †, which is the analyzing power for transversely polarized incident neutrons on the resonance. Its value for the p-wave resonance of the target of ^{139}La can be evaluated by

$$(A_2)_{E_n = E_p} = -\sqrt{\frac{\Gamma_s^n}{\Gamma_p^n}}\sqrt{\frac{\Gamma_{M1}}{\Gamma_{E1}}}\frac{\Gamma_p}{E_p - E_s}(-0.1250x - 0.07395y), \qquad (8-2)$$

for the γ-ray transition of $^{140}La(4^- \to 4^-)$. We obtain

$$|A_2|_{E_n = E_p} \sim 96 \pm 43\%, \qquad (8-3)$$

assuming $|x| = 1$ (Appendix A). More intense neutron beam is necessary for the precise measurement of these observables. The improvement of energy resolution of γ-ray detector is also desirable.

The neutron transmission method is one of the best way to search for T-violating effects, as we can observe T-violating effects in the weak interaction free from FSI. Bunakov, Gudkov and Yamaguchi suggested the enhancement mechanism of PNC effect is also applicable to T-violating effect [32,60,23]. We mention a feasibility of TRI experiment in neutron transmission method below. Interaction between low energy incident neutrons and nuclei is described using forward scattering amplitude f which can be written in the form

$$f = A' + B'\sigma_n \cdot \hat{\mathbf{I}} + C'\sigma_n \cdot \hat{\mathbf{I}} + D'\sigma_n \cdot (\hat{\mathbf{I}} \times \hat{\mathbf{k}}_n). \qquad (8-4)$$

In this case, propagation of incident neutrons through material can be described in the context of neutron optics. The incoming neutron spin state (U_i) is transformed into another one (U_f) which is given as

$$U_f = \delta U_i, \quad \delta = e^{i(n-1)\rho z}, \quad n = 1 + \frac{2\pi}{(\hbar k_n)^2}\rho f, \qquad (8-5)$$

after the propagation of length z in material, where ρ is the number density of nuclei. The δ is

$$\delta = A + B\sigma_n \cdot \hat{\mathbf{I}} + C\sigma_n \cdot \hat{\mathbf{k}}_n + D\sigma_n \cdot (\hat{\mathbf{I}} \times \hat{\mathbf{k}}_n), \qquad (8-6)$$

† P-even T-odd. We cannot test TRI in this observable since FSI is too large.

where $A = \exp(iZA')\cos b$, $B = i\exp(iZA')B'Z(\sin b)/b$,
$C = i\exp(iZA')C'Z(\sin b)/b$, $D = i\exp(iZA')D'Z(\sin b)/b$, $Z = 2\pi\rho z/(\hbar k_n)$ and $b = Z|B' + C'|$. A relation $D' = 0 \rightarrow D = 0$ holds and it is equivalent to $D \neq 0 \rightarrow D' \neq 0$. Therefore a non-zero value of D which is to be observed in the experiment is an unambiguous evidence of the existence of T-odd correlation term D'. In the measurement, we must choose an observable in which no FSI effect is included. Two candidates have been suggested. One is the spin detailed balance with a polarized target[28] and the other is the equality of analyzing power and polarization with a polarized target[29]. The necessary devices for these experiments are (1) neutron polarizer (2) polarized target and (3) neutron spin analyzer. We already mentioned a neutron polarizer. The polarized ^3He is a candidate for the neutron spin analyzer. The technique to polarize ^3He gas is an established one [63]. Recently, high polarization of ^3He in $6 \sim 9atm$ has been reported [64]. In addition, it can also be used as a detector of slow neutrons. But the technique to polarize nuclei (lanthanum etc.) is not yet established.

Dynamic nuclear polarization has been studied for lanthanum trifluoride single crystals in which neodymium ions are diluted ($La_{1-x}Nd_xF_3$[65]). Approximately 1% of ^{139}La polarization was obtained for $x = 0.08\%$ [45].

The neutron spin rotates due to pseudomagnetic field[66] on propagating through a polarized target. If the incident neutron spin rotates on transmission through target material, experimental efficiency for $\sigma_n \cdot (\hat{I} \times \hat{k}_n)$ term is suppressed. The pseudomagnetic rotation can be cancelled by applying a magnetic field antiparallel to the pseudomagnetic field in a spin frozen polarized target. But the coupling energy between nuclear quadrupole moment of ^{139}La and electric field gradient of lanthanum trifluoride crystal causes the overlapping of the levels due to Zeeman splitting in the cancellation field ($\leq 2kG$) [67], and vector polarization decreases. We must overcome the problem. Single crystals of La_2O_3, $LaAlO_3$, La_2O_2S, KBr etc. have high symmetries and the quadrupole couplings are diagonalized about their c-axes. Currently, the g-factors of neodymium ions diluted in these crystals are being studied.

An experimental accuracy of 10^{-2} to 10^{-3} is expected for the size of P-odd T-odd amplitude relative to P-odd T-even one, if we can polarize ^{139}La nuclei more than 20%. The accuracy can be improved up to 10^{-4} with higher nuclear polarization, precise control of magnetic field and more intense neutron beam.

Acknowledgements

The author would like to thank Prof. A. Masaike for his careful advice, helpful discussion and collaboration. He thanks Profs. K. Imai and H. En'yo for their advice and helpful discussions.

He thanks Drs. T. Adachi, S. Ishimoto, Y. Masuda, Prof. K. Morimoto and Ms. Y. Morishita for their collaboration and valuable discussions. He also thanks Profs. C.D. Bowman, J.D. Bowman, C.R. Gould, V.P. Gudkov, S. Penttilä and S.J. Seestrom for their valuable discussions.

He thanks all people at KEK who have constructed, maintained and operated the neutron spallation source.

He gratefully acknowledges Prof. F. Okamura for his kind help in the crystallography, Prof. Y. Uchida for his kind help in ESR study of lanthanum trifluoride crystal and Dr. Y. Takahashi for his valuable discussions on single crystals of lanthanum compounds.

Finally, he would like to thank all his family, especially his wife for their great support throughout his studies.

References

1) T.D. Lee and C.N. Yang, Phys. Rev. **104** (1956) 254
2) C.S. Wu et al., Phys. Rev. **105** (1957) 1413
3) D.H. Wilkinson, Phys. Rev. **109** (1958) 1603
4) D.E. Nagle et al., in High Energy Physics with Polarized Beams and Targets, ed. G.H. Thomas, AIP Conference Proceedings No. 51, (American Institute of Physics, New York, 1978), p.224.
5) R. Balzer et al., Phys. Rev. **C30** (1984) 1409
6) P. von Rossen et al., Polarization Phenomena in Nuclear Physics-1980, Santa Fe, eds. D.E. Nagle et al., AIP Conference Proceedings No. 69, (American Institute of Physics, New York, 1981), p. 1442.
7) V. Yuan et al., Phys. Rev. Lett. **57** (1986) 1680
8) Yu.G. Abov et al., Phys. Lett. **12** (1964) 25
9) J.L. Alberi et al., Phys. Rev. Lett. **29** (1972) 518
10) J.F. Cavignac et al., Phys. Lett. **B67** (1977) 148
11) V.M. Lobashov et al., Nucl. Phys. **A197** (1972) 241
12) C.A. Barnes et al., in Unification of Elementary Forces and Gauge Theory, eds. D. Cline and F. Mills, (Harwood, London, 1978), p.235

13) E.G. Adelberger et al., Phys. Rev. Lett. **34** (1975) 402
14) V.M. Lobashov et al., Yad. Fiz. **15** (1972) 1142
[Sov. J. Nucl. Phys. **15** (1972) 632
15) H. Benkoula et al., Phys. Lett. **B71** (1977) 287
16) G.V. Danilyan et al., Pis'ma Zh. Eksp. Teor. Fiz. **24** (1976) 380
[JETP Lett. **24** (1976) 344]
17) E. Kuphal et al., Nucl. Phys. **A234** (1974) 308
18) P. Jenschke and P. Bock, Phys. Lett. **B31** (1970) 65
E.D. Lipson et al., Phys. Lett. **B35** (1971) 307
19) K.S. Krane et al., Phys. Rev. **C5** (1972) 1663
20) S.W. Herb et al., Phys. Rev. Lett. **39** (1977) 252
21) M. Forte et al., Phys. Rev. Lett. **45** (1980) 2088
22) O.P Sushkov and V.V.Flambaum, Usp. Fiz. Nauk. **136** (1982) 2
[Sov. Phys. Usp. **25** (1982) 1]
23) Y. Yamaguchi, J. Phys. Soc. Jpn. **57** (1988) 1518(L); ibid 1522(L);
ibid 1525(L); ibid 2331; ibid 3339; ibid 3344
24) Y. Yamaguchi, Prog. Theor. Phys. **85** (1991) 101
N. Ishikawa, Master thesis submitted to Tokai Univ. (unpublished, in Japanese)
25) L. Stodolsky, Nucl. Phys. **B197** (1982) 213
26) P.K. Kabir, Phys. Rev. **D25** (1982) 2013
27) V.E. Bunakov and V.P. Gudkov, Nucl. Phys. **A401** (1983) 93
28) L. Stodolsky, Phys. Lett. **172B** (1986) 5
29) P.K. Kabir, Phys. Rev. Lett. **60** (1988) 686
30) J.H. Christenson et al., Phys. Rev. Lett. **13** (1964) 138
31) G.Lüders, Ann. Phys. **2** (1957) 1
32) V.E. Bunakov and V.P Gudkov,
Tests of Time Reversal Invariance in Neutron Physics, 1987.
Proc. of the Aqueduct Conference Center Workshop
on Tests of Time Reversal Invariance in Neutron Physics
N.R. Roberson, C.R. Gould and J.D. Bowman (ed.).
p.175, World Scientific Publishing
33) L. Stodolsky,
Tests of Time Reversal Invariance in Neutron Physics, 1987.
Proc. of the Aqueduct Conference Center Workshop
on Tests of Time Reversal Invariance in Neutron Physics

N.R. Roberson, C.R. Gould and J.D. Bowman (ed.).
p.12, World Scientific Publishing
34) A. Hallin et al., Phys. Rev. Lett. **52** (1984) 337
35) C.G. Callan et al., Phys. Rev. **162** (1967) 1494
36) D. Thompson, Nucl. Inst. Meth. **A284** (1989) 40
37) I.S. Altarev et al., Pis'ma Zh. Eksp. Teor. Fiz. **44** (1986) 360
[JETP Lett. **44** (1986) 460]
38) V.P. Gudkov, Private communication
39) V.V.Flambaum and O.P.Sushkov, Nucl. Phys. **A435** (1985) 325
40) V.P. Alfimenkov et al., Nucl. Phys. **A398** (1983) 93
41) S.A. Biryukov et al., Yad. Fiz. **45** (1987) 1511
[Sov. J. Nucl. Phys. **45** (1987) 937]
42) Y. Masuda et al., Nucl. Phys. **A478** (1988) 737c
Y. Masuda et al., Nucl. Phys. **A504** (1989) 269
43) V. Yuan et al., (to be published)
44) J.R. Vanhoy et al., Z. Phys. A331 (1988) 1
45) Y. Masuda et al., 18th INS International Symposium on Physics
with High-Intensity Hadron Accelerators, Tokyo, March 14-16, 1990
46) N. Watanabe et al., 9th Meeting of International Collaboration on Advanced
Neutron Sources (ICANS-IX), SIN, Villingen, Switzerland.
September 22-26, 1986.
N. Watanabe, 10th Meeting of International Collaboration on Advanced
Neutron Sources (ICANS-IX), Los Alamos, New Mexico, U.S.A.
October 3-7, 1988.
47) H.M.Shimizu et al., 11th Meeting of International Collaboration on Advanced
Neutron Sources (ICANS-XI), KEK, Tsukuba, Japan.
October 22-26, 1990.
48) Y. Masuda et al., Nucl. Inst. Meth. **A264** (1988) 169
49) W. de Boer et al., Phys. Rev. **B12** (1975) 847
W. de Boer, CERN 74-11, Laboratory I, Nuclear Physics Division (1974)
50) V.I. Lushchikov et al., Yad. Fiz. **10** (1969) 669
[Sov. J. Nucl. Phys. **10** (1970) 669]
51) S. Hiramatsu et al., J. Phys. Soc. Jpn. **45** (1978) 949
52) N. Hoshizaki and A. Masaike, Jpn. J. App. Phys. **25** (1986) L244
53) S. Ishimoto et al., Jpn. J. App. Phys. **25** (1986) L246

54) H. Kobayashi et al., Nucl. Inst. Meth. **A270** (1988) 106
55) L.B. Hughes et al., Nucl. Phys. **89** (1966) 241
56) L.V. Groshev et al., Nuclear Data Tables **A5** (1968) 1
57) R.M. Moon et al., Phys. Rev. **181** (1969) 920
58) M. Forte, Fundamental Physics with Reactor Neutrons and Neutrinos, 1977.
Institute of Physics Conference Series N^o42. von Edigy. T. (ed.).
Chap. 2, p.86 Bristol and London: Institute of Physics 1978
59) S.F. Mughabghab et al., Neutron Cross Sections (Academic Press, New York, 1981)
60) V.E. Bunakov and V.P. Gudkov, Z. Phys. **A308** (1982) 363
61) J.D. Bowman et al., Phys. Rev. Lett. **65** (1990) 1192
62) C.M. Frankle et al., (to be published)
63) K.P. Coulter et al.,
Tests of Time Reversal Invariance in Neutron Physics, 1987.
Proc. of the Aqueduct Conference Center Workshop
on Tests of Time Reversal Invariance in Neutron Physics
N.R. Roberson, C.R. Gould and J.D. Bowman (ed.).
p.140, World Scientific Publishing
64) O.Häusser et al., 4th Conference on the Intersections between Particles and Nuclear Physics, Tucson, May 24-29, 1991
65) M.B. Schultz and C.D. Jeffries, Phys. Rev. **149** (1966) 270
66) H. Glättli, J. de Phys. **40** (1979) 629
67) K. Lee et al., Phys. Rev. **150** (1966) 168

Appendix A. Correlation Coefficients in (n,γ) Cross Section

The correlation coefficients which appear in $(\vec{n},\vec{\gamma})$ reaction cross section are discussed (see Eq. (2-1) for definition). Their explicit expressions in the experiment in which incident neutrons are longitudinally polarized and the helicity of γ-rays is not observed are described in the former part of this section. Other important correlation terms are described in the latter part of this section.

If the incident neutrons are longitudinally polarized and the helicity of γ-ray is not observed in Eq. (2-1), we obtain,

$$\sigma_{cap}(\theta_\gamma) = \frac{1}{2}\Big(a_0 + a_1 \hat{\mathrm{k}}_\mathrm{n}\cdot\hat{\mathrm{k}}_\gamma + a_3((\hat{\mathrm{k}}_\mathrm{n}\cdot\hat{\mathrm{k}}_\gamma)^2 - \frac{1}{3}) + a_9\sigma_\mathrm{n}\cdot\hat{\mathrm{k}}_\gamma + a_{10}\sigma_\mathrm{n}\cdot\hat{\mathrm{k}}_\mathrm{n} + a_{11}((\sigma_\mathrm{n}\cdot\hat{\mathrm{k}}_\gamma)(\hat{\mathrm{k}}_\gamma\cdot\hat{\mathrm{k}}_\mathrm{n}) - \frac{1}{3}\sigma_\mathrm{n}\cdot\hat{\mathrm{k}}_\mathrm{n}) + a_{12}((\sigma_\mathrm{n}\cdot\hat{\mathrm{k}}_\mathrm{n}(\hat{\mathrm{k}}_\mathrm{n}\cdot\hat{\mathrm{k}}_\gamma) - \frac{1}{3}\sigma_\mathrm{n}\cdot\hat{\mathrm{k}}_\gamma)\Big), \tag{$A-1$}$$

where $\sigma_\mathrm{n}\cdot\hat{\mathrm{k}}_\mathrm{n} = p_n$, $\hat{\mathrm{k}}_\mathrm{n}\cdot\hat{\mathrm{k}}_\gamma = \cos\theta_\gamma$. It leads to

$$\sigma_{cap}(\theta_\gamma) = \frac{1}{2}\Big(a_0 + a_1\cos\theta_\gamma + a_3(\cos^2\theta_\gamma - \frac{1}{3}) + p_n\Big(a_{10} + (a_9 + \frac{2}{3}a_{12})\cos\theta_\gamma + a_{11}(\cos^2\theta_\gamma - \frac{1}{3})\Big)\Big). \tag{$A-2$}$$

The explicit expressions of the correlation coefficients in the case of single γ-ray transition to a definite final state are given below. Intrinsic parity of the final state is assumed to be the same as that of the compound state. The dominant parity favored transition is M1 transition while the dominant parity unfavored one is E1.

$$a_0 = \sum_{J_s}|V_1(J_s)|^2 + \sum_{J_p j}|V_2(J_p j)|^2 \tag{$A-3a$}$$

$$a_1 = 2Re\sum_{J_s J_p j} V_1(J_s)V_2^*(J_p j)P(J_s J_p \tfrac{1}{2} j 1 I F) \tag{$A-3b$}$$

$$a_3 = Re\sum_{J_p j J_p' j'} 3\sqrt{10}V_2(J_p j)V_2^*(J_p' j')P(J_p J_p' j j' 2 I F)\begin{Bmatrix} 2 & 1 & 1 \\ 0 & \frac{1}{2} & \frac{1}{2} \\ 2 & j & j' \end{Bmatrix} \tag{$A-3c$}$$

$$a_9 = -2Re\Big(\sum_{J_s J_s'} V_1(J_s)V_3^*(J_s')P(J_s J_s' \tfrac{1}{2}\tfrac{1}{2} 1 I F) + \sum_{J_p j J_p' j'} V_2(J_p j)V_4^*(J_p' j')P(J_p J_p' j j' 1 I F)6\begin{Bmatrix} 0 & 1 & 1 \\ 1 & \frac{1}{2} & \frac{1}{2} \\ 1 & j & j' \end{Bmatrix}\Big) \tag{$A-3d$}$$

$$a_{10} = -2Re\sum_{J_s}\left(V_2(J_p = J_s, \frac{1}{2})V_3^*(J_s) + V_1(J_s)V_4^*(J_p = J_s, \frac{1}{2})\right) \qquad (A-3e)$$

$$a_{11} = Re\sum_{J_s J_p}\left(V_2(J_p, \frac{3}{2})V_3^*(J_s) + V_1(J_s)V_4^*(J_p, \frac{3}{2})\right)\sqrt{3}P(J_s J_p \frac{1}{2}\frac{3}{2}2IF) \qquad (A-3f)$$

$$a_{12} = -2Re\sum_{J_p j J_p' j'} V_2(J_p j)V_4^*(J_p' j')P(J_p J_p' j j' 1IF)18\begin{Bmatrix} 2 & 1 & 1 \\ 1 & \frac{1}{2} & \frac{1}{2} \\ 1 & j & j' \end{Bmatrix} \qquad (A-3g)$$

The I, J_s, J_p and F are spins of target nucleus, s-wave resonance, p-wave resonance and final state, respectively. The j is the total angular momentum of the incident neutron defined by Eq. (6-11) ($j = \frac{1}{2}$ or $\frac{3}{2}$). The V_i's are the invariant amplitudes defined as

$$V_1 = -\frac{1}{2k}\frac{\sqrt{3}}{2}\frac{T_s A_{M1}(1+\alpha)}{E_n - E_s + \frac{i}{2}\Gamma_s}, \qquad (A-4a)$$

$$V_2(j) = -\frac{1}{2k}\frac{\sqrt{3}}{2}\frac{T_p(j)A_{E1}}{E_n - E_p + \frac{i}{2}\Gamma_p}, \qquad (A-4b)$$

$$V_3 = -\frac{1}{2k}\frac{\sqrt{3}}{2}\frac{T_s W A_{E1}(1+\beta)}{(E_n - E_p + \frac{i}{2}\Gamma_p)(E_n - E_s + \frac{i}{2}\Gamma_s)}, \qquad (A-4c)$$

$$V_4(j) = -\frac{1}{2k}\frac{\sqrt{3}}{2}\frac{T_p(j)W A_{M1}(1+\gamma)}{(E_n - E_s + \frac{i}{2}\Gamma_s)(E_n - E_p + \frac{i}{2}\Gamma_p)}, \qquad (A-4d)$$

where

$$T_s = \eta_s\sqrt{\Gamma_s^n(E_n)}, \qquad (A-5a)$$

$$T_p(j) = \eta_{pj}\sqrt{\Gamma_{pj}^n(E_n)}, \qquad (A-5b)$$

$$A_{M1(E1)} = \eta_\gamma\sqrt{\Gamma_{M1(E1)}}. \qquad (A-5c)$$

The α, β and γ represent the contribution of far s-wave resonances. They are zero if only one s-wave resonance contributes. Corresponding diagrams are shown in Fig. A - 1. The η's are the phase factors and almost equal to ± 1 in the low energy neutron capture reaction[39]. The T_s and $T_p(j)$ are the reduced T-matrix elements for s-wave resonance and p-wave resonance, respectively. The A_{M1} and A_{E1} are the reduced T-matrix elements for parity-favored and parity-unfavored γ-ray transitions, respectively. The E_n is the incident neutron energy. The E_s and E_p are the resonance energies of s- and p-wave resonances. The Γ_s and Γ_p are the resonance widths of s- and p-wave

resonances. The Γ_s^n and Γ_p^n are the neutron widths of s- and p-wave resonances. The Γ_{M1} and Γ_{E1} are widths of parity-favored and parity-unfavored γ-ray transitions. The function P is defined by Eq. (6-15). Substituting the invariant amplitudes (V_i's) into Eq. (A-3), the explicit expressions of correlation coefficients are obtained. We discuss the size of each coefficient relative to the p-wave resonance cross section †.

$$A_i = \frac{a_i}{a_{0p}} \qquad (A-6)$$

The a_{0p} is given as $a_{0p} = \sum_j |V_2(J_p j)|^2$. This definition is useful only in the vicinity of the p-wave resonance. If we go far from the p-wave resonance, the denominator in Eq. (A-6) becomes too small and the resonance cannot be observed in the experiment. If we assume that only one s-wave resonance exist close to the p-wave resonance, we obtain

$$A_1 = \eta_\gamma\frac{1}{(E_n - E_s)^2 + \frac{\Gamma_s^2}{4}}\sqrt{\frac{\Gamma_s^n}{\Gamma_p^n}\frac{\Gamma_{M1}}{\Gamma_{E1}}}((E_n - E_p)(E_n - E_s) + \frac{\Gamma_s\Gamma_p}{4})\sum_j \xi_j P(J_s J_p \frac{1}{2} j 1IF) \qquad (A-7a)$$

$$A_3 = 3\sqrt{10}\sum_{jj'}\xi_j\xi_{j'}P(J_p J_p j j' 2IF)\begin{Bmatrix} 2 & 1 & 1 \\ 0 & \frac{1}{2} & \frac{1}{2} \\ 2 & j & j' \end{Bmatrix} \qquad (A-7b)$$

$$A_9 = -2\eta_\gamma\frac{W}{(E_n - E_s)^2 + \frac{\Gamma_s^2}{4}}\frac{\Gamma_s^n}{\Gamma_p^n}\sqrt{\frac{\Gamma_{M1}}{\Gamma_{E1}}}\Big((E_n - E_p)P(J_s J_s \frac{1}{2}\frac{1}{2}1IF) + 6(E_n - E_s)\frac{\Gamma_p^n}{\Gamma_s^n}\sum_{jj'}\xi_j\xi_{j'}P(J_p J_p j j' 1IF)\begin{Bmatrix} 0 & 1 & 1 \\ 1 & \frac{1}{2} & \frac{1}{2} \\ 1 & j & j' \end{Bmatrix}\Big) \qquad (A-7c)$$

$$A_{10} = -2x\frac{W}{(E_n - E_s)^2 + \frac{\Gamma_s^2}{4}}\sqrt{\frac{\Gamma_s^n}{\Gamma_p^n}}\left((E_n - E_s) + (E - E_p)\frac{\Gamma_{M1}}{\Gamma_{E1}}\right) \qquad (A-7d)$$

$$A_{11} = \sqrt{3}y\frac{W}{(E_n - E_s)^2 + \frac{\Gamma_s^2}{4}}\sqrt{\frac{\Gamma_s^n}{\Gamma_p^n}}\left((E_n - E_s) + (E_n - E_p)\frac{\Gamma_{M1}}{\Gamma_{E1}}\right)P(J_s J_p \frac{1}{2}\frac{3}{2}2IF). \qquad (A-7e)$$

$$A_{12} = -36\eta_\gamma\frac{W}{(E_n - E_s)^2 + \frac{\Gamma_s^2}{4}}\sqrt{\frac{\Gamma_{M1}}{\Gamma_{E1}}}(E_n - E_s)\sum_{jj'}\xi_j\xi_{j'}P(J_p J_p j j' 1IF)\begin{Bmatrix} 2 & 1 & 1 \\ 1 & \frac{1}{2} & \frac{1}{2} \\ 1 & j & j' \end{Bmatrix}. \qquad (A-7f)$$

† The A_i's are defined as $A_i = a_i/a_0$ in *Ref.*39.

Typically,

$$\begin{cases} \Gamma_s, \Gamma_p \ll E_p - E_s, \\ \sqrt{\dfrac{\Gamma_s^n}{\Gamma_p^n}} \simeq 10^3, \\ \sqrt{\dfrac{\Gamma_{M1}}{\Gamma_{E1}}} \simeq 10^{-2} \sim 10^2. \end{cases} \qquad (A-8)$$

Therefore we can rewrite the expressions in the vicinity of the p-wave resonance ($E_n \sim E_p$) as Eq. (6-13). We can omit A_{12} since its contribution is $\Gamma_p^n/\Gamma_s^n(\sim 10^{-6})$ times smaller compared with that of A_9.

We discuss the case of the p-wave resonance of the target of ^{139}La at $E_n = 0.734eV$ below (see Fig. A-2). We take the s-wave resonance at $E_n = -48.63eV$ as the neighboring s-wave resonance since it is the nearest to the p-wave resonance. The ground state of ^{139}La has $I^\pi = 7/2^+$ and neutron orbital angular momentum is $l = 1$. The dominant γ-ray transition near Q-value is the transition into the state of $F^\pi = 4^-$ of ^{140}La [55,56]. Therefore the allowed γ-ray transition is $M1$ and forbidden one is $E1$. Substituting $I = 7/2$, $J_s = 4$, $J_p = 4$ and $F = 4$ into Eq. (A-7), we obtain the following relations.

$$A_1 \sim \eta_\gamma(-0.1250x + 0.1479y)\frac{1}{(E_p - E_s)}\sqrt{\frac{\Gamma_s^n}{\Gamma_p^n}\frac{\Gamma_{M1}}{\Gamma_{E1}}}(E_n - E_p) \qquad (A-8a)$$

$$A_3 = 3\sqrt{10}(0.1029xy - 0.0174y^2) \qquad (A-8b)$$

$$A_9 \sim -2 \times (-0.1250)\eta_\gamma \frac{W}{(E_p - E_s)^2}\frac{\Gamma_s^n}{\Gamma_p^n}\sqrt{\frac{\Gamma_{M1}}{\Gamma_{E1}}}(E_n - E_p) \qquad (A-8c)$$

$$A_{10} \sim -2x\frac{W}{E_p - E_s}\sqrt{\frac{\Gamma_s^n}{\Gamma_p^n}} \qquad (A-8d)$$

$$A_{11} \sim \sqrt{3}(-0.5636y)\frac{W}{E_p - E_s}\sqrt{\frac{\Gamma_s^n}{\Gamma_p^n}} \qquad (A-8e)$$

Other important correlation coefficients are a_2 and a_{13} corresponding to $\sigma_n \cdot (\hat{k}_n \times \hat{k}_\gamma)$ and $\sigma_\gamma \cdot \hat{k}_\gamma$, respectively (see Eq. (2-1)). The a_2 corresponds to the analyzing power for transversely polarized incident neutrons, while a_{13} corresponds to the circular polarization of emitted γ-rays induced by unpolarized incident neutrons (P_γ). Their explicit expression are given as

$$a_2 = -2Im \sum_{J_s J_p j} V_1(J_s)V_2^*(J_p j)\beta_j P(J_s J_p \frac{1}{2} j 1 I F), \qquad (A-9a)$$

$$a_{13} = 2Re\left(\sum_{J_s} V_1(J_s)V_3^*(J_s) + \sum_{J_p j} V_2(J_p j)V_4^*(J_p j)\right), \qquad (A-9b)$$

where

$$\beta_j = \begin{cases} 1, & j = \frac{1}{2}, \\ -\frac{1}{2}, & j = \frac{3}{2}. \end{cases} \qquad (A-10)$$

If we divide them by a_{0p}, we obtain

$$A_2 = -\eta_\gamma\sqrt{\frac{\Gamma_s^n}{\Gamma_p^n}}\sqrt{\frac{\Gamma_{M1}}{\Gamma_{E1}}}\frac{\Gamma_p}{(E_p - E_s)^2}\left((E_n - E_s) - \frac{\Gamma_s}{\Gamma_p}(E_n - E_p)\right) \times \sum_j \xi_j\beta_j P(J_s J_p \frac{1}{2} j 1 I F), \qquad (A-11a)$$

$$A_{13} \sim 2\eta_\gamma \frac{W}{(E_p - E_s)^2}\sqrt{\frac{\Gamma_{M1}}{\Gamma_{E1}}}\frac{\Gamma_s^n}{\Gamma_p^n}(E_n - E_p). \qquad (A-11b)$$

The following relations are important.

$$\frac{A_9}{A_{13}} = -P(J_s J_s \frac{1}{2}\frac{1}{2} 1 I F) \qquad (A-12a)$$

$$(A_2)_{E_n = E_p} = -\eta_\gamma\sqrt{\frac{\Gamma_s^n}{\Gamma_p^n}}\sqrt{\frac{\Gamma_{M1}}{\Gamma_{E1}}}\frac{\Gamma_p}{E_p - E_s}\sum_j \xi_j\beta_j P(J_s J_p \frac{1}{2} j 1 I F) \qquad (A-12b)$$

Substituting $I = 7/2$, $J_s = 4$, $J_p = 4$ and $F = 4$ into Eq. (A-12), we obtain the following relations.

$$\frac{A_9}{A_{13}} = 0.1250 \qquad (A-13a)$$

$$(A_2)_{E_n = E_p} = -\eta_\gamma\sqrt{\frac{\Gamma_s^n}{\Gamma_p^n}}\sqrt{\frac{\Gamma_{M1}}{\Gamma_{E1}}}\frac{\Gamma_p}{E_p - E_s}(-0.1250x - 0.07395y) \qquad (A-13b)$$

The P_γ, which is usually measured in the experiment, is given as

$$P_\gamma = A_{13}\frac{\sigma_p}{\sigma_{cap}}, \qquad (A-14)$$

when the γ-rays are detected for whole angle and incident neutron are unpolarized.

Appendix B. Dynamic Polarization

"Dynamic Polarization" is a well established method to obtain a high vector nuclear polarization by pumping nuclear spins in a material applying microwave which resonates paramagnetic centers. An overview of the principle of dynamic polarization is discussed in this section. We write spins of electron and nucleus as **s** and **I**, respectively.

For simplicity, we discuss only the system which consists of paramagnetic centers and one kind of nuclei of $I = 1/2$. The total hamiltonian of the spin system in a magnetic field is given as

$$H = H_{sz} + H_{Sz} + H_{ss} + H_{II} + H_{sI} + H_{RF}, \qquad (B-1)$$

where the spin-lattice interaction is ignored. The first and second terms represent the Zeeman energy terms of electron and nucleus, respectively. The third, fourth and fifth terms represent spin-spin interactions between electrons, nuclei and electron-nucleus, respectively. The last term is a possible effect of oscillating magnetic field of the applied microwave. We discuss the simplest case of that only one electron and one proton are included. The hamiltonian of this system is given as

$$H = H_Z + H_{sI} + H_{ss}, \qquad (B-2a)$$

$$H_Z = H_{sz} + H_{I_z} + H_{sI} + H_{RF}. \qquad (B-2b)$$

The H_Z is diagonal when we take the state vector of this system as $|s_z, I_z\rangle$ with the quantization axis which is parallel to the direction of the applied magnetic field. When we denote magnetic substates of $\pm 1/2$ as $\pm$, each state satisfies the following relations.

$$\begin{cases} H_Z|+-\rangle = (E_s + E_I)|+-\rangle, \\ H_Z|++\rangle = (E_s - E_I)|++\rangle, \\ H_Z|--\rangle = (-E_s + E_I)|--\rangle, \\ H_Z|-+\rangle = (-E_s - E_I)|-+\rangle. \end{cases} \qquad (B-3)$$

Off-diagonal components are included in H_{sI}. They can be evaluated in the first order perturbation as

$$\begin{cases} |a\rangle = |-+\rangle + \epsilon^*|--\rangle, \\ |b\rangle = |--\rangle + \epsilon|-+\rangle, \\ |c\rangle = |++\rangle + \epsilon^*|+-\rangle, \\ |d\rangle = |+-\rangle + \epsilon|++\rangle. \end{cases} \qquad (B-4)$$

When H_{sI} is assumed to be the dipole interaction as

$$H_{sI} = \frac{\hbar^2 \gamma_e \gamma_I}{r^3}\left(\mathbf{s}\cdot\mathbf{I} - \frac{3(\mathbf{s}\cdot\mathbf{r})(\mathbf{I}\cdot\mathbf{r})}{r^2}\right), \qquad (B-5)$$

the ϵ is given as

$$\epsilon = \frac{3}{4}\frac{\hbar\gamma_e}{r^3 H}\sin\theta\cos\theta e^{-i\phi}, \qquad (B-6)$$

where the H is the magnitude of external magnetic field, and θ and ϕ are spherical angles of the vector $\mathbf{r}$ which connects the electron and proton. Transitions of $|a\rangle \leftrightarrow |c\rangle$ and $|b\rangle \leftrightarrow |d\rangle$ are allowed transitions. When the microwave is applied at $\nu_0 (= 2E_s/h)$, strong electron spin resonance (ESR) is observed. Transitions of $|a\rangle \leftrightarrow |d\rangle$ and $|b\rangle \leftrightarrow |c\rangle$ are forbidden transitions. The microwave of $\nu = \nu_0 \pm \Delta\nu (= 2(E_s \pm E_S)/h)$ induces a weak electron spin resonance corresponding to the forbidden transition. The probability of the forbidden transition is known to be $4|\epsilon|^2$ times that of allowed transition by evaluating a matrix element of H_{RF} between two admixed states[49]. Therefore, the absorption of the applied microwave power behaves as schematically shown in Fig. B-2 against the frequency. (But the ESR peaks of the forbidden transitions are not observed in ordinary experiment since they are $|\epsilon|^2$ times that of the allowed transition.) The population of the states $|a\rangle, |b\rangle, |c\rangle, |d\rangle$ obey the Boltzmann distribution when no microwave is applied. The polarization p of a particle whose spin is J is given as

$$p = \frac{1}{J}\frac{\sum_{m=-J}^{J} mN_m}{\sum_{m=-J}^{J} N_m}, \qquad (B-7)$$

where N_m is the population of a magnetic substate. The population is given as

$$N_m \propto e^{-\frac{m\hbar\gamma H_0}{kT}}, \qquad (B-8)$$

where the H_0 is the magnitude of the applied magnetic field. The polarization p is given as

$$p = \frac{2J+1}{2J}\coth\left(\frac{2J+1}{2J}\frac{\mu H_0}{kT}\right) - \frac{1}{2J}\coth\left(\frac{1}{2J}\frac{\mu H_0}{kT}\right). \qquad (B-9)$$

The polarization of a free electron is -99.75% with a $25kG$ magnetic field at $0.5K$ while the polarization of a proton is only 0.51%.

For a dynamic polarization, a microwave is applied at $\nu = \nu_0 \pm \Delta\nu$. Let us consider the case of $\nu = \nu_0 - \Delta\nu$. If no microwave is applied, the electron-proton system stays

in the lowest energy state, namely $|a\rangle$, with a large probability which is determined by thermal equilibrium. The microwave induces the forbidden transition between $|b\rangle \leftrightarrow |c\rangle$. The double spin-flip transition pushes up the state to higher energy state. The electron spin is flipped to the original spin direction through a spin-lattice relaxation typically within the time of the order of *msec*, while proton spin is flipped very slowly within the time of the order of *sec*. The large difference between these two relaxation times causes a net transition of

$$|b\rangle \rightarrow |c\rangle \rightarrow |a\rangle.$$

The interaction which is responsible for the double spin-flip transition is the dipole interaction included in H_{sI}. The probability of the forbidden transition is proportional to $|\epsilon|^2 \propto r^{-6}$. Therefore only the neighboring nuclei around a radical electron are polarized through this mechanism. The nuclear polarization is transferred to remote nuclei through spin-spin coupling ($I^i_{\pm} I^j_{\mp}$). This mechanism is referred to as "spin diffusion". The characteristic time for spin diffusion is order of *sec*. The "spin diffusion" works well when two nuclear spins have an identical magnetic moment and the magnitudes of spin. Finally we can obtain a very high polarization in a material uniformly.

When a microwave frequency is set at $\nu = \nu_0 + \Delta\nu$, the net transition of

$$|a\rangle \rightarrow |d\rangle \rightarrow |b\rangle.$$

is enhanced. Then a negative nuclear polarization is obtained. Therefore the nuclear polarization curve against the microwave frequency is dispersive shape as shown in Fig. B-2. Both positive- and negative-nuclear polarization can be obtained by choosing the microwave frequency with a fixed magnetic field.

Appendix C. Time Reversal Invariance in Neutron Transmission

We describe T-violating observables in low-energy neutron transmission experiment, below [28,29]. We write the scattering amplitude for forward scattering as

$$f = A' + B'\sigma_n \cdot \hat{I} + C'\sigma_n \cdot \hat{I} + D'\sigma_n \cdot (\hat{I} \times \hat{k}_n). \qquad (C-1)$$

The incoming neutron spin state represented by U_i is transformed into U_f given as

$$\begin{aligned} U_f &= \delta U_i, \\ \delta &= e^{i(n-1)\rho z}, \\ n &= 1 + \frac{2\pi}{(\hbar k_n)^2}\rho f, \end{aligned} \qquad (C-2)$$

after the propagation of length z in a material whose number density is ρ. The δ is given as

$$\delta = A + B\sigma_n \cdot \hat{I} + C\sigma_n \cdot \hat{k}_n + D\sigma_n \cdot (\hat{I} \times \hat{k}_n), \qquad (C-3)$$

where

$$\begin{aligned} A &= e^{iZA'} \cos b, \\ B &= ie^{iZA'} B' \frac{\sin b}{b} Z, \\ C &= ie^{iZA'} C' \frac{\sin b}{b} Z, \\ D &= ie^{iZA'} D' \frac{\sin b}{b} Z, \\ Z &= \frac{2\pi}{\hbar k_n}\rho z, \\ b &= Z|B' + C'|. \end{aligned}$$

The most important point is that ($D' = 0 \rightarrow D = 0$). It is equivalent to ($D \neq 0 \rightarrow D' \neq 0$). Therefore a non-zero value of D which is to be observed in experiment is an unambiguous evidence of the existence of T-odd correlation term D'.

We assume the σ_n, $\hat{I}$ and $\hat{k_n}$ are perpendicular to each other and $\sigma_n // x$, $\hat{I} // y$ and $\hat{k_n} // z$. When we define

$$\begin{aligned} \mathbf{E} &\equiv B\hat{I} + C\hat{k_n} + D\hat{I} \times \hat{k_n} \\ &= \begin{pmatrix} B \\ D \\ C \end{pmatrix}, \end{aligned} \qquad (C-4)$$

the δ can be written as

$$\delta = A + \sigma_n \cdot \mathbf{E}. \qquad (C-5)$$

The analyzing power and polarization vector in this process, which are represented by A and P, respectively, are given as

$$\mathbf{A} \equiv Tr(\delta^\dagger \sigma_n \delta) = 4\mathbf{ReA^*E} - 2\mathbf{iE^*} \times \mathbf{E}, \qquad (C-6a)$$

$$\mathbf{P} \equiv Tr(\sigma_n \delta^\dagger \delta) = 4\mathbf{ReA^*E} + 2\mathbf{iE^*} \times \mathbf{E}. \qquad (C-6b)$$

Therefore, the following relations are obtained.

$$\mathbf{A}+\mathbf{P} = 8ReA^*\mathbf{E} = 8\begin{pmatrix} ReA^*B \\ ReA^*D \\ ReA^*C \end{pmatrix} \qquad (C-7a)$$

$$\mathbf{A}-\mathbf{P} = -4i\mathbf{E^*} \times \mathbf{E} = 4\begin{pmatrix} -ImC^*D \\ -ImB^*C \\ ImB^*D \end{pmatrix} \qquad (C-7b)$$

The $(\mathbf{A}+\mathbf{P})_y$, $(\mathbf{A}-\mathbf{P})_x$ and $(\mathbf{A}-\mathbf{P})_z$ are proportional to D which signals T-violation. It is natural to assume that the magnitude of A is biggest among those of A, B, C and D. The $(\mathbf{A}+\mathbf{P})_y$ is expected to be the biggest T-violating observable among them.

In a similar way, we can find other observables which are sensitive to T-violation. We use $Prob(i \to j)$ to represent the expectation value of the transmitted neutron polarization in the direction j with 100% polarized incident neutrons in the direction i.

$$\begin{aligned} Prob(i \to j) &= Tr\left(\frac{1+(\sigma_n)_j}{2}\delta^\dagger \frac{1+(\sigma_n)_i}{2}\delta\right) \\ &= \frac{1+\delta_{ij}}{2}|A|^2 + \frac{1-\delta_{ij}}{2}|\mathbf{E}|^2 \\ &\quad + ReA^*(E_i+E_j) + i\frac{\epsilon_i^{kl}-\epsilon_j^{kl}}{2}E_k^*E_l + ReE_i^*E_j + \epsilon_{ij}{}^k ImA^*E_k \end{aligned} \qquad (C-8)$$

The δ_{ij} and ϵ_{ijk} are given as follows.

$$\delta_{ij} = \begin{cases} 1 & (i=j) \\ 0 & (i \neq j) \end{cases}$$

$$\epsilon_{ijk} = \begin{cases} 1 & (\text{if } ijk \text{ is an even permutation of } 123) \\ -1 & (\text{if } ijk \text{ is an odd permutation of } 123) \\ 0 & (\text{otherwise}) \end{cases}$$

We find several observables which are proportional to D among the following observables.

$$Prob(+i \to -i) - Prob(-i \to +i) = -2i(\mathbf{E^*} \times \mathbf{E})_i = 4\begin{pmatrix} ImC^*D \\ ImB^*C \\ ImB^*D \end{pmatrix} \qquad (C-9a)$$

$$Prob(+i \to +i) - Prob(-i \to -i) = 4ReA^*E_i = 4\begin{pmatrix} ImA^*B \\ ImA^*D \\ ImA^*C \end{pmatrix} \qquad (C-9b)$$

Those are $Prob(+x \to -x) - Prob(-x \to +x)$, $Prob(+y \to +y) - Prob(-y \to -y)$ and $Prob(+z \to -z) - Prob(-z \to +z)$.

Appendix D. Numerical Simulation

Numbers of neutrons which are captured by the resonance cross section for two helicities ($N^\pm$) consist of $N_i^\pm$ which are numbers of neutrons captured by the resonance cross section after being scattered elastically for i times. The $N_i^\pm$ depend on the energy of incident neutrons, so do $N^\pm$.

$$N^\pm(E_n) = \sum_{i=0}^{\infty} N_i^\pm(E_n) \qquad (D-1)$$

The E_n dependence of resonance cross section obtained in experiment was used to include the effect of Doppler broadening as a spreading of resonance width. The N_i's were calculated as

$$\begin{aligned} N_0^\pm(E_n) &= \int d\Omega \int_{V_B} \frac{d^3r}{S_B} e^{-n\sigma_{tot}^\pm z} n \frac{d\sigma_{res}^\pm}{d\Omega} = \frac{\sigma_{res}^\pm}{\sigma_{tot}^\pm}(1-e^{n\sigma_{tot}^\pm t}), \\ N_1^\pm(E_n) &= \int dE_1 \int d\Omega_1 \int_{V_B} \frac{d^3r_1}{S_B} e^{-n\sigma_{tot}^\pm z_1} n \frac{d\sigma_{sc}}{d\Omega_1} \kappa(E_1, E_n; \hat{k}_n, \vec{\Omega}_1) \frac{\sigma_{res}^\pm}{\sigma_{tot}^\pm}(1-e^{n\sigma_{tot}^\pm \ell(\vec{r}_1,\vec{\Omega}_1)}), \\ N_2^\pm(E_n) &= \int dE_2 \int dE_1 \int d\Omega_2 \int_{V_B} \frac{d^3r_1}{S_B} \int_V \frac{d^3r_2}{S} e^{-n\sigma_{tot}^\pm z_1} n \frac{d\sigma_{sc}}{d\Omega_{12}} \kappa(E_1, E_2; \hat{k}_n, \hat{\vec{r}}_{12}) \\ &\quad \times e^{-n\sigma_{tot}^\pm |\vec{r}_{12}|} n \frac{d\sigma_{sc}}{d\Omega_2} \kappa(E_2, E_n; \hat{\vec{r}}_{12}, \vec{\Omega}_2) \frac{\sigma_{res}^\pm}{\sigma_{tot}^\pm}(1-e^{n\sigma_{tot}^\pm \ell(\vec{r}_2,\vec{\Omega}_2)}), \\ &\vdots \end{aligned} \qquad (D-2)$$

where

$$\begin{aligned} \sigma_{tot}^\pm &= \sigma_{sc} + \sigma_{con} + \sigma_{res}^\pm, \\ \sigma_{res}^\pm &= \sigma_{r0}(1 \pm p_n A_L), \\ \vec{r}_{12} &= \vec{r}_2 - \vec{r}_1, \\ \hat{\vec{r}}_{12} &= \frac{\vec{r}_2 - \vec{r}_1}{|\vec{r}_2 - \vec{r}_1|}, \end{aligned}$$

and

E_n	: incident neutron energy,
p_n	: incident neutron polarization,
A_L	: longitudinal asymmetry,
σ_{tot}	: total cross section,

σ_{sc}	: scattering cross section,
σ_{con}	: continuum cross section,
σ_{res}	: resonance cross section,
n	: number density of target nuclei,
V	: target volume,
V_B	: intersection between target volume and incident beam,
S	: cross section of V,
S_B	: cross section of V_B,
$\ell(\vec{r},\vec{\Omega})$	: target thickness for the neutron which is scattered at the point $\vec{r}$ and propagated parallel to $\vec{\Omega}$.

The function κ is unity only when arguments are allowed in elastic scattering kinematically, otherwise it is zero. The $\vec{\Omega}$, $\vec{\Omega}_1$, $\vec{\Omega}_2$, ... are unit vector variables which run over whole solid angle. The Ω_{12} is the solid angle of the volume d^3r_2 seen from the point $\vec{r}_1$.

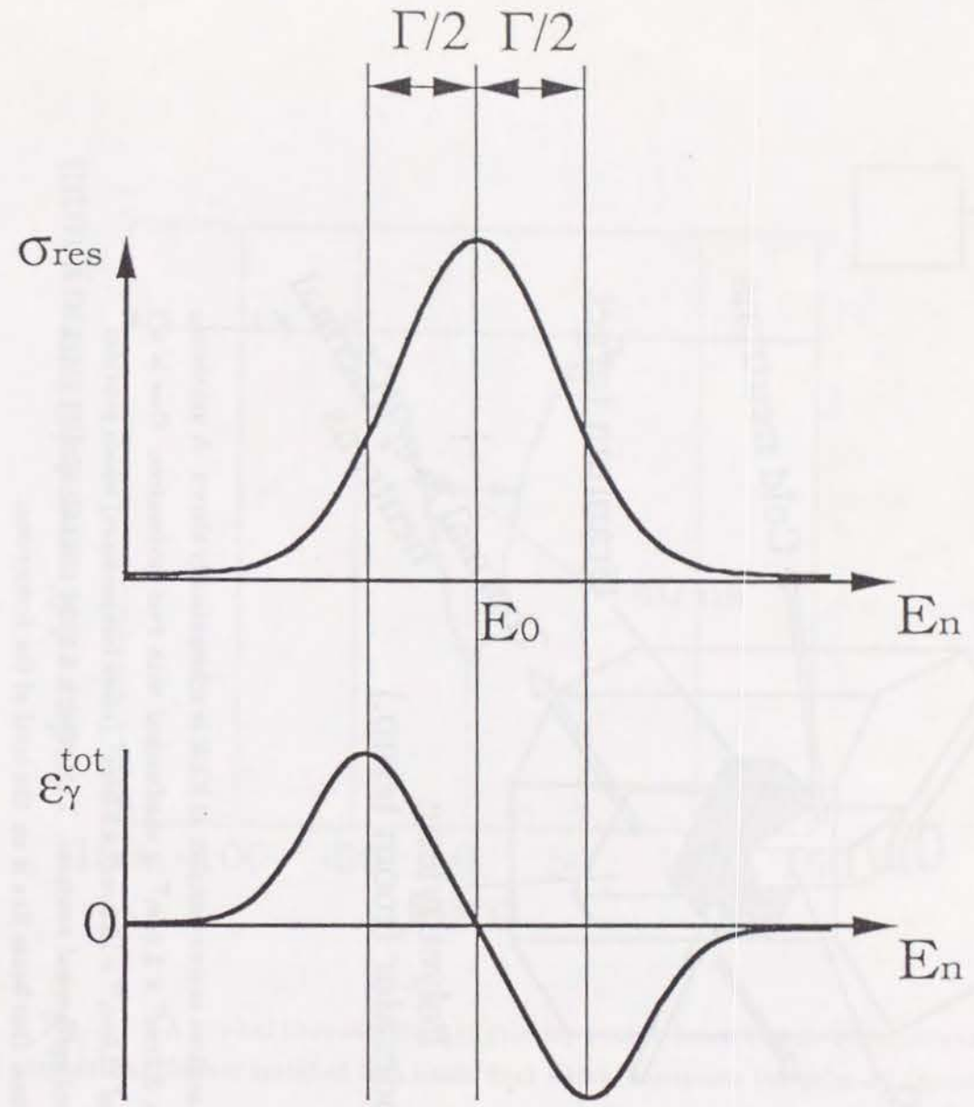

Fig. 2-1 The E_n dependence of $\epsilon_\gamma^{tot} = a_\gamma \cdot (\sigma_{res}/\sigma_{cap})$ in the vicinity of the p-wave resonance is shown. The E_0 and Γ are the resonance energy and the resonance width of the resonance, respectively.

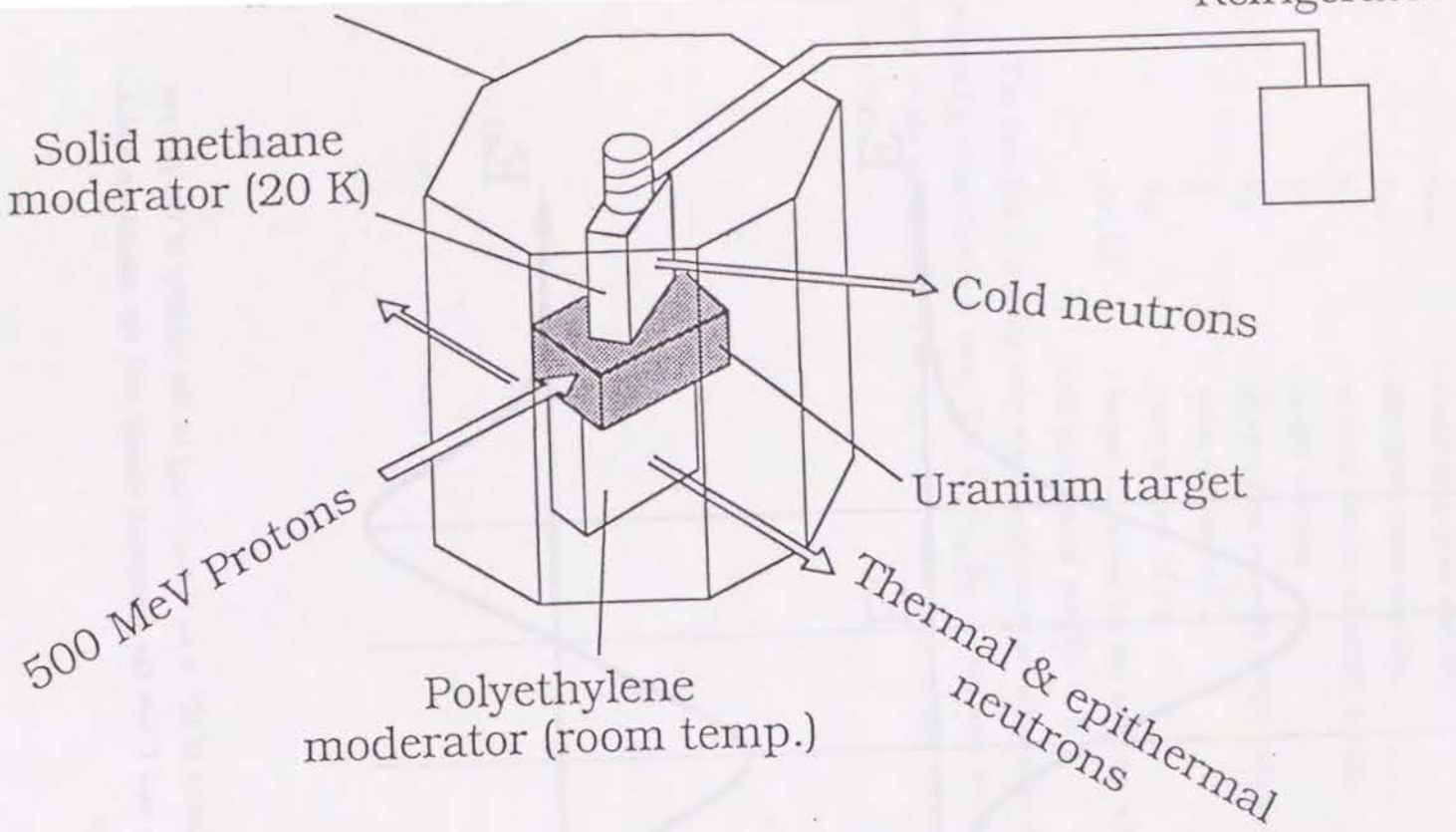

Fig. 3-1-1 The neutron source complex at KEK is schematically shown. A uranium target of $7.8cm^W \times 5.7cm^H \times 3.0cm^T$ is sandwiched with two moderators. One is a polyethylene block of $10.0cm^W \times 10.0cm^H \times 5.0cm^T$ (room temperature) which provides thermal neutrons and epithermal neutrons. The other is a solid methane ($20K$) which provides cold neutrons. Our beam line is on the level of the former one.

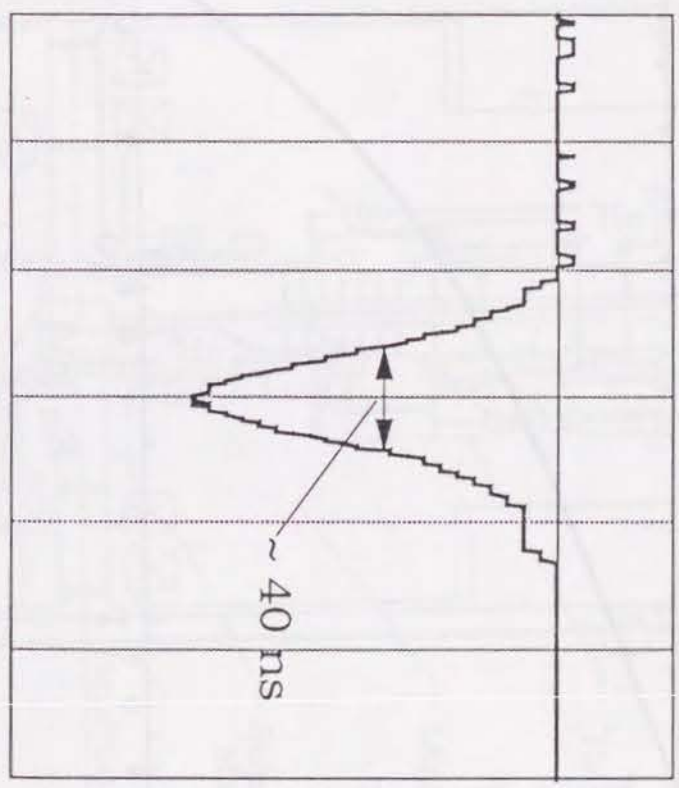

Fig. 3-1-2 A typical time structure of primary proton beam bunch. (The output of a current transformer installed in a beam duct which transports the primary protons.)

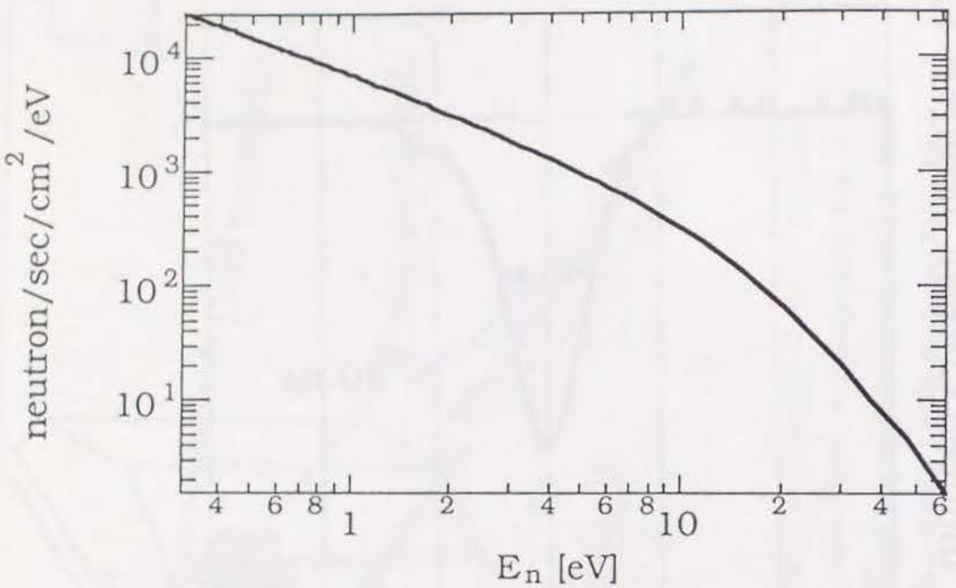

Fig. 3-1-3 Neutron intensity at PEN beam line upstream the polarized proton filter versus incident neutron energy. The intensity of the primary proton beam was $7 \times 10^{11}[proton/pulse] \times 20[pulse/sec]$.

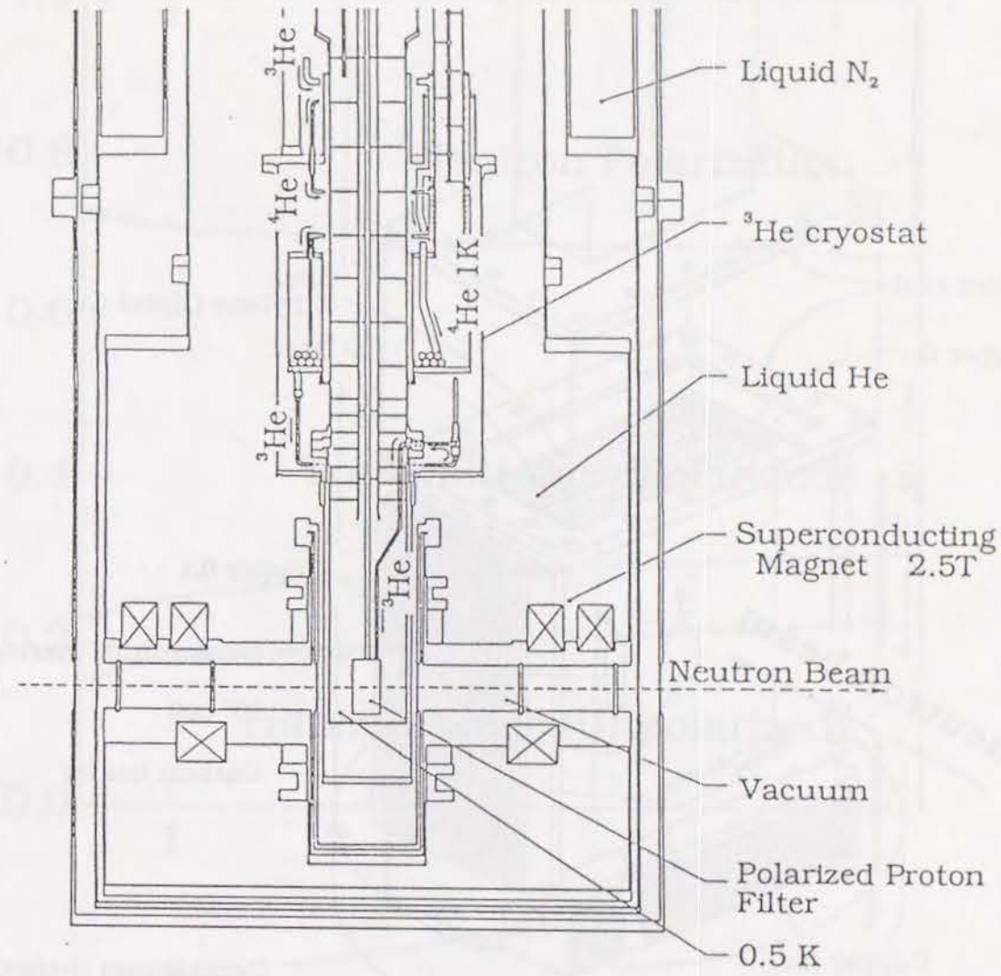

Fig. 3-2-1 The arrangement of the dynamically polarized proton filter as a neutron-spin polarizer.

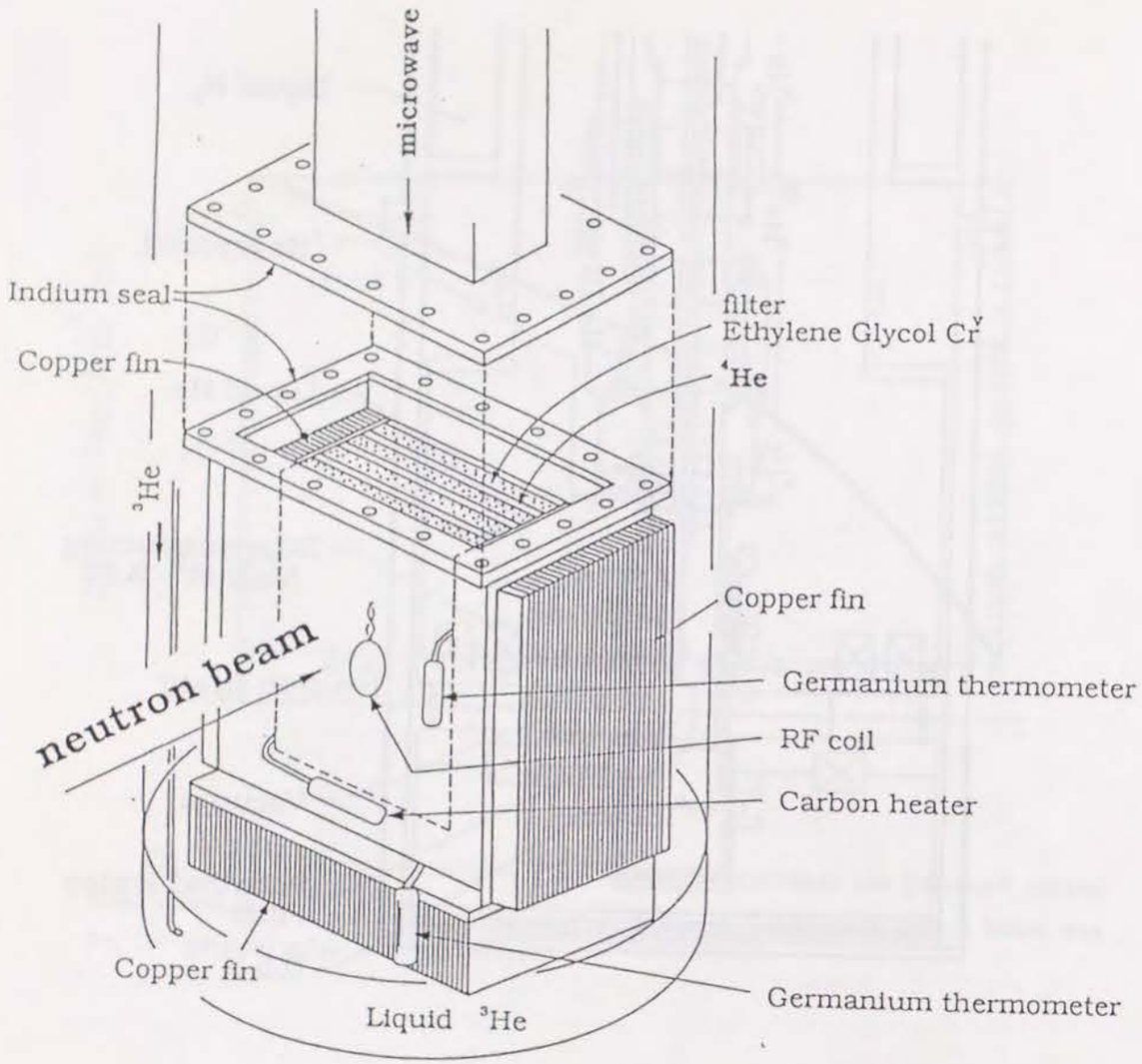

Fig. 3-2-2 The configuration of the copper box cavity containing five layers of ethylene glycol (Cr^V). The box is helium tight and filled with liquid ^4He for heat conductor between the ethylene glycol layer and the box. The walls of the box were grooved and formed into fins. The depths of the grooves are from 0.5 to 1cm. The thickness of the fins is around 0.03cm and the gap between the fins is 0.03cm. The bottom of the box is immersed in a liquid ^3He bath.

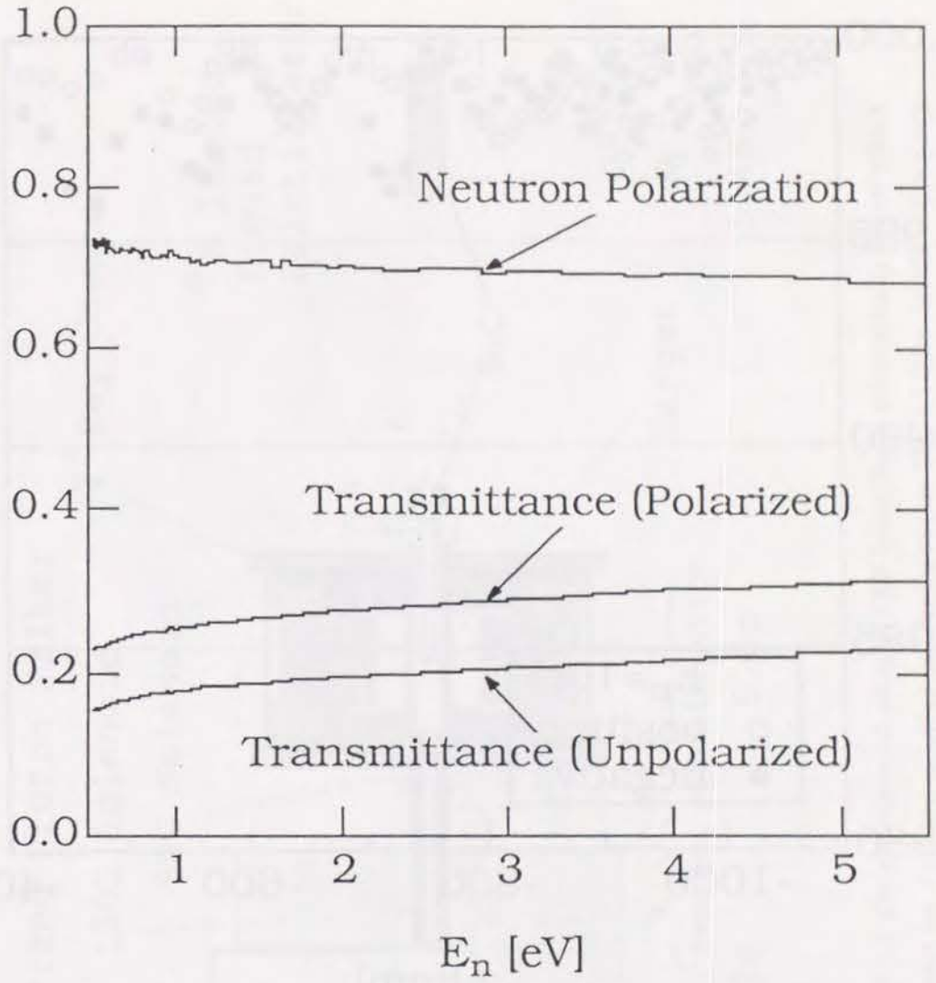

Fig. 3-2-3 Neutron polarization is plotted with transmittance of polarized and unpolarized filter.

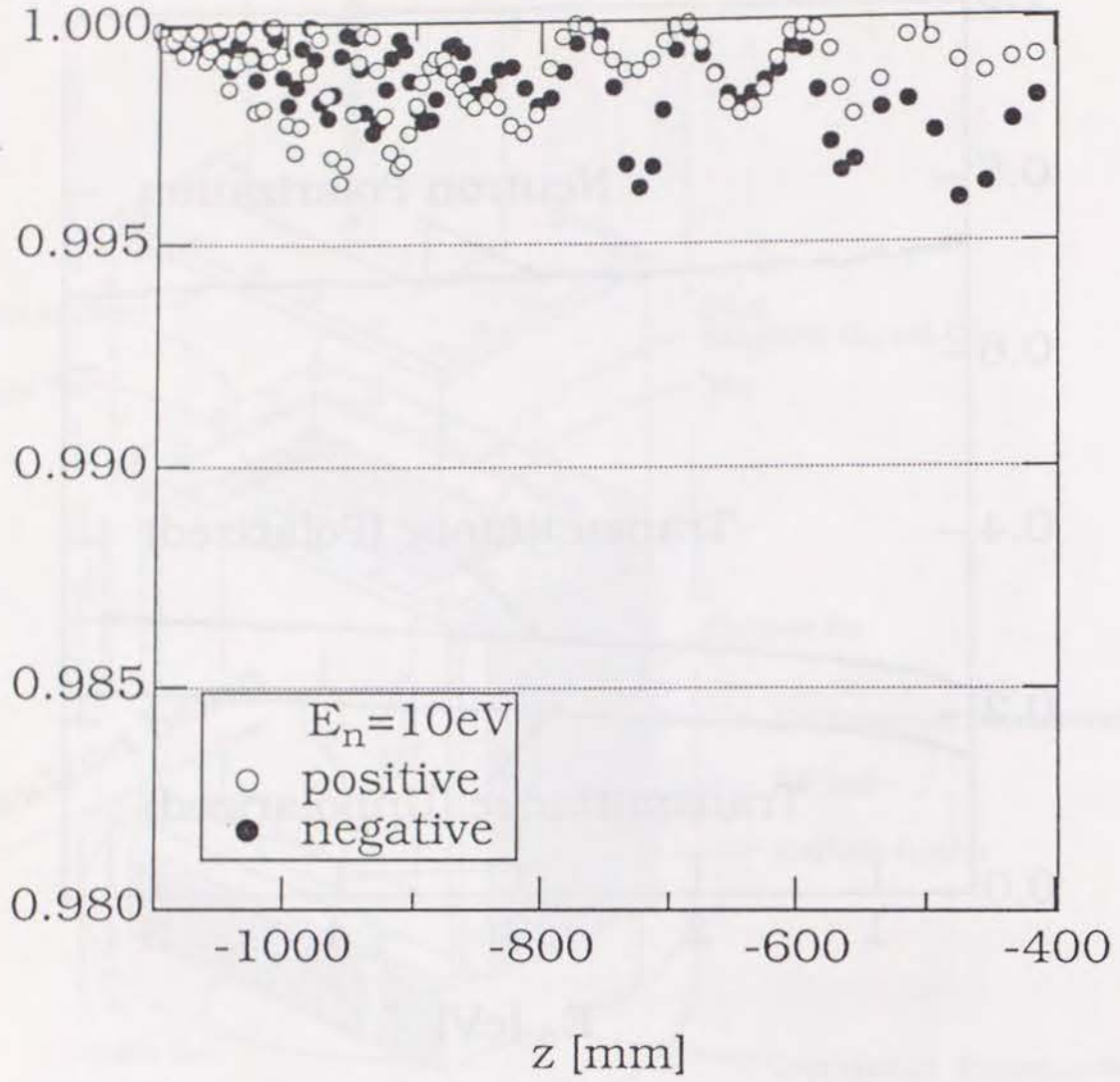

Fig. 3-2-4 The $\cos\eta$ which was calculated from the actual magnetic field versus the z-coordinate which is the distance from the center of target. Open and closed circles represent the values of $\cos\eta$ with magnetic fields for positive and negative helicity neutrons. The target center is at $z = 0$.

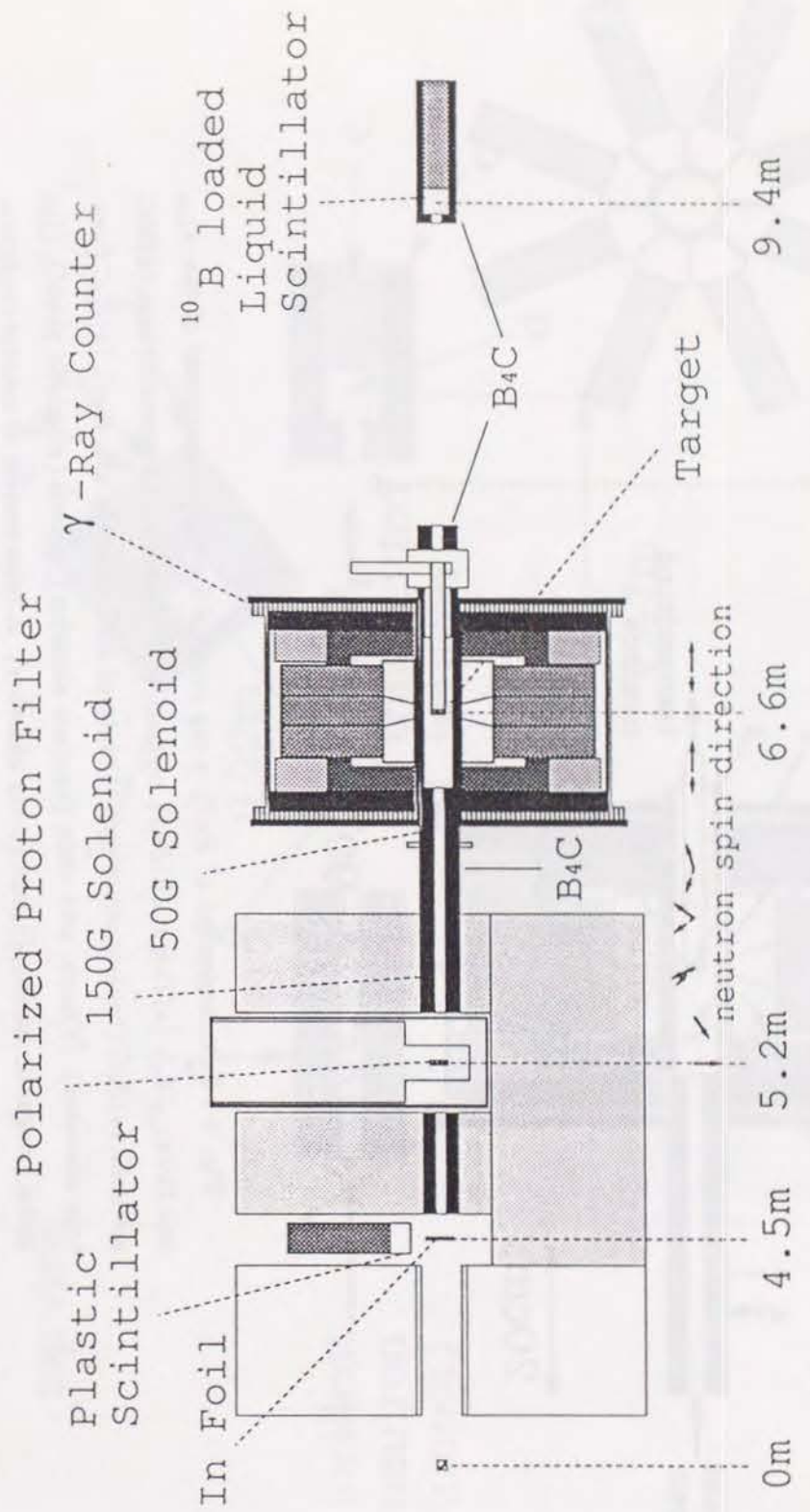

Fig. 4-1-1 The experimental setup of PEN beam line is schematically shown with a γ-ray counter for $A_{L,\gamma}$ and $a_{L,\gamma}(\theta_\gamma)$ measurement (see Fig. 4-1-2 for details of the γ-ray counter).

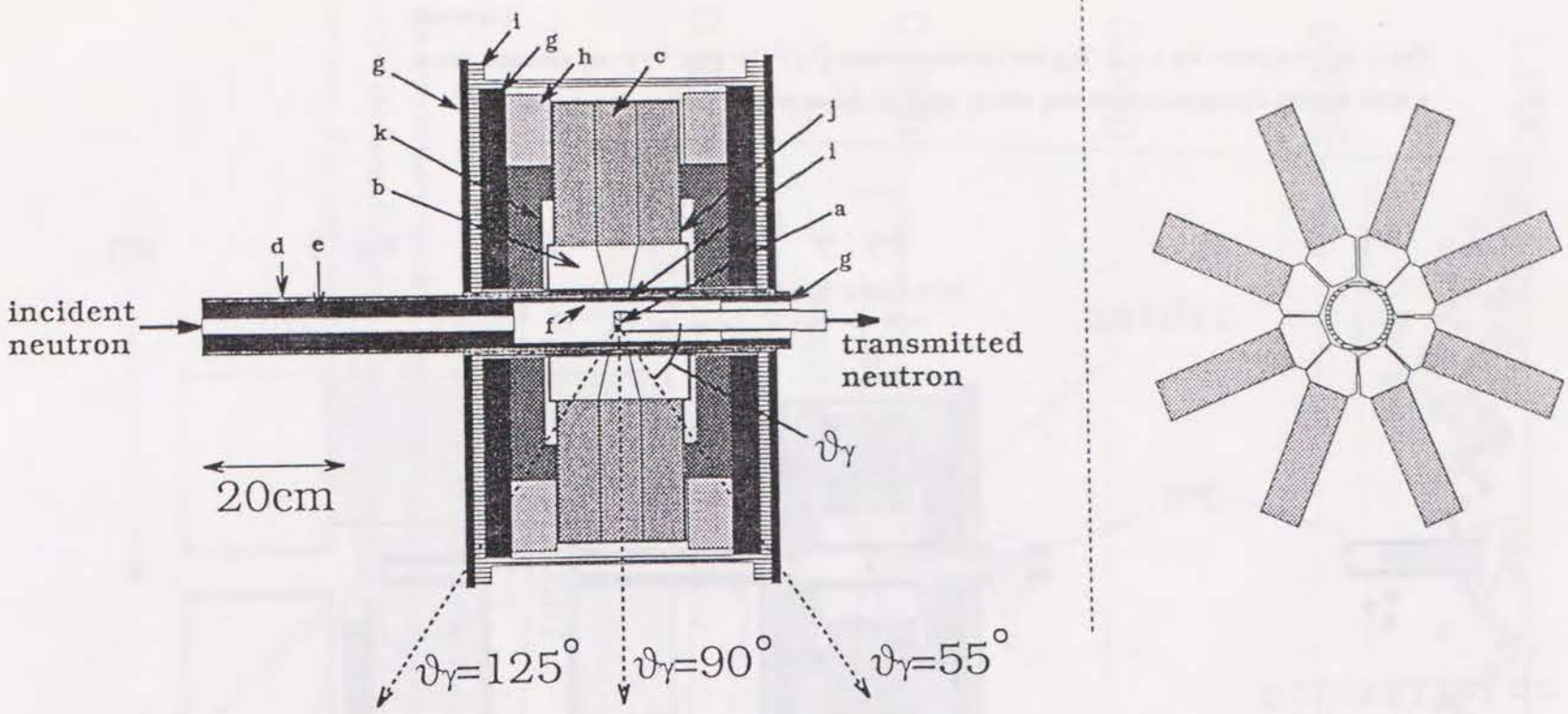

Fig. 4-1-2 Arrangement of BaF_2 γ-ray counter for the measurement of the $A_{L,\gamma}$ and the $a_{L,\gamma}(\theta_\gamma)$. (a)Target, (b)$BaF_2$ crystals, (c)UV sensitive photomultipliers, (d)$50G$ solenoid, (e)B_4C (neutron absorber), (f)sintered B_4C (neutron absorber), (g)B_4C (neutron absorber), (h)boric acid resin (neutron absorber), (i)iron (magnetic shield), (j)μ metal (magnetic shield), (k)lead (γ-ray absorber). A cross section of counter configuration seen from down stream on the beam line is shown in the right hand side. The BaF_2 crystals are arranged to detect γ-rays at θ_γ = 55°, 90° and 125°. The BaF_2 crystals cover 85% of 4π steradians in total.

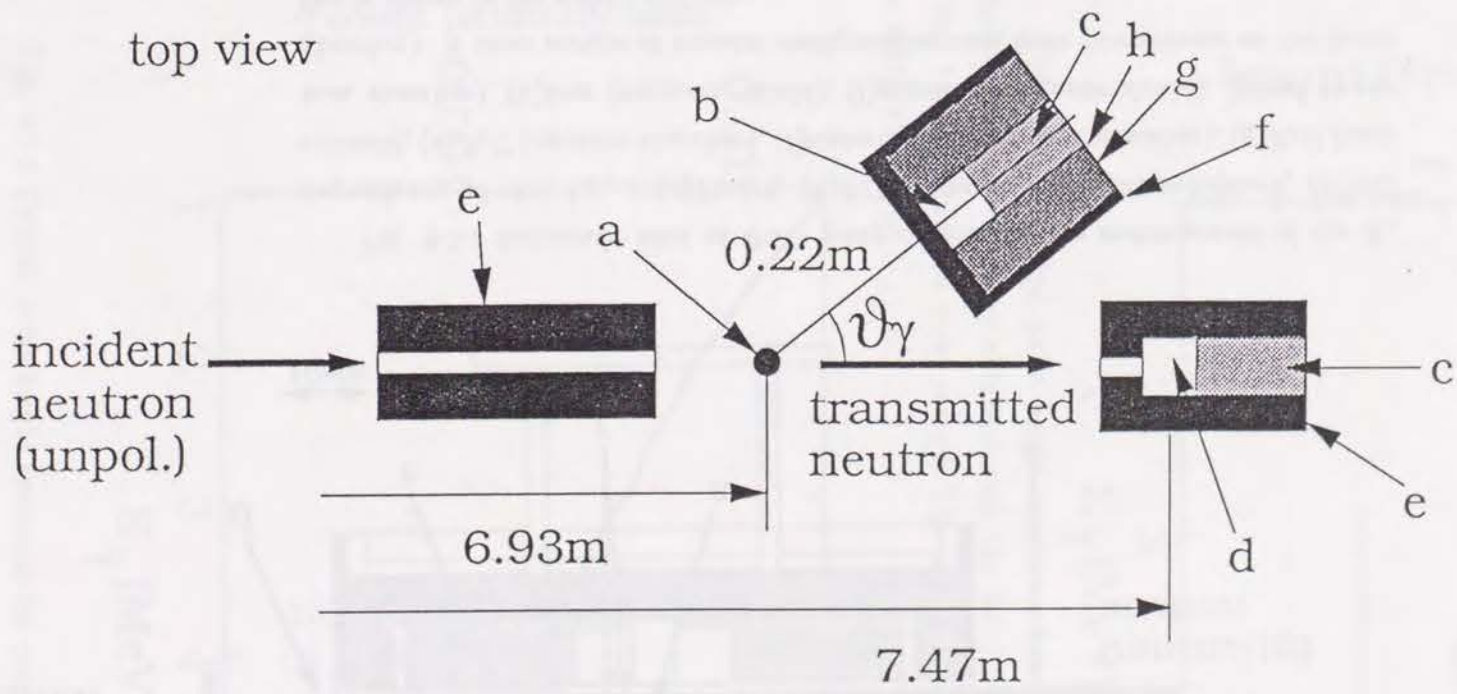

Fig. 4-2-1 The schematic view of experimental arrangement of $\sigma_{res}^{Unpol}(\theta_\gamma)$ measurement. (a)Target, (b)BGO crystals, (c)photomultipliers, (d)^{10}B loaded liquid scintillator, (e,f)B_4C (neutron absorber), (g)lead, (h)iron (magnetic shield).

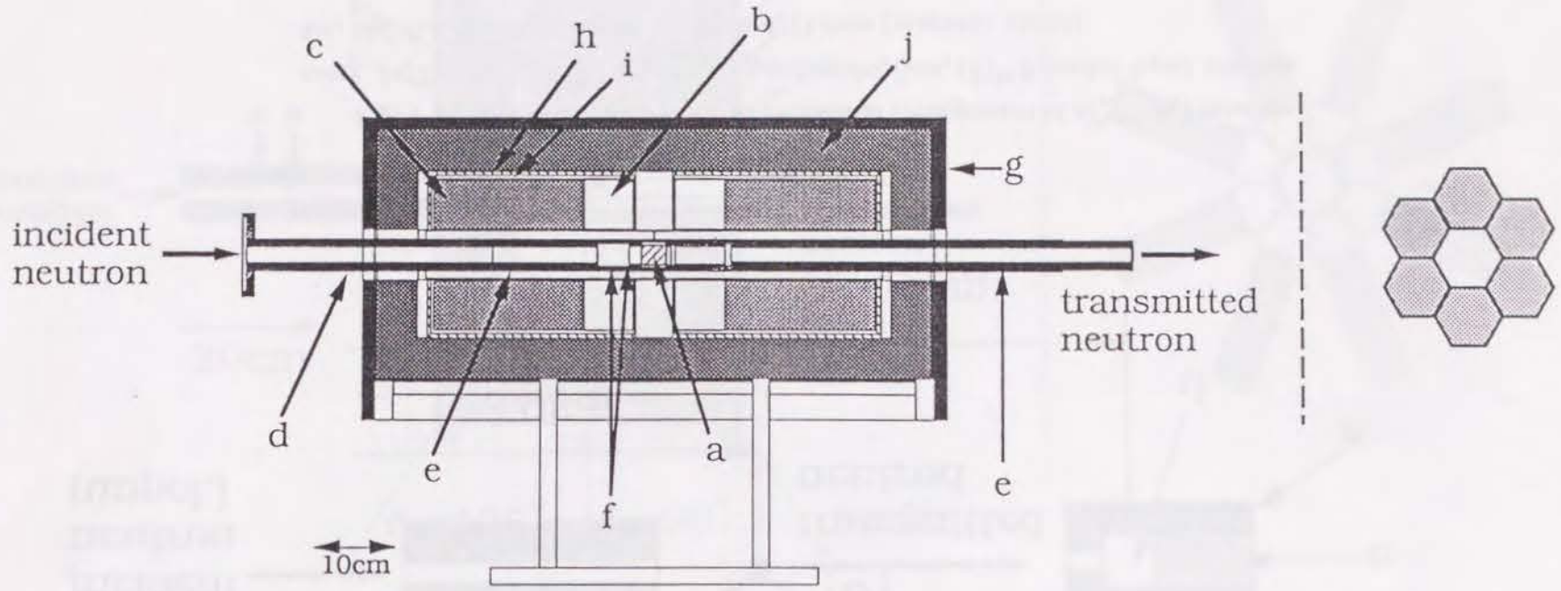

Fig. 4-3-1 Schematic view of BGO γ-ray counter for the measurement of the E_γ dependence of the $A_{L,\gamma}$. (a)Target, (b)BGO crystals, (c)photomultipliers, (d)$50G$ solenoid, (e)B_4C (neutron absorber), (f)sintered B_4C (neutron absorber), (g)B_4C (neutron absorber), (h)iron (magnetic shield), (i)μ metal (magnetic shield), (j)lead (γ-ray absorber). A cross section of counter configuration seen from downstream on the beam line is shown in the right hand side.

Fig. 4-3-2 A typical pulse height spectrum for γ-rays from $^{12}C^*(4.43MeV)$ of Am/Be radioactive source obtained with the BGO counter. The horizontal axis is scaled by fully absorbed γ-ray energy. The energy resolution was was 13% in FWHM for $4.43MeV$ γ-rays.

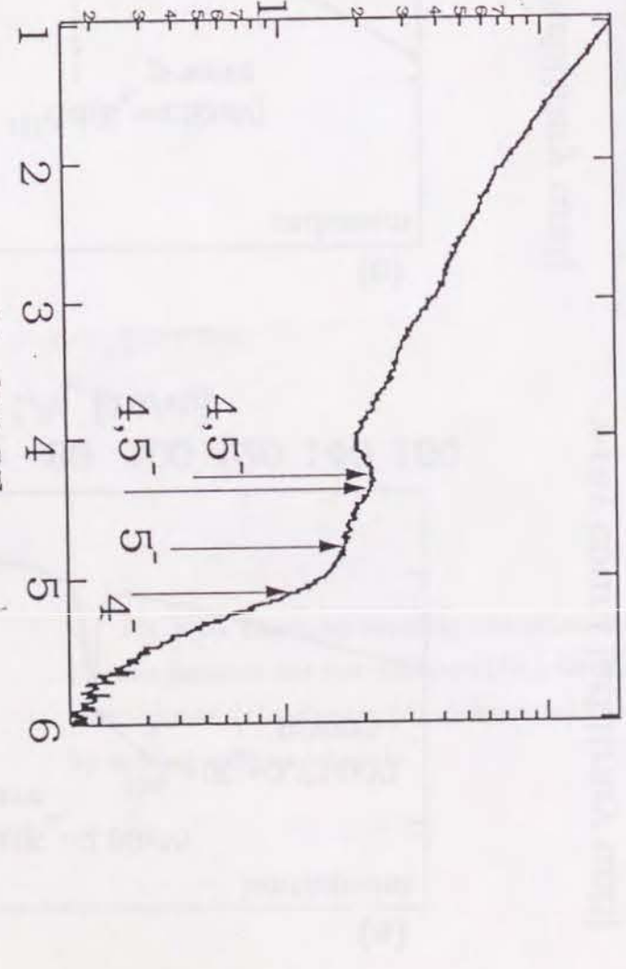

Fig. 4-3-3 Typical pulse height spectrum for γ-rays from $La(n,\gamma)$ (E_n = 0.46 ~ 1.4eV) obtained with BGO counter. The horizontal axis is scaled by fully absorbed γ-ray energy. The labels show the spin/parity of the final states of expected γ-ray transitions.

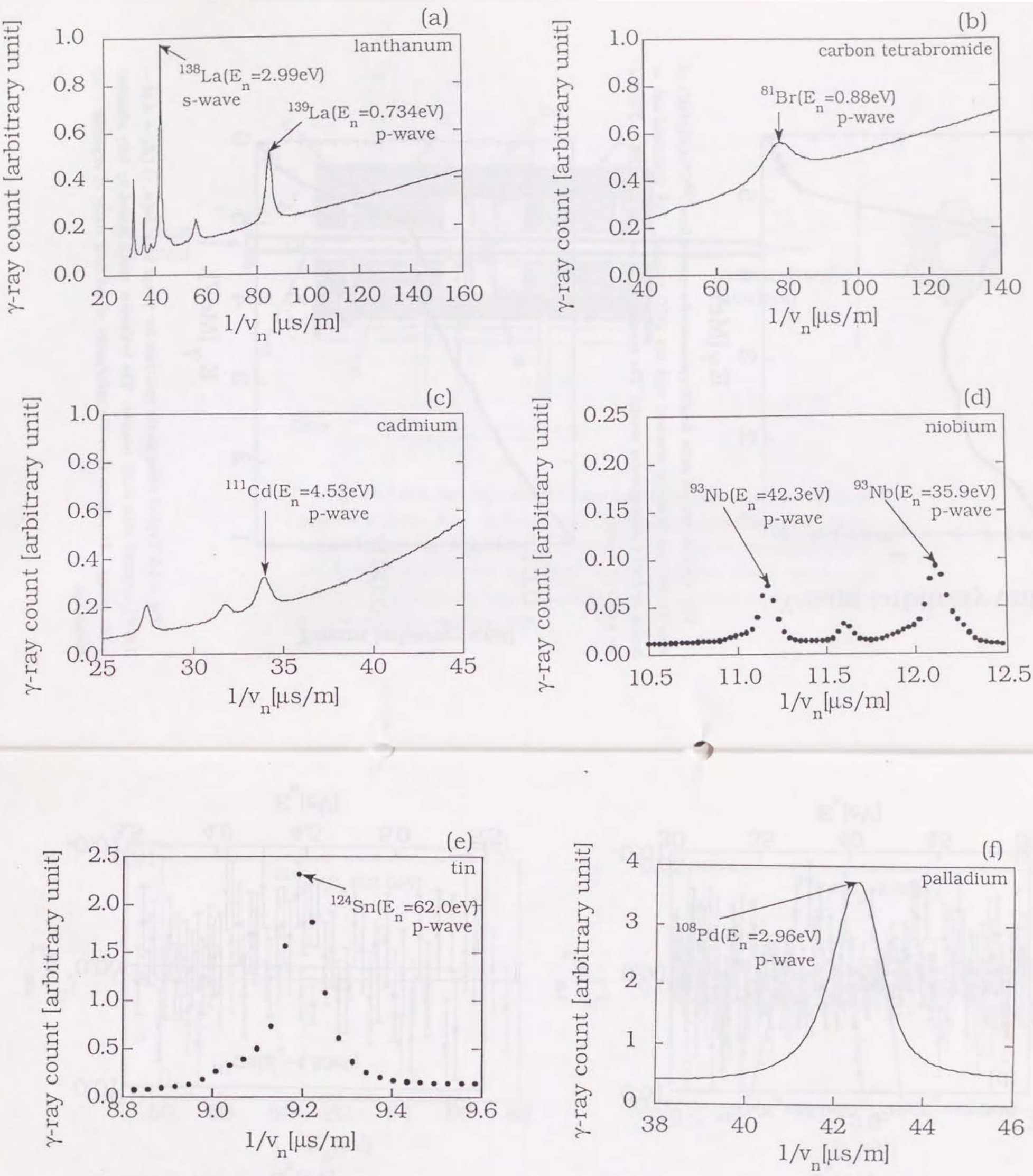

Fig. 5-1-1 The γ-ray counting rate obtained with the γ-ray counter discussed in §4-1 versus incident neutron velocity ($1/v_n$) for the targets of (a) lanthanum, (b) carbon tetrabromide, (c) cadmium, (d) niobium, (e) tin and (f) palladium. They are normalized by incident neutron intensity.

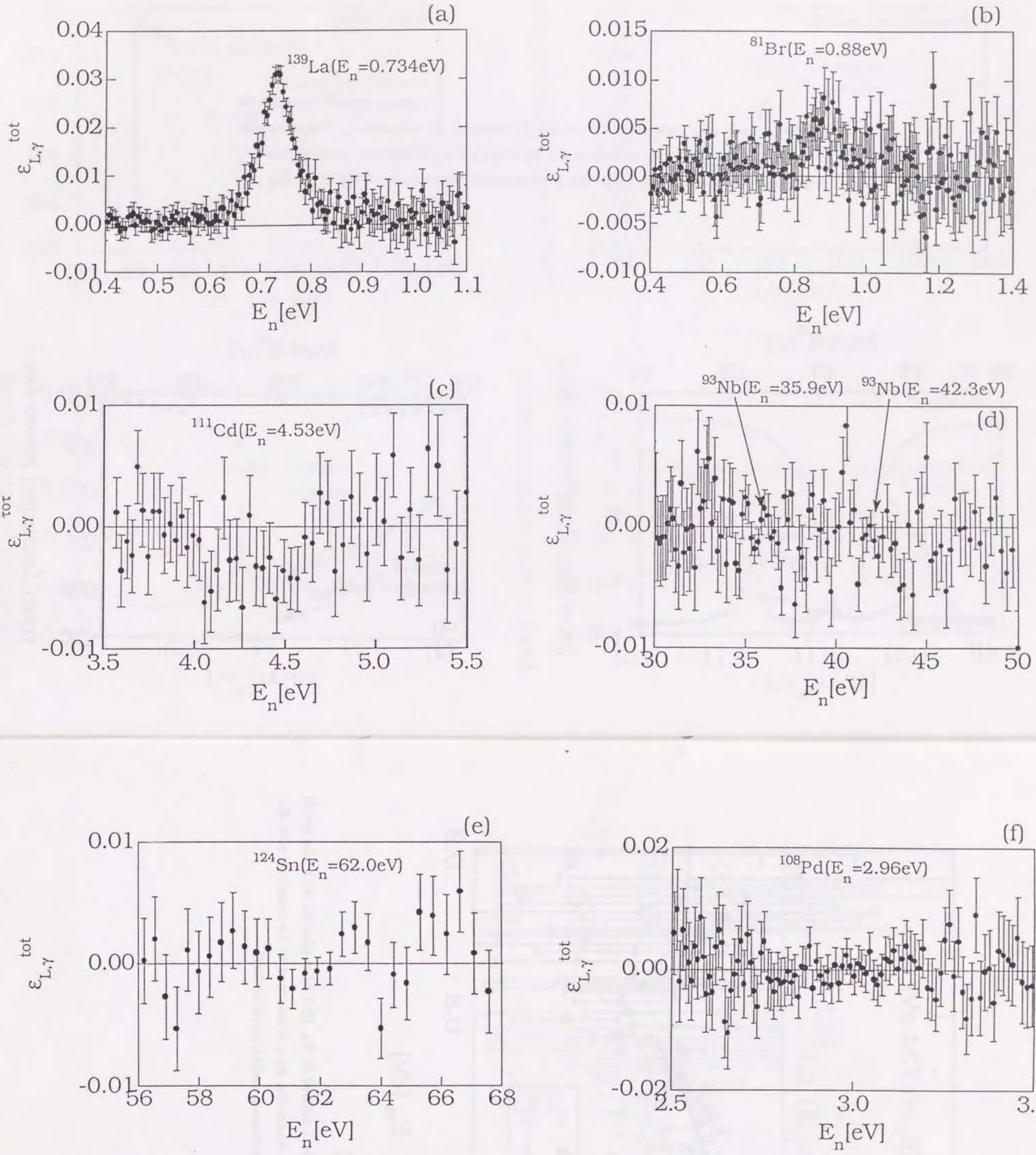

Fig. 5-1-2 The $\epsilon^{tot}_{L,\gamma}$ (Eq. (5-1-1)) versus incident neutron energy for the targets of (a) lanthanum, (b) carbon tetrabromide, (c) cadmium, (d) niobium, (e) tin and (f) palladium.

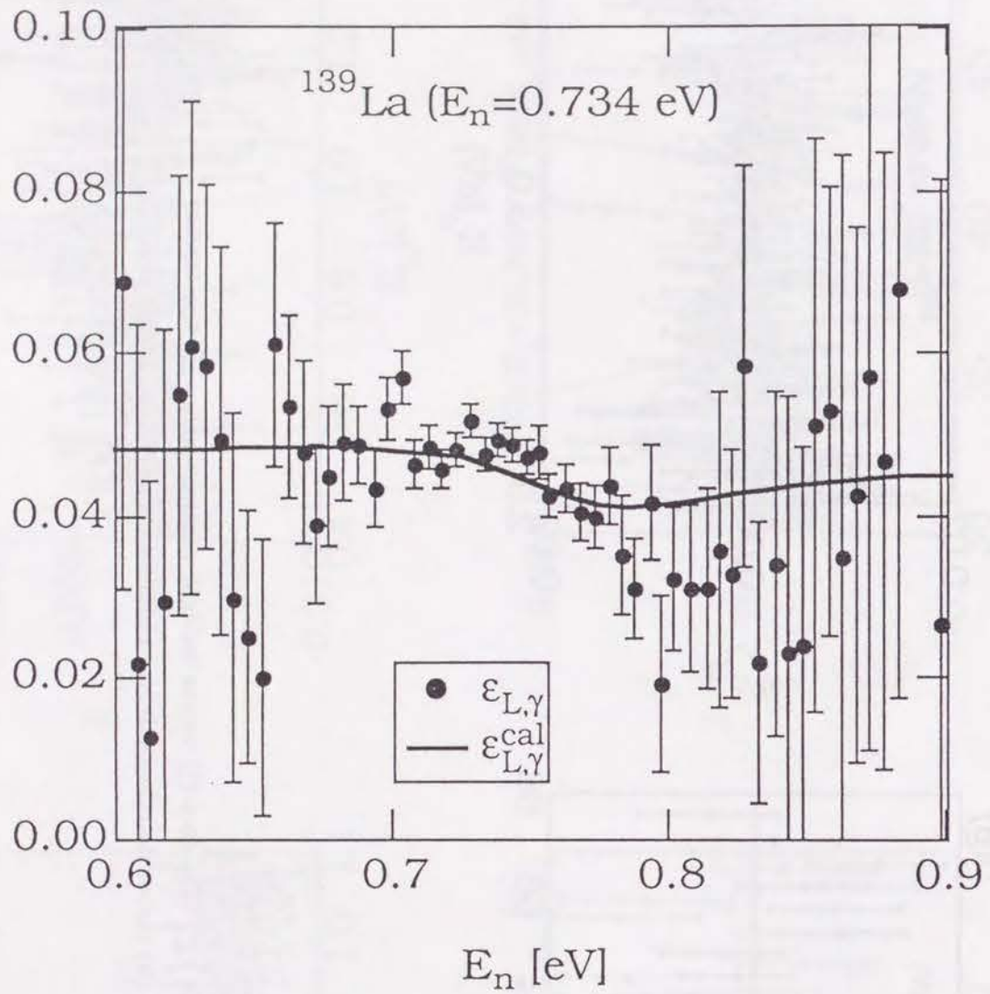

Fig. 5-1-3 The $\epsilon_{L,\gamma}$ (black circles) defined in Eq. (5-1-5) is plotted with the result of numerical simulation (solid line) where the $A_{L,\gamma}$ is assumed to be constant with E_n. The target was $1cm$ thick metal lanthanum cooled down to $35K$.

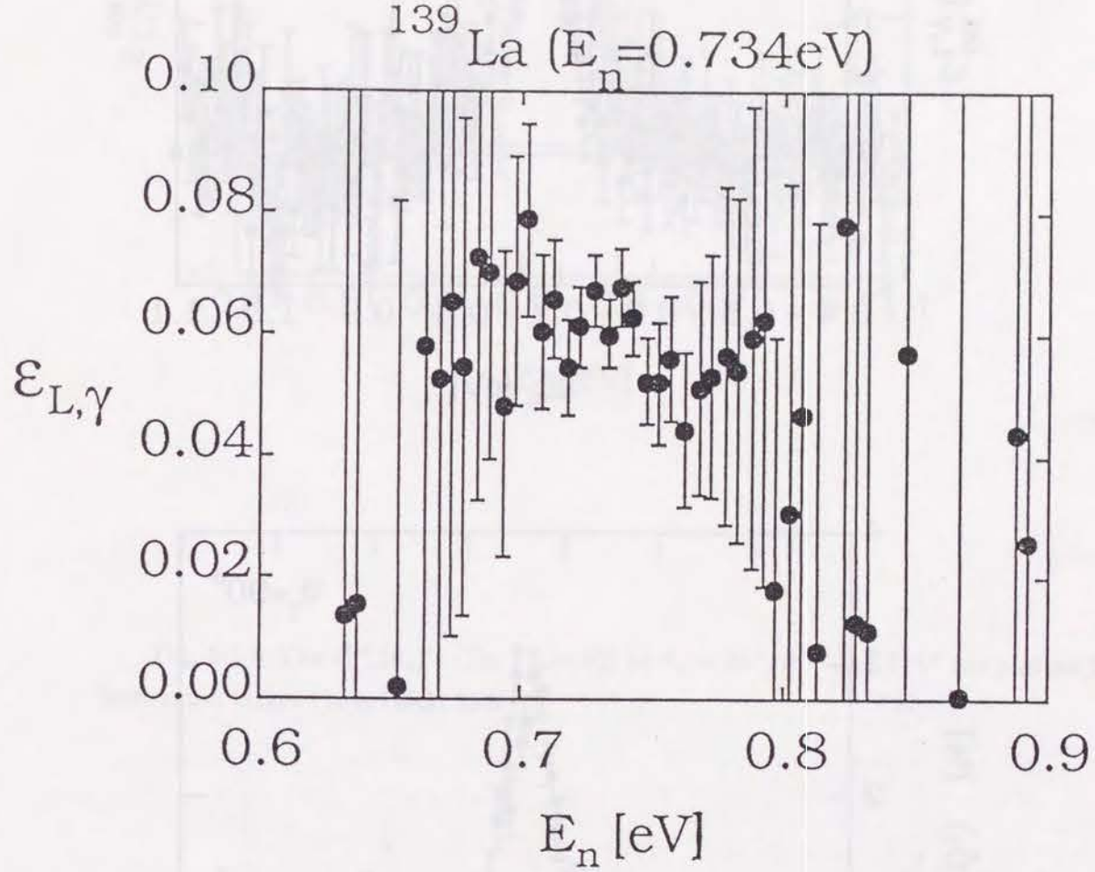

Fig. 5-1-4 The $\epsilon_{L,\gamma}$ (Eq. (5-1-5)) for $0.3cm$ thick metal lanthanum target cooled down to $9K$.

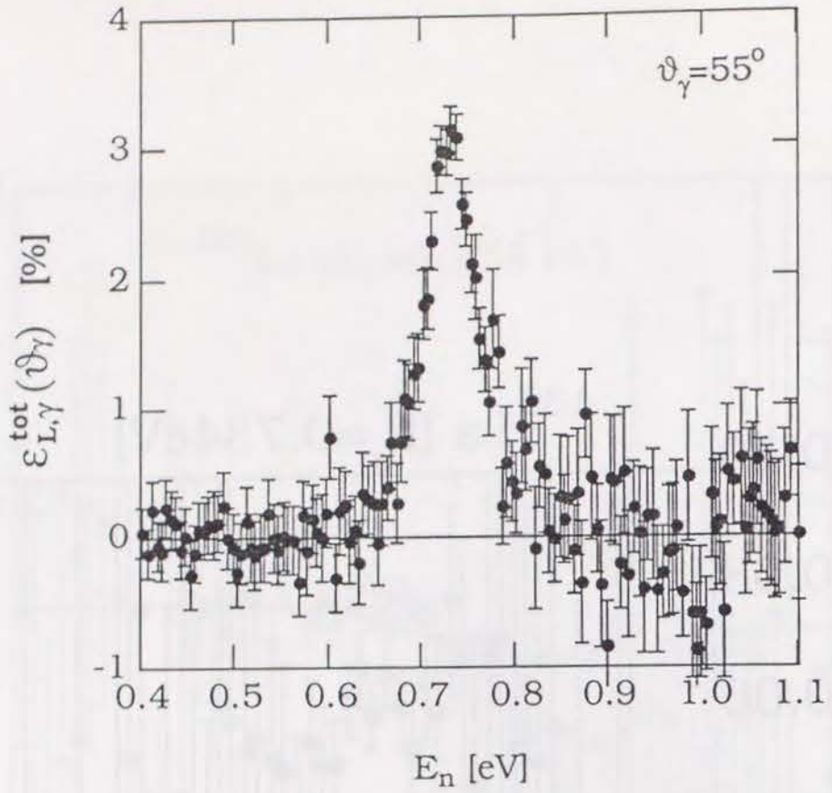

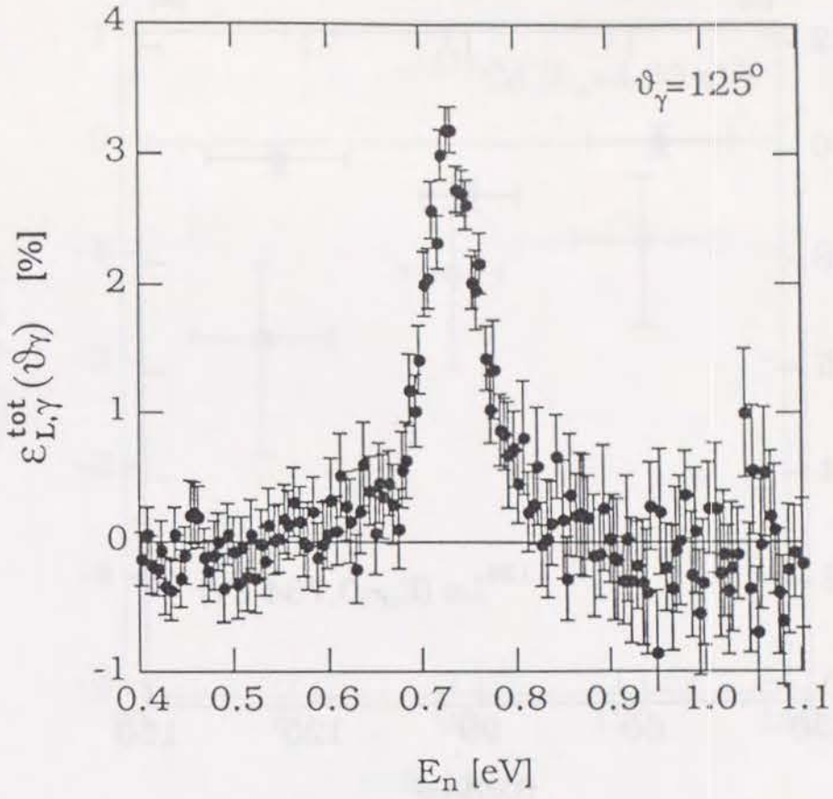

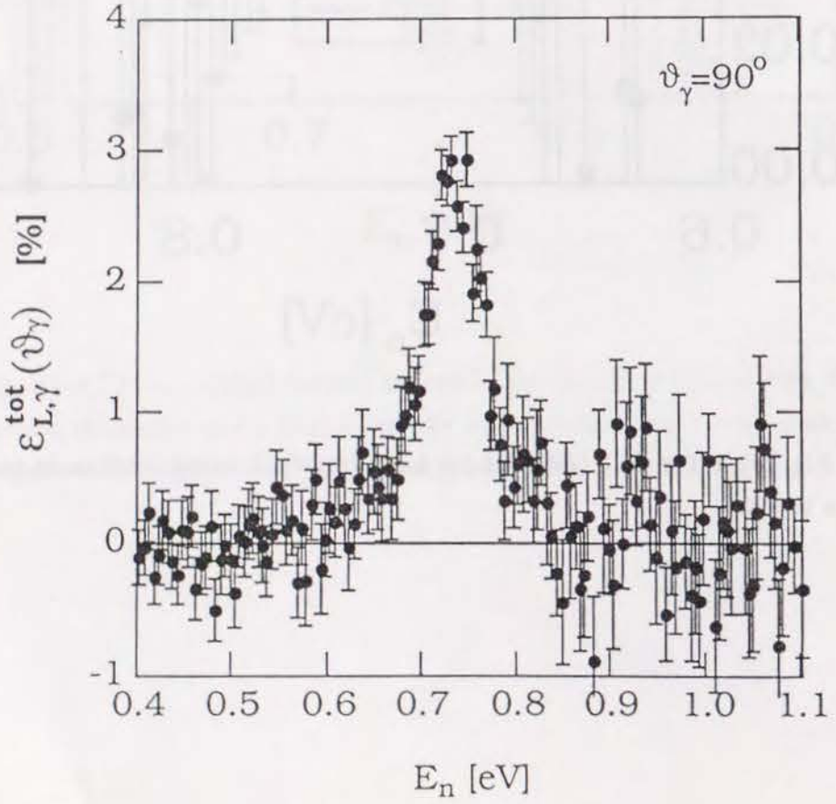

Fig. 5-1-5 The $\epsilon^{tot}_{L,\gamma}(\theta_\gamma)$'s (Eq. (5-1-10)) at $\theta_\gamma = 55°$, 90° and 125° are plotted for lanthanum target ($1cm$-thick, $35K$).

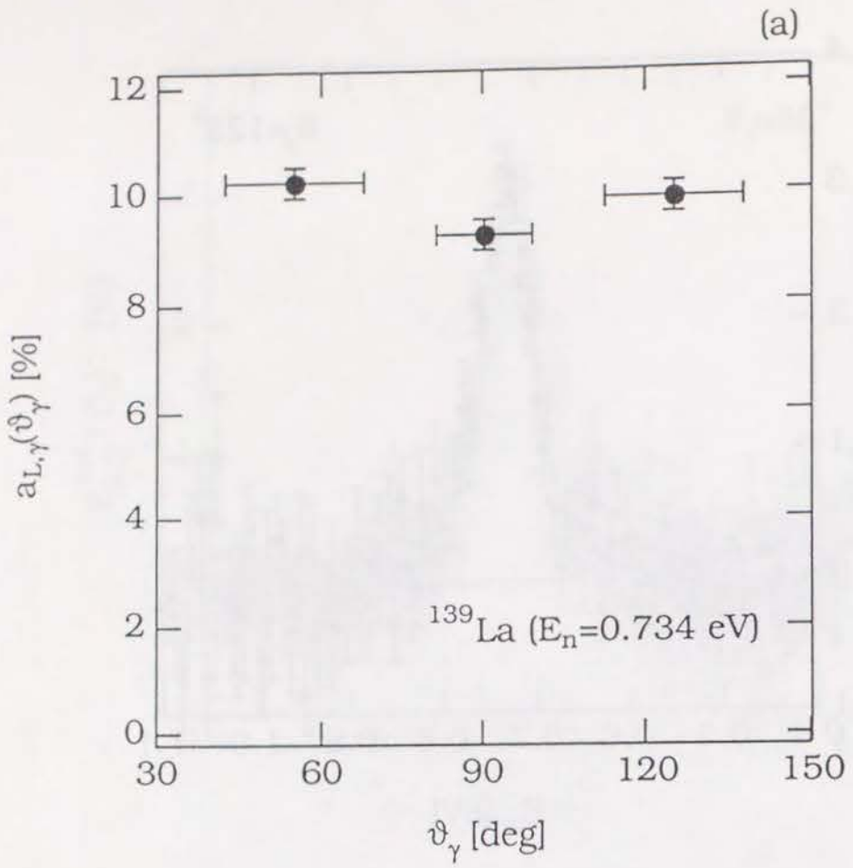

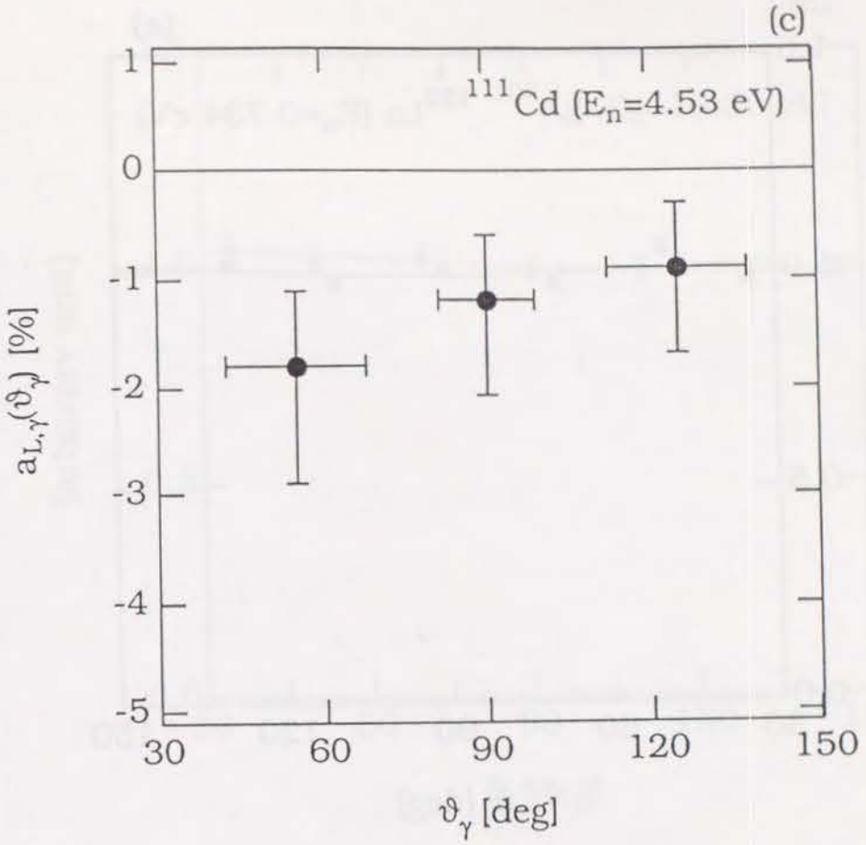

Fig. 5-1-6 The values of $a_{L,\gamma}(\theta_\gamma)$ (Eq. (2-6)) obtained with $E_{\gamma,thres} \sim 1MeV$ versus θ_γ for the p-wave resonances of the targets of (a) $^{139}La(E_n = 0.734eV)$, (b) $^{81}Br(E_n = 0.88eV)$ and (c) $^{111}Cd(E_n = 4.53eV)$.

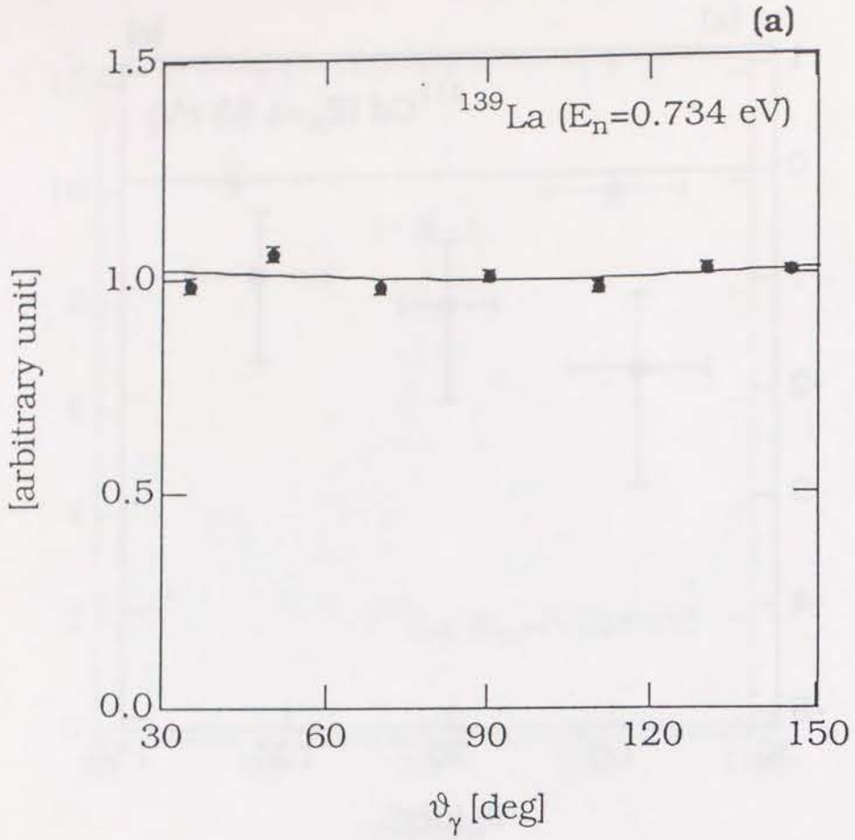

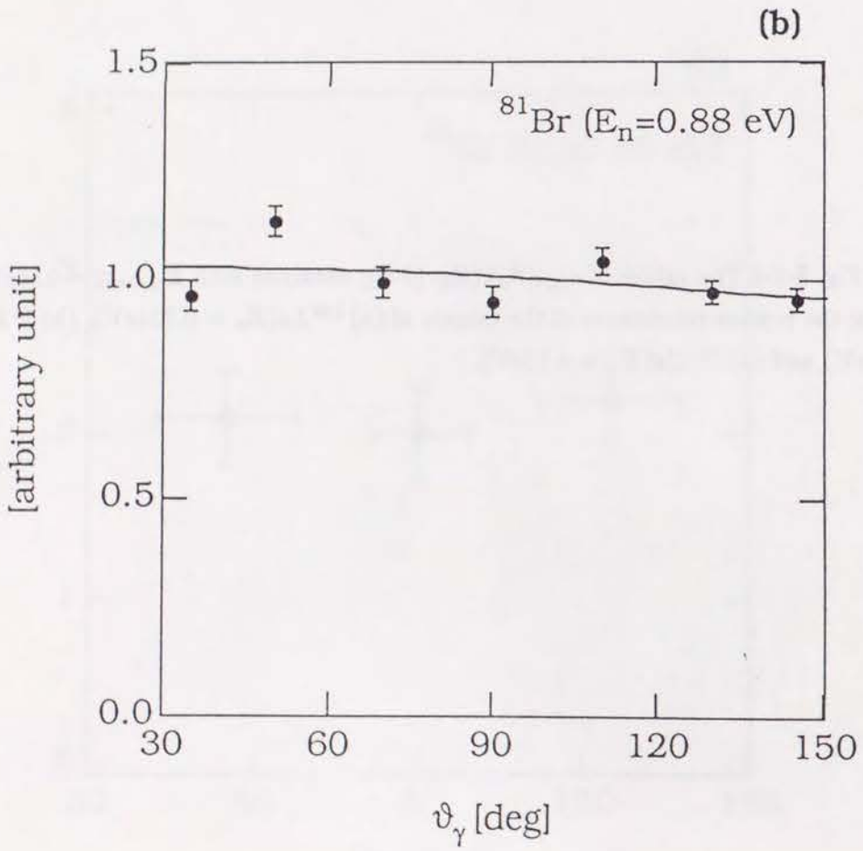

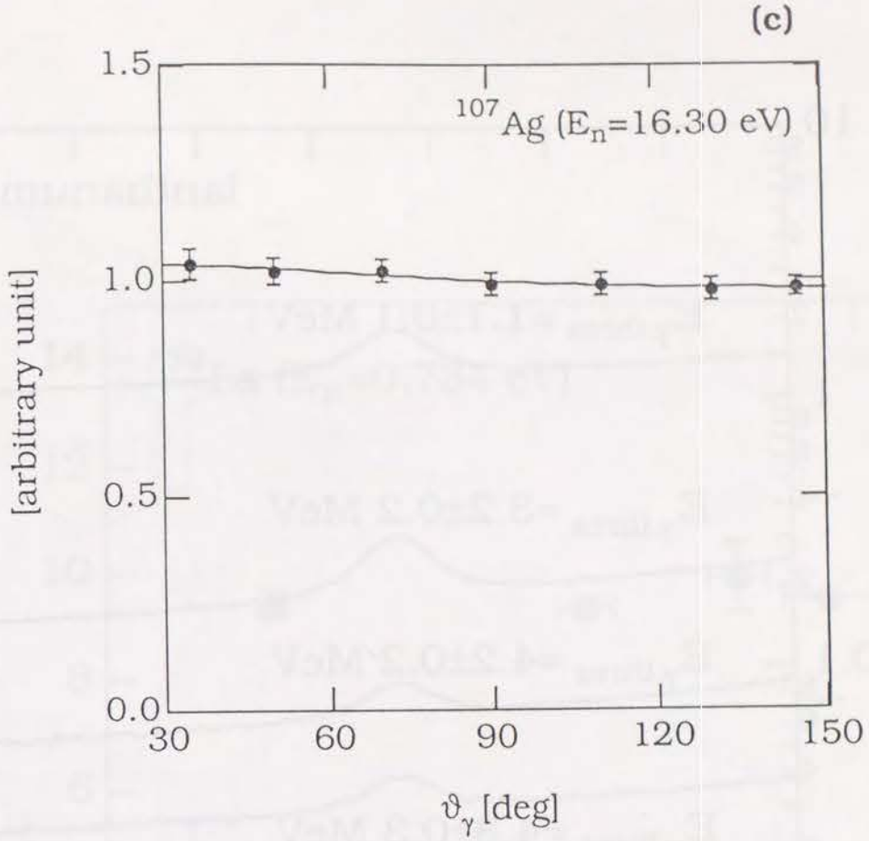

Fig. 5-2-1 The $\sigma_{res}^{Unpol}(\theta_\gamma)$ (Eq. (2-11)) with $E_{\gamma,thres} \sim 1MeV$ for the p-wave resonances of the targets of (a) $^{139}La(E_n = 0.734eV)$, (b) $^{81}Br(E_n = 0.88eV)$ and (c) $^{107}Ag(E_n = 16.30eV)$.

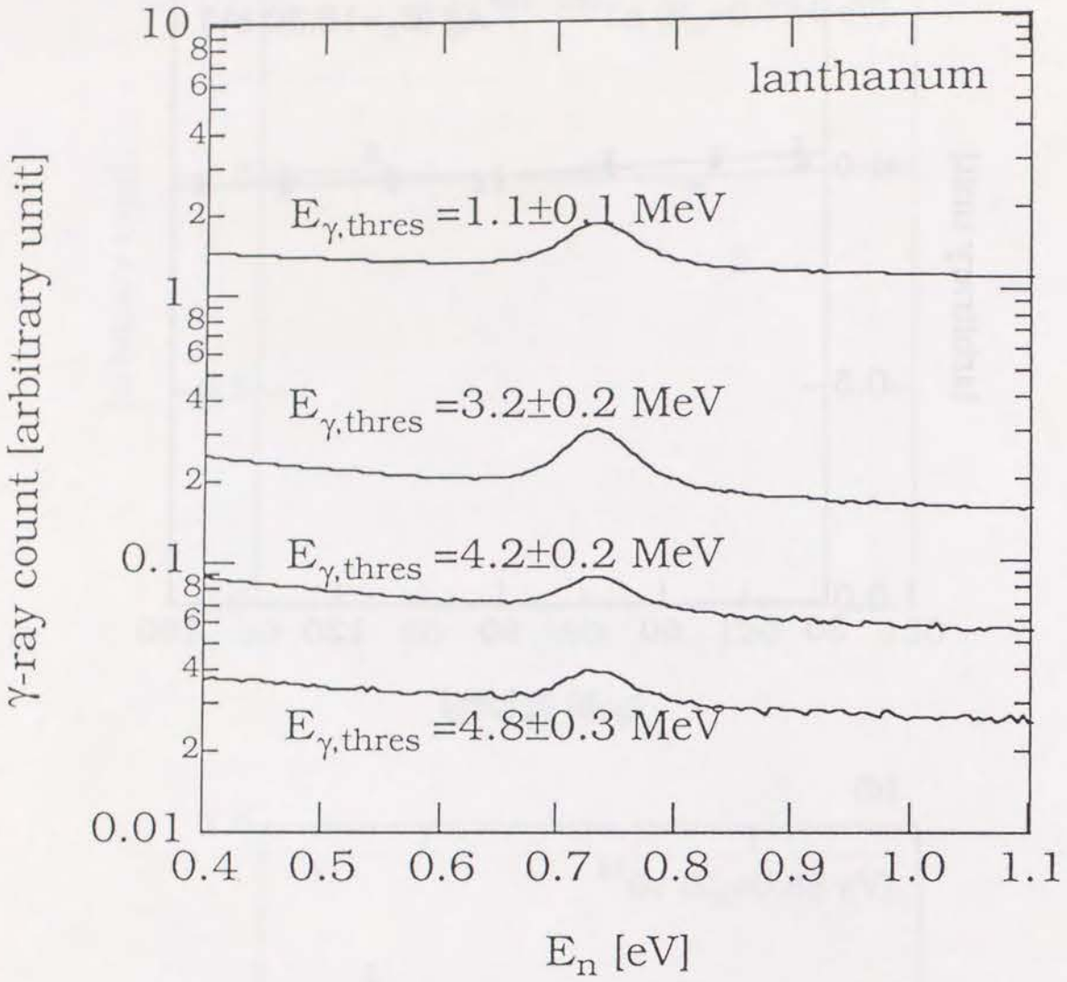

Fig. 5-3-1 The γ-ray counting rates are plotted for several $E_{\gamma,thres}$. The target was a 3.0cm thick metal lanthanum (room temperature).

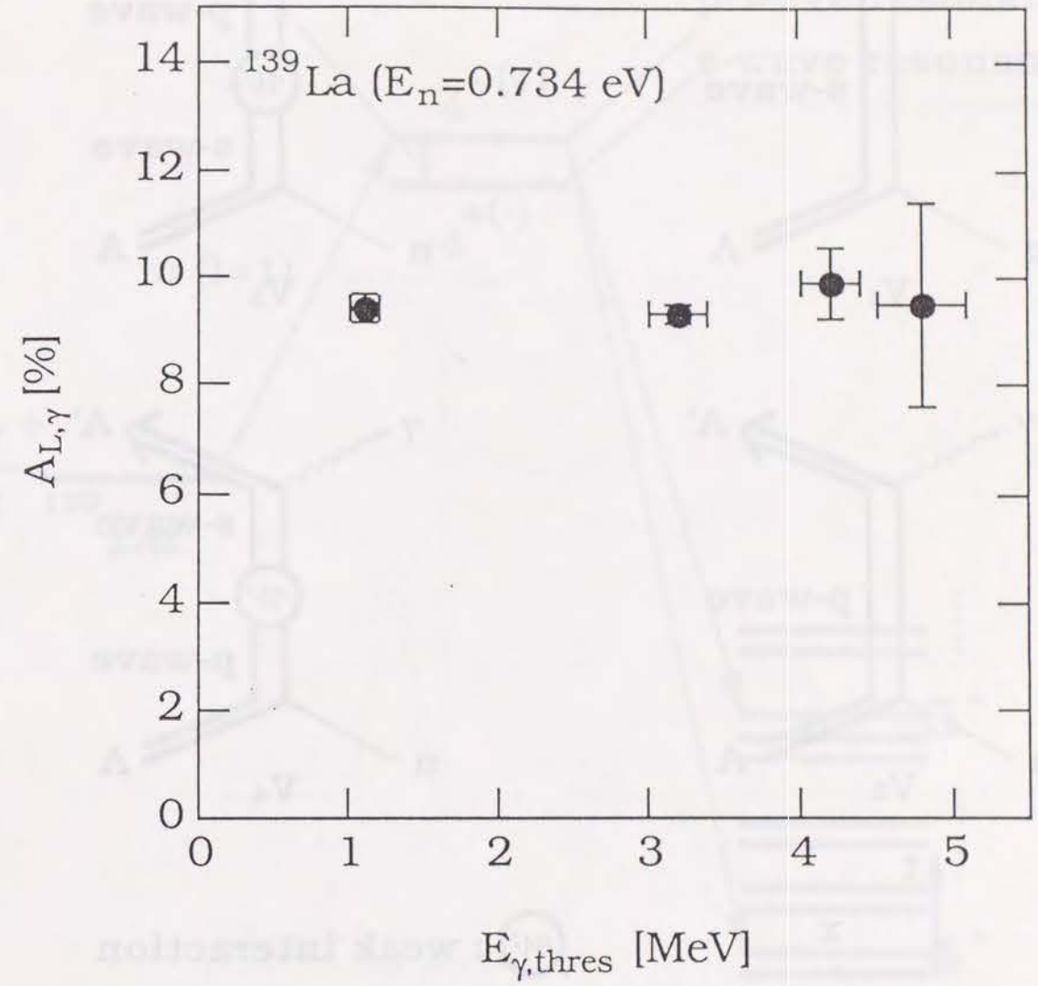

Fig. 5-3-2 The $A_{L,\gamma}$ for the p-wave resonance of the target of $^{139}La(E_n = 0.734eV)$ versus $E_{\gamma,thres}$.

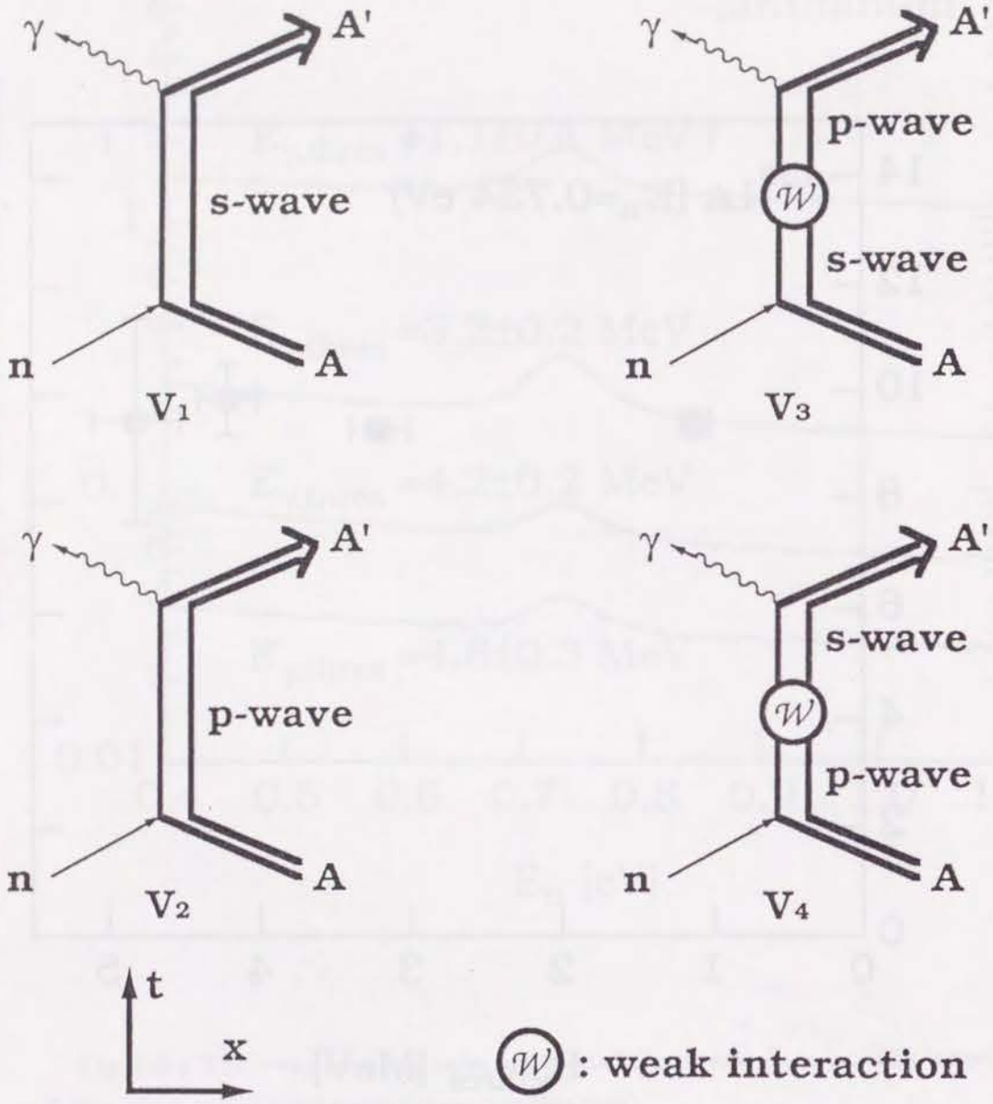

Fig. A-1. The diagrams of invariant amplitudes[37].

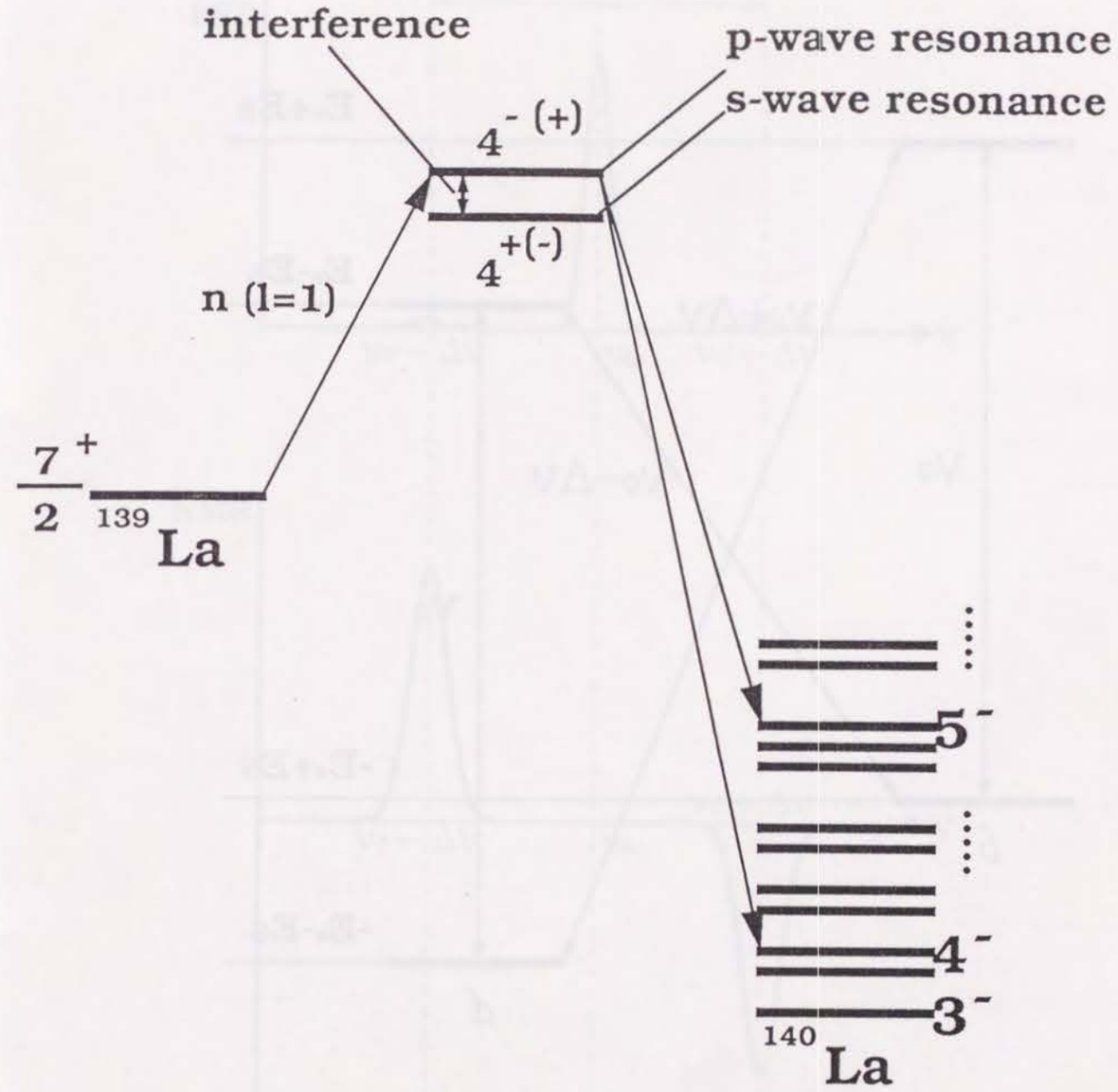

Fig. A-2. The reaction of $^{139}La(\vec{n},\gamma)$ is illustrated.

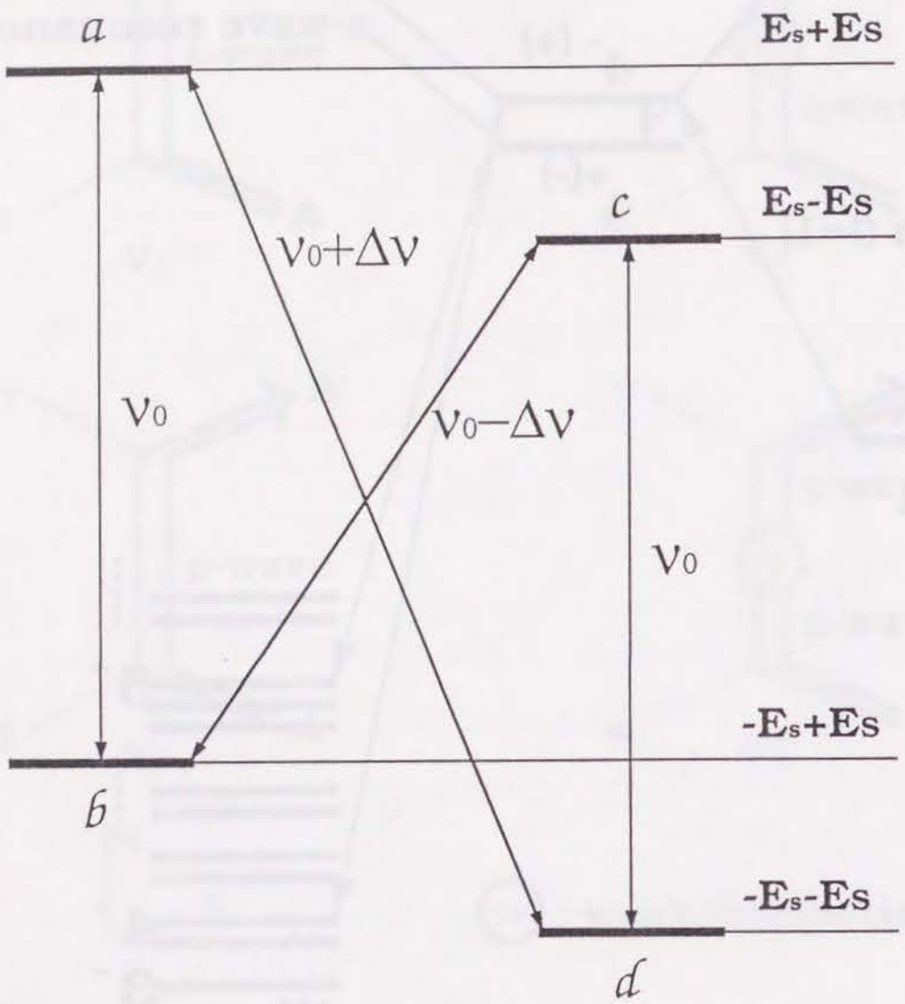

Fig. B-1. Energy levels in the simplest system which consists of an electron and a proton are illustrated.

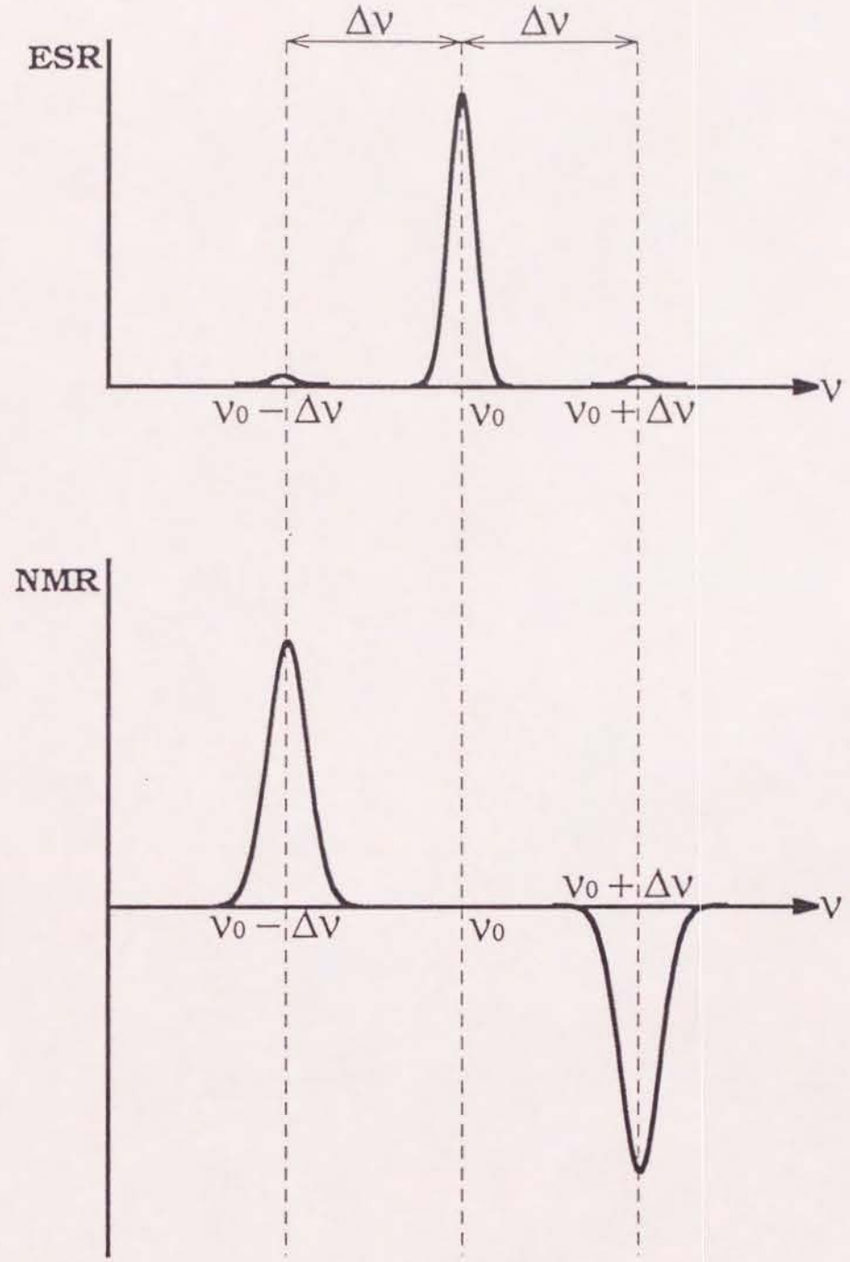

Fig. B-2. The ESR and NMR curves versus the frequency of the applied microwave.